UNIVERSITÀ DEGLI STUDI DI TRIESTE

XXXVII CICLO DEL DOTTORATO DI RICERCA IN

NANOTECNOLOGIE

Borsa MIUR/Ateneo cofinanziata dal Dipartimento di Fisica su fondi CNR-IOM

NANOMECHANICAL SYSTEMS FOR UNDERSTANDING THE BEHAVIOUR OF MECHANICALLY ACTIVATED ION CHANNEL

Settore scientifico-disciplinare: **FIS/03**

DOTTORANDA

GIORGIA DEMONTIS

COORDINATORE

PROF. ALBERTO MORGANTE

SUPERVISORE DI TESI
DTT.SSA LAURA ANDOLFI

CO-SUPERVISORE DI TESI
DTT. MARCO LAZZARINO

ANNO ACCADEMICO 2023/2024

“It always seems impossible until it’s done.”

Nelson Mandela

‘*’Ai miei genitori,*

a mia nonna,

a mia sorella,

alla mia famiglia tutta,

ancora e vento della mia vita’’

ACKNOWLEDGMENTS

I would like to thank financial support from the *Doctoral School of Nanotechnology* of the *University of Trieste*, the *Istituto Officina dei Materiali - Consiglio Nazionale delle Ricerche* (CNR-IOM) of Trieste and the *PRIN2020* project *Touch on a chip*.

I would like to express my deepest gratitude to *Professor Heppenstall* for granting me the opportunity to join his laboratory in SISSA and for fully integrating me into their research team. I would also like to thank Dr. *Fernanda De Castro Reis* for their constant support and guidance, particularly in molecular biology. I am especially grateful for their encouragement and for allowing me unrestricted access to all the laboratory equipment and reagents, which greatly facilitated my experiments on primary DRG neurons while maintaining the highest ethical standards for animal care.

I thank all the people from the PhD's administrative office of the *Department of Physics* of the *University of Trieste* in particular *Ottavia Umani* for providing satisfactory feedbacks in very short time and guidance throughout the complexity of bureaucracy.

I would like to thank Dr. *Francesco Taberner* from the *Instituto de Neurocienci*as in Alicante for kindly providing the PIEZO2-green lantern DNA construct.

I am also grateful to Dr. *Ilaria Tonazzini* of *Consiglio Nazionale delle Ricerche – Istituto Nanonoscienze* (CNR-NANO) of Pisa, for her contributions and expertise that she generously shared with me and the productive discussions.

I would like to express my deepest gratitude to my supervisor, Dr. *Laura Andolfi*, for her continuous step by step support both professionally and emotionally, for the shared expertise, and fruitful conversations that have been a constant source of inspiration throughout my PhD journey.

Finally, thanks to all my colleagues for the help, support and collaboration which have accompanied me along this wonderful PhD journey.

PREFACE

In 2021, Ardem Patapoutian and David Julius were awarded the Nobel Prize in Physiology or Medicine for their groundbreaking discoveries regarding the mechanisms through which humans perceive temperature and touch, senses that are fundamental to our connection with the external world and with others. This recognition holds particular relevance in the context of the Covid-19 pandemic, a period during which physical contact and proximity, so essential to human experience, were temporarily restricted to protect public health.

The discovery of mechanically activated channels in mammals, PIEZO channels, has revolutionized our understanding of mechanotransduction, the process by which cells convert mechanical stimuli into biochemical signals. These channels play a pivotal role in a wide spectrum of physiological functions, ranging from tactile perception, proprioception to vascular regulation and neurophysiology. Furthermore, their involvement in various pathologies has underscored their therapeutic potential. Despite significant advancements, many aspects of their gating mechanisms and functionality remain poorly understood.

This thesis aims to further improve our understanding of PIEZO channels activation through the application of advanced nanotechnological tools. The objective is to explore how mechanical forces in terms of stimulus duration, directionality and geometric cues influence the activation and cellular localization of these channels, thereby contributing to the resolution of existing gaps in this field of study.

The *Chapter 1* provides an overview of the fundamental role of mechanical forces in cell biology, focusing on mechanosensitive ion channels. The discussion is further extended to the identification, structure, and physiological functions of PIEZO channels, highlighting their involvement in the somatosensory system.

The *Chapter 2* explores both traditional techniques and innovative experimental nanotechnological tools employed to study the activation of mechanosensitive channels, examining their respective strengths and limitations. Particular attention is given to advanced techniques such as Atomic Force Microscopy (AFM), Fluidic Force Microscopy (FluidFM), and the use of micro- and nano-structured substrates to investigate channel behavior.

In *Chapter 3***,** the focus shifts to PIEZO2, to gain insights into its activation by exploiting a well-characterized model. The study utilizes AFM, a technique that stands out for its precision in applying a localized mechanical stimuli on a cell, allowing a fine control over the force and pressure applied.

In this case, however, the mechanical stimulus engages the entire cell, rather than targeting specific regions.

In *Chapter 4*, Fluidic Force Microscopy, a novel AFM-based approach, is exploited to apply a localized mechanical stimulation at the level of the plasma membrane. This chapter investigates the behavior of mechanosensitive ion channels in dorsal root ganglion neurons, a physiological context where PIEZO2 is endogenously expressed.

Finally**,** *Chapter 5* focuses on how topographical and mechanical inputs can influence cellular orientation and PIEZO2 localization within a cell. Micro-patterned substrates with a particular periodicity were created and employed for this purpose. This work was conducted in strict collaboration with the group of Dr. Ilaria Tonazzini Istituto di Nanoscienze-Consiglio Nazionale delle Ricerche (CNR-Nano Pisa).

ABSTRACT

Studying mechanosensitive channels is essential because they serve as key mediators in how cells sense and respond to physical forces, which are fundamental to many physiological functions. These channels translate mechanical stimuli into biochemical signals, involved in physiological and pathological conditions.

This thesis advances the field of mechanotransduction by investigating the activation mechanisms of PIEZO2 channels under diverse mechanical conditions, including variations in force intensity, stimulus duration, and directional application. It also examines how geometric cues can influence channel localization. By utilizing advanced nanotechnological approaches—Atomic Force Microscopy (AFM) and Fluidic Force Microscopy (FluidFM)—the study seeks to overcome the limitations of traditional methods in studying mechanically activated channels.

The research highlights the response of PIEZO2 in transfected cells to low-pressure, short-duration stimuli applied by AFM, revealing both individual and collective cellular behaviors under mechanical stress. Additionally, the local stimulation of dorsal root ganglion (DRG) neuron membranes with FluidFM, employing both positive and negative pressures, demonstrates that membrane deformation activates calcium mechanosensitive channels, with a stronger response observed at longer culture times.

The results also show that physical cues from the cellular microenvironment influence not only the morphology of DRG neurons, but also the localization of PIEZO2 channels in transfected cells. These findings contribute to enhance our understanding of PIEZO2 activation and its role in mechanotransduction, potentially guiding the development of therapeutic strategies for diseases associated with mechanosensitivity.

TABLE OF CONTENTS

CHAPTER 1

Mechanotransduction and mechanosensitive channels

1.1. Mechanical forces in cell biology

The concept that physical properties influence biological structure and function has deep roots in cell biology and physiology. Cell behavior is now commonly regarded as being affected not only by chemical signals, but also by the mechanical qualities of both the cells and their environment (Y. Li et al., 2021). The complex biological process by which cells sense and respond to these mechanical stimuli by converting them into biochemical signals is named mechanotransduction. This process plays a crucial role in regulating a broad spectrum of physiological functions and cellular behaviors (Di et al., 2023). Cells are susceptible to external forces that can be characterized as tensile, compressive, or shear stress (***Figure 1.1***):

Tensile or stretching forces that involve pulling or stretching a cell, in a tissue under tension, like muscle fibers or skin. For instance, during muscle contraction, stretching of epithelial tissues, cell migration.

Compressive forces that compress or squeeze cells, often seen in tissues subjected to pressure as bone cells (osteocytes) under mechanical load, cartilage under joint compression.

Shear Stress that acts parallel to the cell surface, causing layers of fluid or tissue to slide past each other. Endothelial cells lining blood vessels experience shear stress from blood flow, especially in arteries.

These mechanical cues are given by the neighboring cells in respiration, blood flow, muscle contractions and etc. The pre-stressed contractile machinery of cells responds immediately to micrometric and nanometric variations in their environment's geometry, topography, or spatial distribution (C. S. Chen et al., 2003). In response to external mechanical forces, the contractile apparatus of cell generates an opposing force within the extracellular matrix (ECM). As a result, the ECM starts a remodeling process to restore homeostasis and strengthen adhesions against increased forces. Cytoskeletal components, such as microtubules and actin filaments, counterbalance the tensile withstanding compressive forces in pre-stressed elements (Fletcher & Mullins, 2010). Intermediate filaments aid in the long-distance transmission of force and the structural integration of the cytoplasm and nucleus.

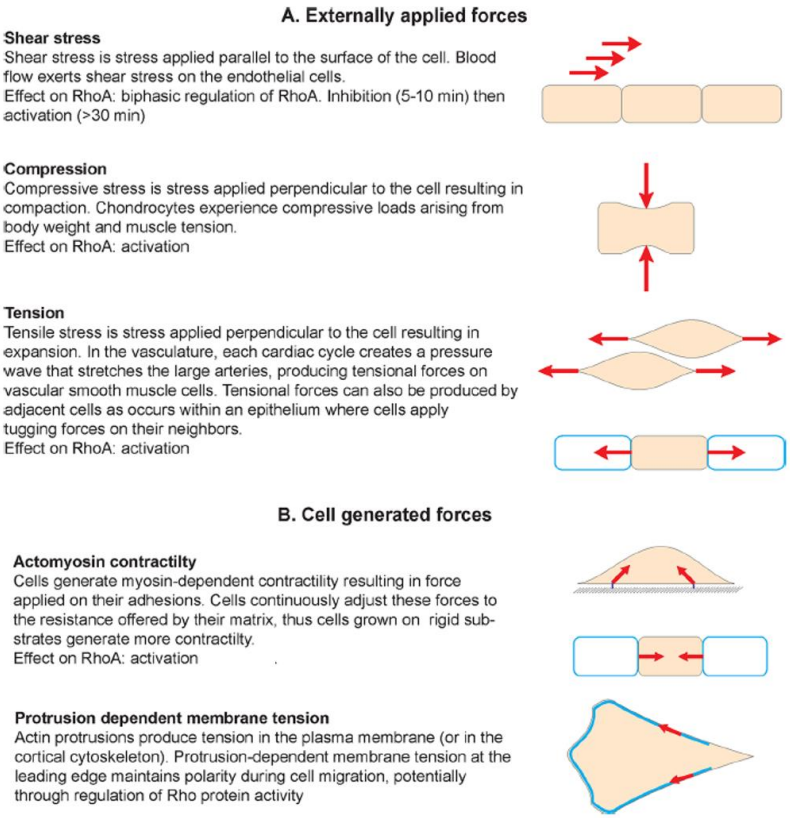

Figure1.1 **Mechanical forces experienced by cells.** Scheme illustrating the main forces to which cells are subjected (*passive forces*) and those generated by cell in various processes. Image from (Lessey et al., 2012).

Considering the endogenous forces during cytoskeletal assembly, intermolecular bonding forces attract neighboring filament subunits, creating tension. These forces are balanced by resistance to compression, with the cytoskeletal components and associated proteins featuring stiff and flexible regions that impart elasticity and pre-stress to the filaments. This structural arrangement enables the system to withstand deforming forces such as extension, bending, and compression (Chaudhuri et al., 2007). Cells can generate forces by the actomyosin apparatus, that produces tensional forces by remodeling and exerting traction on cell-cell and cell-matrix adhesions, creating a baseline tension within the cell. This contractile tension exemplifies the feedback mechanism that a cell employs to link external and internal mechanotransduction events (C. S. Chen, 2008). Variations in the stress versus strain equilibrium can influence which mechanosensors collaborate to orchestrate a coordinated response and dictate how the signal is integrated.

1.1.1. Mechanical forces from microenvironment shape cell behavior and fate

Mechanical forces are now recognized as essential regulatory mechanisms for maintaining tissue integrity and function in human organs. These forces govern critical processes such as morphogenesis, organ homeostasis, and gene expression (Alvarez & Smutny, 2022).

Moreover, mechanical stimuli are vital for the function of tissues like bone, cartilage, and muscle, and they play a key role in preserving the integrity of systems that rely on mechanical regulation, such as the cardiovascular and respiratory systems (Jung & Donahue, 2007).

Mechanical forces originating from microenvironment are essential in driving collective cell migration, a process at the base of embryonic development, morphogenesis, immune system surveillance, and wound healing (Ventura & Sedzinski, 2022). Unlike chemical signals, the mechanical properties of the microenvironment offer sustained cues that influence cellular behavior over prolonged periods and across large spatial dimensions. In the absence of injury, the mechanical characteristics of the extracellular matrix (ECM) change gradually, affecting large physical areas across multiple cell lengths. As a result, mechanical signals are enduring, continually influencing cells even as they migrate over long distances (Afzal et al., 2016).

These cues include ECM rigidity and topographical features, which recent research has shown to play a critical role in regulating various cellular processes in stem cells, such as maintaining their potency, promoting division and differentiation, influencing metabolism and migration, and mediating interactions with neighboring cells (Kshitiz, 2013).

Macroscale forces alter the strength of cell-cell or cell-matrix associations, activating mechanosensors and transmitting signals through the cellular network via the cell membrane, adhesion receptors, and focal adhesions. These mechanotransduction events allow the cell to discern the mechanical nature, stiffness, and specific types of ECM fibers, influencing downstream signaling and cytoskeletal reorganization that lead to altered cell morphology (Cukierman et al., 2001; Geiger & Bershadsky, 2002).

To ensure proper function, cells within a tissue need to establish, maintain, and restore their optimal morphological and mechanical conditions, a process known as mechanical homeostasis (Eichinger et al., 2021). Loss of mechanical homeostasis is closely linked to the onset and progression of various pathological conditions, including cardiovascular diseases such as cardiomyopathy (Cook et al., 2014; Grolleman et al., 2023) and aneurysms (C.J.Cyron,J et al, 2014) as well as cancer (Jaalouk & Lammerding, 2009).

In order to maintain mechanical homeostasis, it is essential that mechanoreciprocity is finely tuned. Mechanoreciprocity refers to the dynamic, bidirectional mechanical interactions between a cell and

its surrounding ECM-rich microenvironment (De Luca et al., 2021; Eichinger et al., 2021; Van Helvert et al., 2018).

Key elements involved in maintaining mechanical homeostasis include ECM components such as collagens and elastin, which provide structural support and transmit mechanical forces. These components interact with transmembrane receptors like integrins, which connect the ECM to intracellular structures via integrin-associated linker proteins (e.g., talin and vinculin). These linker proteins, in turn, anchor integrins to the cytoskeleton, comprised of actin filaments, non-muscle myosin, and related proteins, that propagate mechanical forces within the cell. Cells first perceive ECM mechanical properties and subsequently modulate them to maintain optimal conditions (Humphrey et al., 2014). Disruptions in these interconnected processes can lead to pathological conditions such as fibrosis or other diseases. Consequently, tissue stiffness is highly controlled in healthy tissue, but variations in its mechanical properties often lead to the onset of disease.

For example, in cancer, tumors frequently exhibit increased stiffness compared to surrounding healthy tissue, while cancer cells themselves tend to soften (LiKang Chin et al., 2016). Tumor mechanosensing involves intricate mechanical interactions between cancer cells, the extracellular matrix (ECM), and the tumor microenvironment (Gargalionis et al., 2018).

The cell mechanoreceptors detect extracellular mechanical changes, including different types of forces and stress, activating oncogenic signaling pathways that promote cancer initiation, growth, survival, angiogenesis, invasion, metastasis, and immune evasion (Mierke, 2024). Additionally, increased ECM stiffness and enhanced activation of mechanosensitive transcriptional regulators (transcription factors and cofactors) are strongly associated with resistance to anticancer drugs (Jahin et al., 2023).

1.1.2. The cell mechanotransduction machinery

Mechanotransduction is a highly coordinated process that involves several key cellular components, each playing a vital role in sensing and responding to mechanical stimuli. Integrins, which are transmembrane receptors, serve as a critical bridge between the extracellular matrix (ECM) and the cytoskeleton. By linking these two structures, integrins enable the transmission of mechanical forces from the ECM into the cell, triggering a cascade of intracellular signaling pathways. Once inside the cell, the cytoskeleton, composed of actin filaments, microtubules, and intermediate filaments, takes over. This dynamic structure acts as a network that distributes mechanical forces throughout the cell, with proteins like actin, myosin, and vinculin playing central roles in the process. At the molecular level. Focal Adhesion Kinase (FAK) is activated upon integrin engagement, further amplifying the mechanical signal. FAK is instrumental in regulating cellular adhesion, migration, and survival in

response to these mechanical stimuli (Di et al., 2023). Another crucial component is the YAP/TAZ transcriptional co-activators, which belong to the Hippo signaling pathway. Sensitive to changes in mechanical forces, YAP/TAZ translocate to the nucleus, where they influence gene expression, regulating important cellular behaviors such as proliferation, differentiation, and apoptosis. Interestingly, recent studies suggest that the nucleus itself can function as both a mechanosensor and mechanotransducer, responding to mechanical forces and potentially influencing nuclear processes (Kirby & Lammerding, 2018; Lammerding & Kirby, 2018). Nuclear responses to mechanical force can induce modification in chromatin structure and transcriptional dynamics, leading to alterations in cellular states (Hampoelz & Lecuit, 2011). These mechanically-driven modifications help maintain chromatin and nuclear integrity, preventing deformities in nuclear shape and preserving genome stability (Uhler & Shivashankar, 2017). It will very important elucidating the relationship between nuclear mechanics and gene expression regulation, as understanding these processes is crucial to fully comprehending how these processes guide cell fate during development (Alvarez & Smutny, 2022).
Of great relevance in mechanotransduction are the mechanically activated ion channels, which open or close in response to mechanical forces, allowing ions to flow into or out of the cell. As illustrated in ***Figure 1.2***, mechanosensitive channels form pores in the cellular plasma membrane and their probability of opening increases in response to mechanical forces. When these channels open, ions move passively through the pore, driven by their electrochemical gradients. The ion flow generates a current across the membrane. These channels often exhibit selectivity for specific ions, and the direction of the current (inward or outward) is determined by both the electrochemical gradient and the specific ion that the channel permits to pass through (Martinac & Poole, 2018). Together, these components form a complex and finely tuned system that ensures cells can sense, adapt to, and respond to the mechanical properties of their environment.

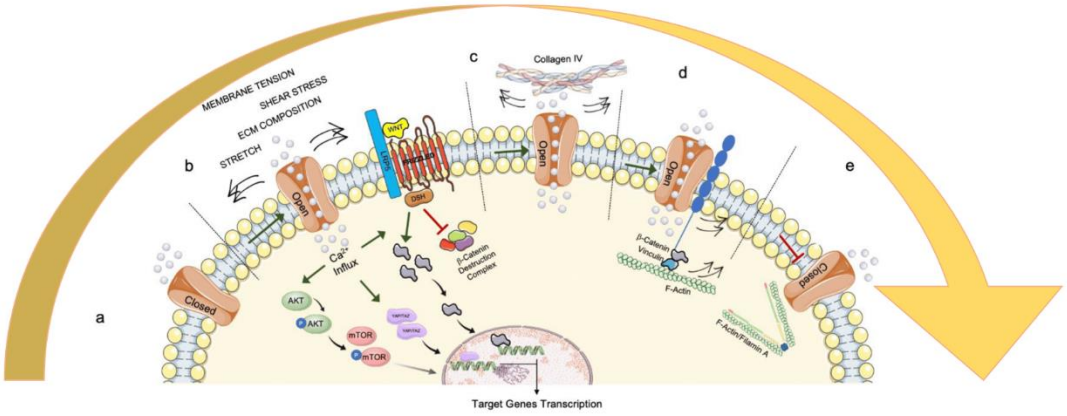

Figure 1.2 **Scheme illustrating Piezo mechanosensitive ion channel regulation and interplay with some of key players involved in cellular mechanotransduction**. **(a)** Resting state: in absence of mechanical stimuli, Piezo channels remain closed, blocking the passage of ions such as calcium (Ca^{2+}). No mechanical forces are acting on the lipid bilayer, and the channels stay in their inactive conformation. **(b)** Mechanotransduction activation: upon mechanical stimulation such as membrane tension, shear stress, or ECM composition changes Piezo channels open due to forces transmitted through the lipid bilayer. This allows an influx of Ca^{2+} ions, which triggers downstream signaling pathways like AKT/mTOR**,** WNT/β-Catenin, and YAP/TAZ**,** leading to transcription of target genes that regulate cell behavior (Pathak et al., 2014; Qin et al., 2021; Sforna et al., 2022) **(c)** Collagen IV influence: the ECM component Collagen IV can induce Piezo channel opening. The mechanical presence of collagen directly influences Piezo activation, facilitating the mechanical signal transduction process.(Gaub & Müller, 2017) **(d)** Piezo interaction with E-Cadherin/β-Catenin/F-Actin complex: Piezo associates with the E-Cadherin/β-Catenin/F-Actin complex, which generates intracellular forces that promote the opening of the channel. (J. Wang et al., 2022). **(e)** Desensitization by Filamin A: Filamin A, an actin-binding protein, interacts with Piezo channels to desensitize them, inhibiting further activation (Retailleau et al., 2015).
Image adapted from (Tortorella & , Chiara Argentati , Carla Emiliani, Francesco Morena, 2022)

1.2. The identification of mechanically activated ion channels

The concept of mechanically activated ion channels was first introduced in 1950 by Bernard Katz, from studies of specialized mechanosensory neurons, and later revisited by Georg von Békésy, highlighting the idea that ion channels could be activated by mechanical forces (Martinac, 2004). This theory obtained substantial support in 1979 when Hudspeth and Corey demonstrated the direct activation of ion channels by mechanical stimuli, showing rapid current responses to physical inputs (D. P. Corey & Hudspeth, 1979). In 1984, stretch-activated ionic currents were recorded also in chick skeletal muscle cells, providing further evidence of mechanosensitive ion channels (Guharay & Sachs, 1984).

Later, the first mechanosensitive channel (MC) to be cloned was the bacterial MscL channel, known for its role in releasing osmotic pressure in cells (Sukharev et al., 1994). Although prokaryotic MS channels have been identified and studied for over 25 years (Martinac et al., 1990), the molecular identities of MS cation channels in mammals have remained unknown.

In 2010 Árnadóttir and Chalfie (Árnadóttir & Chalfie, 2010) proposed several criteria to define a mechanosensitive channel:

- **Expression in mechanosensory organs**: MS channels must be located in organs specifically responsible for mechanosensory functions.
- **Loss of function**: Removing the MS channels from sensory cells should result in the loss of the mechanical response, with no indirect effects due to developmental issues.
- **Response to mutagenesis**: Altering the physical properties of these channels (e.g., through mutagenesis) should directly change the mechanical response.
- **Activation by force**: Heterologously expressed MS channels must still be activated by mechanical force when placed in different contexts (i.e., in systems other than the native environment).

In same years, the Patapoutian's group discover in mammals a family of mechanically activated protein, which they named PIEZO, derived from the ancient Greek word for *pressure*. In 2010 they identified the gene encoding the PIEZOl ion channel by combining microarray analyses with RNA interference (RNAi) techniques: targeting over 50 genes. The PIEZO1 channel was discovered through electrophysiology experiments in which pressure was applied to cells, revealing its activation in response to mechanical stimuli. Following this, they identified a second homologous protein, PIEZO2, which shares similar mechanosensitive properties (Coste et al., 2010).
Together with PIEZOs, several members of the Transient Receptor Potential (TRP) ion channel family were suggested to be mechanosensitive. Among them, in particular, TRPV4 shows a weak response to membrane stretch (Strotmann et al., 2000) and no response to cellular indentation (Servin-Vences et al., 2017). In addition, TRPV4 is activated when mechanical stimuli are applied through deflections at cell-substrate contact points (Servin-Vences et al., 2017). However, despite its involvement in various mechanosensory processes, there are no clear evidences that TRPV4 is directly activated by mechanical stimuli (Martinac 2018, White et al., 2016).

1.2.1 PIEZO channels

PIEZO proteins, encoded by the PIEZO1/FAM38A and PIEZO2/FAM38B genes, are approximately 2500 and 2800 amino acids long, respectively, and share approximately 42% sequence identity (Qin et al., 2021). Furthermore, PIEZO channels are found in both vertebrates and invertebrates, plants, and protozoa, but not in yeast and bacteria (J. Wang et al., 2022). They are non-selective channel permeable to Na^+, K^+, Ca^{2+}, Mg^{2+}, with a preference for Ca^{2+} (Coste et al., 2010).
Following their identification, it has been increasingly demonstrated that the PIEZOs play critical roles in various mechanotransduction processes (Ranade, Woo, et al., 2014), including mechanical

nociception (S. E. Kim et al., 2012), gentle touch (Anderson et al., 2017; Faucherre et al., 2014; Ikeda et al., 2014; Ranade, Woo, et al., 2014), proprioception (S.-H. Woo et al., 2015), vascular development and function, and red blood cell volume regulation (Cahalan et al., 2015; Faucherre et al., 2014).

1.2.2 The expression of PIEZOs in cells and tissues

PIEZO channels are widely expressed across various organs and tissues, with distinct distribution patterns reflecting their roles in mechanosensation. PIEZO1 channels are mainly found in bladder urothelial cells (Beča et al., 2021), erythrocytes (Faucherre et al., 2014), vascular endothelial cells (Friedrich et al., 2019), and chondrocytes (Brylka et al., 2024), playing a key role in mechanosensitivity in non-excitable tissues exposed to fluid pressure and flow, such as the kidneys, red blood cells, lung capillaries cells and skeletal muscles (***Figure 1.3***) (Mirzoev, 2023; Miyamoto et al., 2014; Peyronnet et al., 2013; Ranade, Qiu, et al., 2014; Vaisey et al., 2022).

In contrast, PIEZO2 is highly expressed in sensory tissues, particularly in dorsal root ganglia (DRG) sensory neurons (Coste et al., 2010), Merkel cells (S. H. Woo et al., 2014), and muscle spindles (S.-H. Woo et al., 2015), the sensory nerve endings that innervate skeletal muscles, and are essential for proprioception (Nagel & Chesler, 2022) and bladder control (Coste et al., 2010; Marshall et al., 2020). Furthermore, PIEZO2 is found in vagal sensory neurons innervating the airway, where it mediates the autonomic reflex of lung inflation-induced apnea (***Figure 1.3***) (Nonomura et al., 2017).

The differential physiological expression of PIEZO channels reflects their different sensitivity to stresses. PIEZO 1 activity is mainly identified in region where the cell exerts higher traction forces whereas PIEZO2 is important for sensation of airway dilatation, fine touch and proprioception, low-threshold bladder-stretch and urethral micturition (Marshall et al., 2020).

In human, mutations of PIEZO1 or PIEZO2 genes result in altered channel functions, which are linked to a number of diseases (Albuisson et al., 2013; Cahalan et al., 2015; Coste et al., 2013; Fotiou et al., 2015; McMillin et al., 2014; Zarychanski et al., 2012). These studies have revealed that the PIEZO proteins are a physiologically and pathophysiologically important class of biological mechanotransducers.

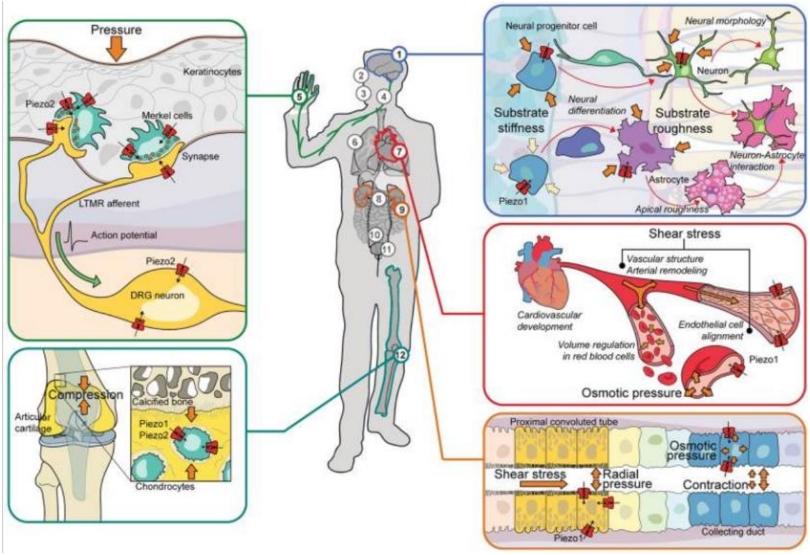

Figure 1.3 Distribution and functional roles of PIEZO channels in mechanosensation. PIEZO1 is predominantly expressed in non-sensory tissues, such as bladder urothelial cells, vascular endothelial cells, chondrocytes,lung capillaries cells, and erythrocytes, where it is responsible for detecting mechanical forces like fluid pressure and shear stress; PIEZO2 is localized in sensory tissues, including DRG neurons, Merkel cells, and muscle spindles, contributing to proprioception, touch sensation, and the autonomic regulation of airway dilation. (Wu et al., 2017)

1.2.3 Physiology and pathology of PIEZO1

Since PIEZO1 is expressed in several cell types, as was previously indicated, it is difficult to assign its significance to a single biological role. Its broad expression reflects its diverse functionality. A comprehensive overview of PIEZO1 role and function is summarized in ***Table 1***. PIEZO1 is essential in numerous mechanotransduction processes, including cardiovascular force sensing, immune regulation, epithelial homeostasis, red blood cell volume control, and bone formation (Zhang et al., 2024). In vascular endothelial cells, PIEZO1 plays a key role as a sensor of shear forces, contributing to the development and regulation of vascular architecture (Ranade, Qiu, et al., 2014). The critical importance of PIEZO1 signaling in the vasculature is emphasized by the fact that its deletion in endothelial cells results in embryonic lethality (Li et al., 2014).

Additionally, PIEZO1 is overexpressed in osteoblasts, where it plays a key role in regulating osteoclast differentiation and bone resorption by controlling the expression of type II and type IX collagen via the YAP signaling pathway. When PIEZO1 is deleted, the communication between osteoblasts and osteoclasts becomes disrupted, leading to an imbalance that results in rapid bone mass loss and increases the risk of spontaneous fractures (Xuehua Li et al., 2019; Lijun Wang et al., 2020). The critical role of PIEZO1 in the central nervous system (CNS) was first highlighted by Koser et al (Koser et al., 2016), who demonstrated that PIEZO1 exhibits a punctate distribution along the axons and growth cones of retinal ganglion cells (RGCs) in *Xenopus*. This study revealed an involvement of PIEZO1 in axonal growth and regeneration processes.

More recent studies have established that PIEZO1 channels are also localized within myelinated axonal tracts in the brains of mice and rats, notably in regions such as the *corpus callosum* and *cerebellar arbor vitae*, with substantial expression in CNS neurons, particularly those of the frontal cortex. This distribution pattern suggests potential therapeutic implications for demyelinating neurodegenerative diseases (Koser et al., 2016). In contrast, PIEZO1 expression is significantly lower in mature oligodendrocytes and astrocytes, underscoring its selective involvement in specific CNS cell types (Velasco-Estevez et al., 2020). Recent findings have demonstrated the presence of PIEZO1 and PIEZO2 channels in the trigeminal sensory neurons, highlighting their potential involvement in migraine-related mechanotransduction (Mikhailov et al., 2019).

***Table1*. PIEZO1 distribution and function (Du et al., 2024).**

Tissue	Cell	Mechanical stimulation	Function	Reference
Vascular system	Endothelium and smooth muscle cells, blood cell	FSS	Vascular development; blood pressure regulation; red blood cell volume regulation	Ranade et al. (2014), Retailleau et al. (2015), Wang et al. (2016), Gudipaty et al. (2017), Murthy et al. (2017), Wong et al. (2018), Beech and Kalli (2019)
Lymphatic system	Lymphatic endothelial cells	FSS	The development and maintenance of lymphatic valves	Nonomura et al. (2018), Choi et al. (2019)
Lung	Alveolar capillary endothelial cells	Alveolar pressure and hydrostatic pressure (HP)	Maintain lung function	Mammoto et al. (2022), Grannemann et al. (2023)
Nerve system	Retinal ganglion cells, neural stem cells	Stretch	Axon growth and regeneration, directs the differentiation of neural stem cells	Koser et al. (2016), Wu et al. (2017)
Gastric mucosa	G cells	Antrum distension	Regulate gastrin secretion	Lang et al. (2018)
Intestines	Intestinal epithelial	HP and shear force	Regulate epithelial function and permeability	Jiang Y. D. et al. (2021), He et al. (2023)
Bladder, and kidney	Bladder and kidney epithelial cells	Shear stress and wall tension	Sense bladder distension and urinary osmolarity, concentrate urine	Michishita et al. (2016), Dalghi et al. (2019)
Tooth	Odontoblasts, dental pulp stem cells (DPSC), Oral squamous cell (OSC)	Intrapulpal pressure changes, extracellular matrix stiffness	Regulate DPSC and OSC proliferation, pulpitis attack and dentin mineralization	Gao et al. 2017, Sato et al. (2018), Hasegawa et al. (2021), Matsunaga et al. (2021)
Cartilage	Chondrocytes	Osmotic stress	Cartilage mechanotransduction	Lee et al. (2014)

1.3 The somatosensory system

In human, the somatosensory system is responsible for detecting stimuli, such as touch, vibration, light, pressure, skin tension, as well as painful stimuli, proprioception, stereoception and temperature. The sensory information originates as neural activity from the stimulation of receptor cells located in specific parts of the body. We can distinguish different types of sensations because the functional differences between sensory systems arise from the various types of stimulus energy that drive them and the distinct pathways each system follows (Kandel, Schwartz, & Jessell, 1991). The functional units responsible for transducing and encoding mechanical stimuli into electrical signals are the dorsal root ganglion (DRG) neurons. Through this process, DRG neurons play a key role in converting mechanical inputs, such as touch and pressure, into signals that can be processed by the nervous

system (Viatchenko-Karpinski & Gu, 2016). These cells provide humans and other animals the ability to recognize the internal and external forces acting on the body, the shapes and textures of objects. DRG are pseudo-unipolar neurons having a cell body (*soma*) with a single axon that bifurcates into two extensions (***Fig. 1.4***). While one axon projects from the soma to the periphery innervating the skin, joint and muscles, the other branch extends from the soma to the spinal cord (Abd-Elsayed et al., 2024). For this reason, they are called peripheral and central branches, respectively.

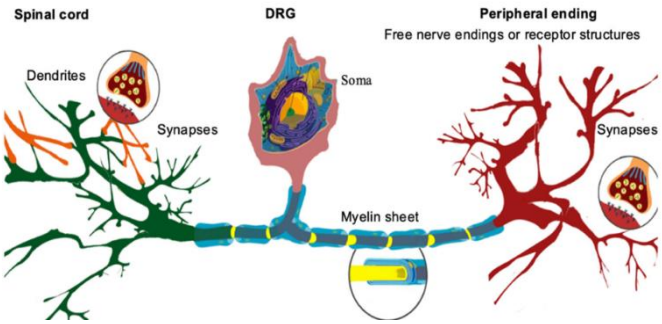

***Figure 1.4* Schematic representation of DRG neurons.** The axon (*yellow*) extends briefly from the soma (*pink*) before branching into two distinct pathways. The peripheral branch leads to free nerve endings or specialized receptor structures such as Merkel cells, Ruffini endings, Meissner's corpuscles, or Pacinian corpuscles in the skin, or innervates peripheral organs, muscles, and joints. The central branch, on the other hand, carries these sensory signals toward the spinal cord. Schwann cells (depicted in *turquoise*) may envelop the axon, forming the protective myelin sheath. Image from (Koll et al., 2020).

1.3.1 PIEZO 2 in mechanosensory system

A key player in the mechanosensory process is the PIEZO2 channel, which is widely expressed in DRG neurons. PIEZO2 has been found to be responsible for light touch and proprioception (Coste et al., 2010). Mice lacking PIEZO2 lost the ability to perceive gentle touch(Ranade, Woo, et al., 2014), while attenuing thermal and pain sensations (Murthy et al., 2018). For this reason, PIEZO2 represents a potential target for treating allodynia, a condition in which a person experiences pain from stimuli that are typically not painful. In the urinary system, innervated by the DRG neurons, PIEZO2 channels are the main traducers of shear stress stimuli and bladder stretching. An interesting paper by Marshall et al. describes the role of PIEZO2 in the bladder urothelium and its innervation by sensory neurons, correlating data from both mice and humans. In case of impaired bladder control, similar effects are observed in humans and mice (Marshall et al., 2020). Additionally, patients have reported difficulty in sensing bladder fullness, indicating that PIEZO2 is essential for low-threshold bladder stretch sensitivity (Xu Li et al., 2022). Additional studies on mouse proprioceptive neurons, which are responsible for the sense of body position in space, have shown that mice lacking PIEZO2 exhibit impaired coordination, frequently stumbling while walking (Florez-Paz et al., 2016). In the respiratory system, PIEZO2 is involved in various functions. In sensory neurons derived from the neural crest of neonatal mice, PIEZO2 is essential for lung expansion. In contrast, in nodose sensory

neurons of adult mice, PIEZO2 is necessary for regulating lung volume (Nonomura et al., 2017). So far, there has been no parallel comparison of lung physiology involving PIEZO2 between mice and human patients. Much work remains to be done to understand the direct or indirect dysfunctions involving PIEZO2 in humans.

1.3.2 Clinical relevance of PIEZO2

Clinical studies on humans have shown that structural mutations or absence of PIEZO channels are linked to a significant decrease in the sense of touch and vibration and, did not develop allodynia (Szczot et al., 2018). Similarly, mutations of PIEZO2 in humans have been associated with deficits in vibration perception and proprioception, leading to impaired awareness of body position and movement (Rezaei & Saghazadeh, 2017). These findings from translational studies reinforce the role of PIEZO2 as a key molecular target for developing therapeutic approaches to treat proprioceptive and somatosensory disorders. Targeting PIEZO2 may offer novel strategies for conditions where mechanosensory dysfunction plays a central role, potentially improving quality of life for affected individuals. Moreover, in humans, gene mutations of the PIEZO2 channel have been linked to additional disorders. For example, gain-of-function mutations in PIEZO2 result in dominant distal arthrogryposis, a condition marked by joint contractures that limit mobility in the hands and feet, and Marden-Walker syndrome, that is a rare defect in embryonic development characterized by multiple joint contractures (Coste et al., 2013). Although these disorders were discovered years ago, only recently, with the identification of PIEZO channels, has it been possible to achieve a comprehensive understanding and reconfirm the importance of the proper functionality of mechanosensitive ion channels. Beyond these specific genetic disorders, PIEZO2 channels are found to have an important role in cancer development and metastasis formation. For instance, PIEZO2 can have a substantial role in aggressive phenotypes of breast cancer (Katsuta et al., 2022). Yang et al have identified PIEZO2 as a novel regulator of tumor angiogenesis and hyperpermeability (Yang et al., 2016). Their *in vitro* studies revealed that knocking down PIEZO2 in endothelial cells suppressed cell proliferation, migration, and invasion of glioma tumor cells.

1.4 Form and function of PIEZO channels

Structurally, PIEZOs have a unique propeller-like shape with a central pore and three curved blades that extend outward in the membrane. This distinctive form allows them to detect changes in membrane tension and curvature. When mechanical stress, such as stretching or pressure, deforms the membrane, the blades flatten, causing the central pore to open. This gating mechanism enables

the rapid influx of cations, such as calcium and sodium, that triggers downstream signaling events. In the following paragraphs, structure features and gating mechanisms will be discussed in details.

1.4.1 PIEZOs structure

PIEZO channels have the largest known ion channel subunits, composed of over 2.500 amino acid residues and bearing no known homology to other cationic ion channels (Jin et al., 2020). Our understanding of the structure-function relationship of PIEZO channel complexes has been greatly enhanced by the determination of their cryo-electron microscopy (cryo-EM) structures, including those of PIEZO1 (Ge et al., 2015; Saotome et al., 2018) and PIEZO2 (Li Wang et al., 2019). These studies revealed key structural features likely involved in their mechanical gating mechanism (Guo & MacKinnon, 2017; Saotome et al., 2016; Zhao et al., 2018). Interestingly, the structure of PIEZO2 was successfully determined, revealing its axial height of 170 Å and a diameter of 280 Å (Zhao et al., 2018). Despite sharing only about 42% sequence homology, PIEZO1 and PIEZO2 exhibit similar structural architectures (Jin et al., 2020).

Their structure is highly distinctive with its homotrimeric complex ***(Fig. 1.5a)*** characterized by four main features (Fang et al., 2021; Tadge et al., 2024) :

- **Three peripherals blades**, known also as arms, that form the large N-terminal region and play an important role as mechanotransduction modules. Each arm consists of nine transmembrane helical units (THUs), with each unit containing four transmembrane segments (TMs), resulting in a total of 36 TMs, plus two additional independent TMs near the pore region, giving the channel its distinctive propeller-like structure (***Fig. 1.5b***).
- **Central ion-conducting pore** formed by the C-terminal region containing the last two TMs.
- **Three intracellular long beams** that connect each arm to the central ion-conducting pore;
- **Extracellular cap domain** located at the top of the central axis.

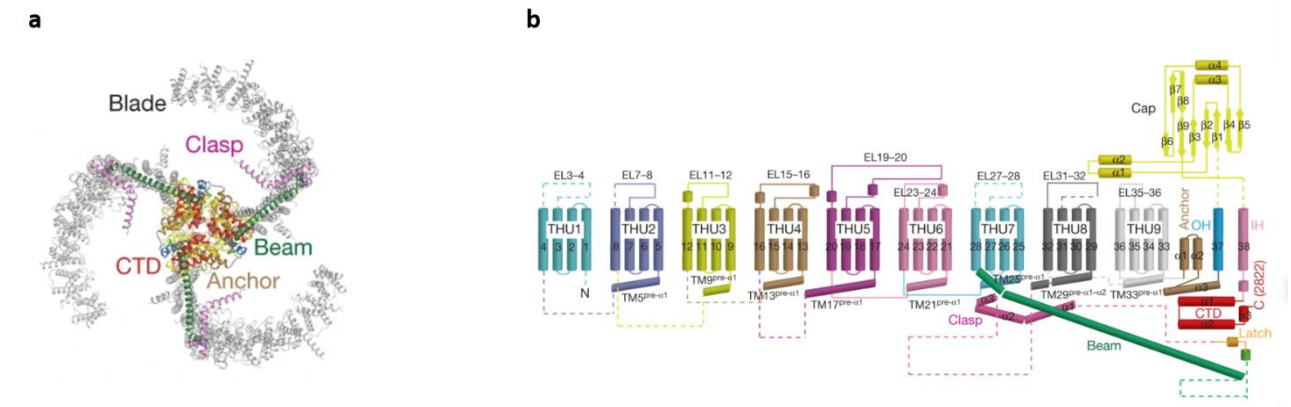

***Figure 1.5* Homotrimeric structure of PIEZO. a)** Cartoon models *r*epresentation of PIEZO's homotrimeric structure with key structural components highlighted, including blades, clasps, beams, anchors, and the C-terminal domain (CTD). **(b)** Schematic of the 38-transmembrane segments (TMs) topology, demonstrating a single "blade" made up of nine transmembrane helical units (THUs), each containing four transmembrane segments (TMs). This leads to a total of 36 TMs in the structure, with two additional TMs near the central pore region. Image adapted from (Li Wang et al., 2019).

Taking into account the PIEZO structural features, a *membrane dome mechanism* has been proposed to explain how PIEZO channels opening in response to mechanical stimuli (Guo & MacKinnon, 2017; Lin et al., 2019) (***Fig. 1.6***). Briefly, PIEZO channels in their closed conformation are proposed to adopt a *dome-like shape*, which serves as a potential energy source for gating. Under membrane tension, the lateral membrane stress flattens the PIEZO dome, increasing the system's energy in proportion to the expansion of the dome's projected area. The opening of the channel is therefore driven by the relative energy difference. This mechanism explains the high sensitivity of PIEZO channels' mechanical gating, which features a cation-selective pore. Although this dome mechanism explains their mechanosensitivity, it does not account for the influence of the surrounding membrane (Fang et al., 2021). Haselwandter et al. proposed the *membrane footprint* hypothesis, which suggests that the PIEZO channel deforms the membrane beyond the channel perimeter, creating a curved footprint that enhances its sensitivity to changes in membrane tension (Haselwandter & Mackinnon, 2018). However, more experiments are needed to shed light and refine this hypothesis.

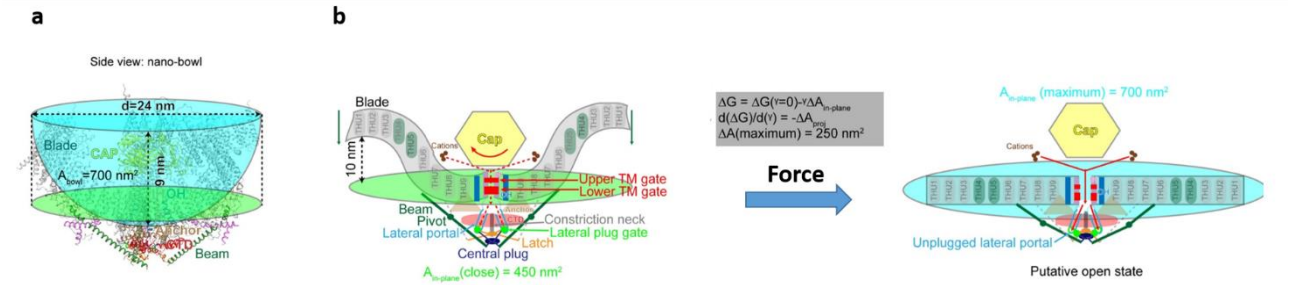

Figure 1.6 **The dome-shaped conformation of PIEZO channels.**
(a) the transmembrane regions of the three blades bend into a dome-like structure, with a mid-plane opening diameter of approximately 24 nm and a depth of 9 nm. The dome in its closed conformation has a surface area of 700 nm² (*blue*), with an in-plane projected area of around 450 nm² (*green*). (**b**) Upon membrane tension the nano-bowl will open reaching a maximal in-plane membrane area of 700 nm². In the *grey* box tension (γ)-induced free energy change upon transition from closed to open: the difference of approximately 250 nm² between these two areas is believed to store potential energy for channel gating. The free energy change (ΔG) required for opening is proportional to the area difference (ΔA) between the closed and open states, which helps explain the channel's mechanosensitivity. Image adapted from (Jiang et al., 2021).

Despite their homology, PIEZO2 differs from PIEZO1 in several key aspects. PIEZO2 follows the "positive-inside" rule for membrane proteins, with TM1-TM38 forming a hydrophobic belt (Al-Lazikani et al., 2008). Notably, the hydrophobic belt created by the distal transmembrane helices of one subunit is positioned significantly above the belt formed by the proximal transmembrane helices of the adjacent subunit.

Furthermore, in opposed to PIEZO1, PIEZO2 inner helix (IH) exhibit two transmembrane constriction sites (F2754, L2743, and E2757) at the pore level, creating a narrowing. These two sites suggest that they function as lower and upper transmembrane gates, governed by the upward and clockwise rotation of the cap (Li Wang et al., 2019). Additionally, lateral portals within the central pores of PIEZO1 and PIEZO2 influence ion permeability, suggesting their potential role in the ion conduction pathway of PIEZO2 (Xu Li et al., 2022; Li Wang et al., 2019).

1.4.2 Pharmacological modulator of PIEZO channels

Small molecules, named Jedi1/2 and Yoda1, have been identified as chemical activators of PIEZO1. These activators can open PIEZO1 ion channels in the absence of mechanical stimulation. Specifically, Jedi1/2 is a hydrophilic chemical activator of PIEZO1 that acts through the peripheral blades, utilizing a lever-like apparatus made of the blades and a beam to control the central ion-conducting pore (Y. Wang et al., 2018). In contrast, Yoda1 acts as a molecular wedge, inducing a

conformational changes that reduces the mechanical threshold required for channel activation (Botello-Smith et al., 2019) (***Fig. 1.7***).

Up to now, no specific chemical activators have been discovered for PIEZO2 and, the reason why PIEZO2 is not efficiently activated by Yoda1 remains unclear (Fang et al., 2021).

Likewise, specific inhibitors of PIEZOs have not been identified so far. However, as other mechanosensitive channels, they are inhibited by gadolinium, ruthenium red (Coste et al., 2012), and GsMTx4, a widely used toxin inhibitor for mechanosensitive channels (Bae et al., 2011). It is believed that GsMTx4 may not directly bind to PIEZO1 but instead exerts its effect by altering the local membrane tension around the channel (Suchyna et al., 2000, 2004). Moreover, Dooku1, a Yoda1 analogue lacking stimulatory effect, antagonizes Yoda1- induced activation of PIEZO1 and aortic relaxation (Evans et al., 2018).

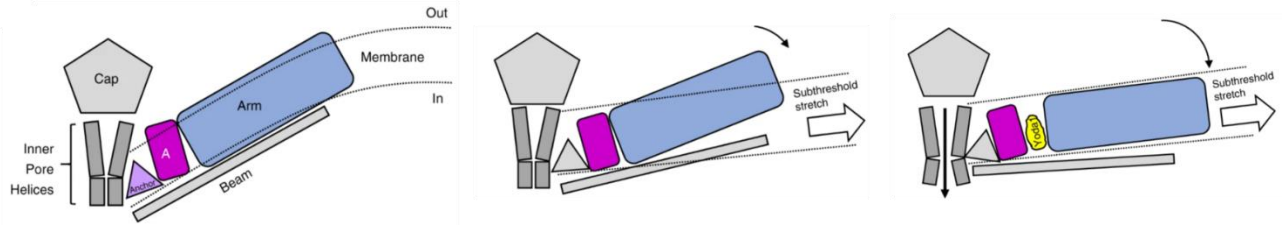

Figure 1.7 **Yoda's activation mechanism of PIEZO1.**
Yoda1 acts as a wedge by separating the first THU (*magenta*) from the adjacent N-terminal arm (*blue*), enhancing the tension-induced extension of the arm and promoting channel opening in response to sub-threshold stimuli. Image adapted from (Botello-Smith et al., 2019).

1.4.3 Gating mechanisms of PIEZO Channels

PIEZO ion channels gate (open and close) in response to mechanical forces, allowing the nonselective flux of cations into the cell, and rapidly inactivate in response to prolonged stimuli (Young et al., 2022). As result they are specialized to transduce mechanical energy into electrochemical signals and mediating diverse mechanotransduction processes throughout the body (Coste et al., 2010; Saotome et al., 2018).

For PIEZO channels, the mechanical energy alone is s enough to lower the energy required for the channel to open. This means that mechanical energy can trigger the channel to switch between open and closed states, adjusting its likelihood of being open, which is known as "open probability".

Whereas, charge movement across the membrane, ligand binding, and temperature can lead to only minimal modulation of PIEZO channel opening. In principle, mechanically derived energy can originate from various sources, which are not necessarily independent, and can act in concert to facilitate PIEZO activation (Haswell et al., 2011; Young et al., 2022).

To describe the gating of PIEZO channels, two widely accepted mechanisms have been proposed: the *force-from-lipids* (Kung, 2005; Martinac et al., 1990) and the *force-from-filament* (Chalfie, 2009; Katta et al., 2015) (***Fig.1.8***).

In the *force -from-lipids*, the channel gating is thought to be influenced directly by the surrounding lipid bilayer of the cell membrane (***Fig.1.8a***). The PIEZO channels are embedded in the membrane, and mechanical tension or deformation of the membrane can lead to a change in the channel's conformation. When the membrane is stretched, it exerts force on the channel, causing it to open and allowing ions to flow through. This model suggests that the mechanical force exerted by the lipid bilayer itself is sufficient to gate the channel without requiring additional structures.

Some researchers reconstituted mouse PIEZO1 in lipid bilayers and showed that an approximate tension of 3.4 mN/m is required to open the channel (C. D. Cox et al., 2017; Murthy et al., 2017; Syeda et al., 2016). PIEZO activity is significantly influenced by the membrane structure and organizzation. The function of the PIEZOs channels has been shown to be significantly impacted by the absence of STOML3 protein, a protein implicated in cholesterol recall (Y. Qi and others, 2015). Furthermore, Ridone et al. demonstrated that PIEZO1 function is directly influenced by the composition of the membrane and the lateral arrangement of cholesterol domains, coordinating the activity of PIEZO1 channel clusters (Ridone et al., 2020). Their results confirmed that both chemical composition of the membrane and the organization of cholesterol domains within it, directly impact PIEZO1 function (Beverley & Levitan, 2024).

The *force-from-filament* proposes that PIEZO channels are gated by mechanical forces transmitted through cytoskeletal elements, such as actin filaments or microtubules, that are physically connected to the channel (***Fig.1.8b***). In this model, mechanical stimuli such as cellular deformation or movement are transmitted to the PIEZO channels through these cytoskeletal structures, which pull on the channels and induce their opening. The force applied by these filaments could either directly pull on the channel or indirectly alter the tension in the surrounding membrane, leading to channel gating.

However, little is known about their activation by mechanical stimuli originating from within the cell. In this regard, a study of Pathak et al (Pathak et al., 2014) support the theory of PIEZO1 gating by forces from cytoskeletal proteins. In detail, they showed that the inhibition of myosin II-associated traction forces suppressed the spontaneous Ca^{2+} transients mediated by PIEZO1, demonstrating that gating of PIEZO1 by traction forces of the cell changes as function of substrate stiffness.

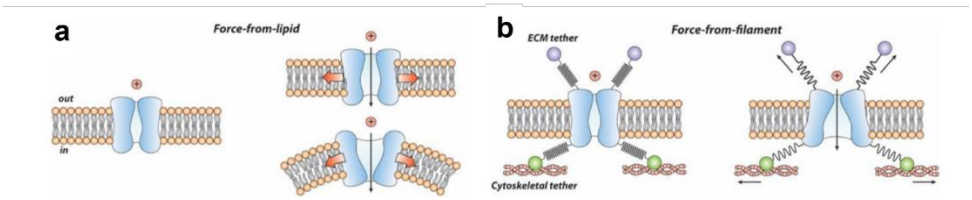

Figure 1.8 **Schematic representation of *Force from lipid* and *Force from filament* mechanism**.
The two generally accepted gating mechanisms based (**a**) on the cell membrane (**b**) or on ECM to cytoskeleton interaction that convey activation force directly to the channels Piezo1. Image adapted from (Ridone et al., 2019).

However, these two mechanisms are likely not mutually exclusive, and PIEZO channels may be gated by a combination of both lipid and filament forces, depending on the cellular context. A recent hypothesis predicts potential spatial and functional cooperativity for the gating of these channels (Young et al., 2022)

Moreover, we have also to consider that under physiological conditions, although thermal energy, voltage, and ligands do directly not activate PIEZOs, they can be important modulators. The local environment can also serve as a significant source of functional modulation and heterogeneity (Young et al., 2022).

CHAPTER 2

Innovative experimental approaches to study mechanosensitive channels

2.1 Tools to study Mechanosensitive Channels activation

A major issue remains: how do mechanosensitive channels sense and transduce mechanical forces into biochemical signals? To answer this question several approaches and methodologies have been developed to reproduce the various physiological forces to which mechanosensitive ion channels are subjected in various organs such as localized stimulus, shear flow, substrate deformation, ultrasound **(*Fig. 2.1*).** Characterizing the function of mechanically activated ion channels is important for understanding the underlying mechanisms of their gating and ion permeation.

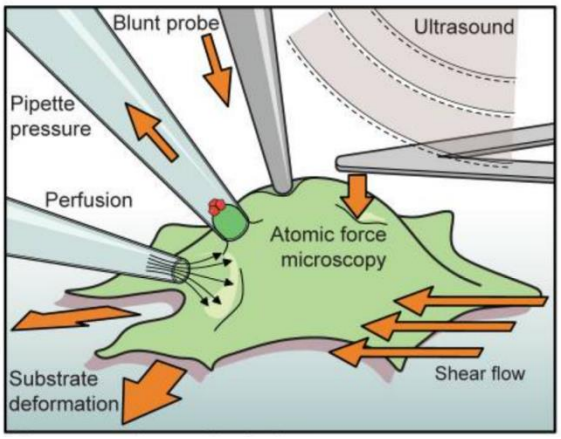

Figure 2.1 **Methods of cellular mechanical stimulation for activating mechanosensitive channels.** Illustration of various methods for cell mechanical stimulation for investigating activation of mechanosensitive channel**s**. Image adapted from (Wu et al., 2017)

Up to now patch-clamp electrophysiology, in combination with stretch and poke stimulation, is the main technique used to study the activation of mechanosensitive channels (***Fig. 2.2***). These approaches have been crucial for investigating the behavior of these channels by measuring ionic currents in response to mechanical stimuli. Although patch-clamp techniques yield valuable data, they lack precise control over the applied forces, they have limited spatial precision and they can disrupt the natural cellular environment, which restricts a deeper understanding of how channels detect and respond to mechanical forces.

To address these shortcomings, nanotechnological techniques such as Optical tweezers (OT), atomic force microscopy (AFM) and Fluid force microscopy (FluidFM) can provide more refined methods that instead can precisely control probe positioning and applied force (intensity and direction) on a single cell, by minimally perturbing cell integrity. This level of precision provides notable advances in studying how mechanosensitive channels activate in respond to a mechanical force applied locally on a cell.

Besides that, further nanotechnological approaches based on microfabrication or design of cell stretcher devices have been developed to uniformly stimulate not only single cell but also cell layer. Microfabrication can be used to shape the topography or change the stiffness of the substrate creating physical cues that enable to investigate how mechanical stimuli from the physical environment affect the behavior and activity of mechanosensitive channels (Bavi et al., 2019). On the other hand, cell stretcher devices can actively stretch the whole cell, or a a cell layer, in one direction or uniformly, thus simulating the physiological tension experienced in tissues, such as during muscle contraction, lung expansion or blood flow (O. Friedrich et al., 2019).

2.2 Electrophysiology

In electrophysiology the patch-clamp technique is considered the gold standard for studying ion channel behavior. It allows for the direct measurement of ion channel-mediated ionic flux across the membrane, either from isolated membrane patches (in cell-attached or excised modes) or through the whole-cell patch-clamp configuration. This enables detailed analysis of ion channel activity across different regions of the plasma membrane. The specific membrane area accessed in each configuration is illustrated in ***Figure 2.2***. The cell is approached with a glass pipette containing an internal solution and a recording electrode ***(Fig. 2.2a)***. By applying a small amount of negative pressure, a tight seal is formed between the cell membrane and the pipette to form a cell-attached patch. The intracellular and extracellular spaces are labelled as IC and EC respectively. Depending on the purpose of the experiment, the cell-attached configuration can allow for the measurement of ion flow through channels occurring across the patch of membrane contained within the pipette (***Fig. 2.2b*** shown in purple). Otherwise, the formation of the membrane seal represents the first step in achieving other patch configurations. By applying a further negative pressure through the patch pipette, the patch of membrane can be breached while maintaining the membrane seal to achieve a whole-cell patch (***Fig 2.2c***). This configuration causes the internal solution of the pipette to become continuous with the intracellular volume of the cell and permits the measurement of ion flow occurring across the entirety of the cell membrane. The remaining two configurations shown: inside-out (***Fig. 2.2d***) and outside-out (***Fig. 2.2e***) are referred to as excised patches as they remove the patch of membrane from the cell. In these latter cases, channel activity across only a small patch of

membrane is measured. The inside-out patch is formed from a cell-attached patch by gently lifting the pipette away from the cell to detach the small patch of membrane free. In this configuration, the inner-side of the membrane is exposed to the bath solution. An outside-out patch is realized by first forming a whole-cell patch and then carefully raising the pipette from the cell to detach the patch of membrane into two segments to either side of the seal which then reform such that the outer side of the membrane is exposed to the bath solution (Richardson et al., 2022).

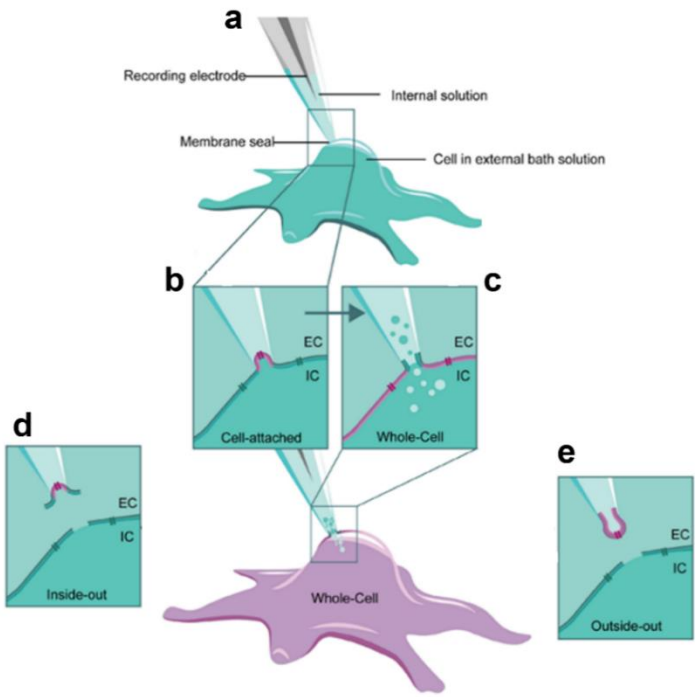

Figure 2.2 **Scheme of patch-clamp in different configurations. (a)** Formation of sealing (**b.c**) for whole cell measurements; (**d,e**) and excision of membrane patch for single channels measurements . In enlarged diagrams, the intracellular and extracellular spaces are indicated by the labels IC and EC, respectively. Image modified from (Richardson et al., 2022)

Patch-clamp in *stretch* and *poke* configuration have been crucial in understanding the ion selectivity of mechanosensitive channels. These approaches have demonstrated that PIEZO channels are cation-selective channels, with a slight preference for Ca^{2+} over other monovalent cations (Coste et al., 2010).

Poke (indentation) configuration (***Fig. 2.3a***) is specifically designed to study how mechanosensitive ion channels respond to localized mechanical forces. In this setup, a glass pipette is used to form a tight seal with the cell membrane, afterward a mechanical force is applied by "poking" or indenting the membrane using an external probe, often using a piezoelectric-driven blunt glass pipette and the patch-clamp setup is used to measure the ionic currents through these channels in real-time. As a consequence, the channels open or close in response to the applied force. In this configuration,

indentation depth can vary and it is difficult to evaluate the membrane tension and number of channels that are activated (Wu et al., 2017). For instance indentation depth can be 5 µm on the soma or 500 nm on the neurites.

In s*tretch* configuration (***Fig. 2.3b***), the first step involves isolating a small patch of membrane by using a fine-tipped glass pipette. The pipette forms a tight, high-resistance seal with the membrane, which ensures that the ionic currents from the mechanosensitive channels within the patch can be accurately measured. Once the patch is formed, mechanical stretch is applied to the membrane. This is typically done applying a negative pressure through the pipette, which stretches the membrane patch inward. This approach simulates mechanical tension on the membrane, mimicking conditions where the cell membrane would stretch in response to forces. Parallel imaging techniques allow for the observation that 'stretch' leads to a global curvature of the membrane. By measuring the curvature (patch radius) and applied pressure, membrane tension can be derived through the application of Laplace's law (Charles D. Cox et al., 2016; Lewis & Grandl, 2015).

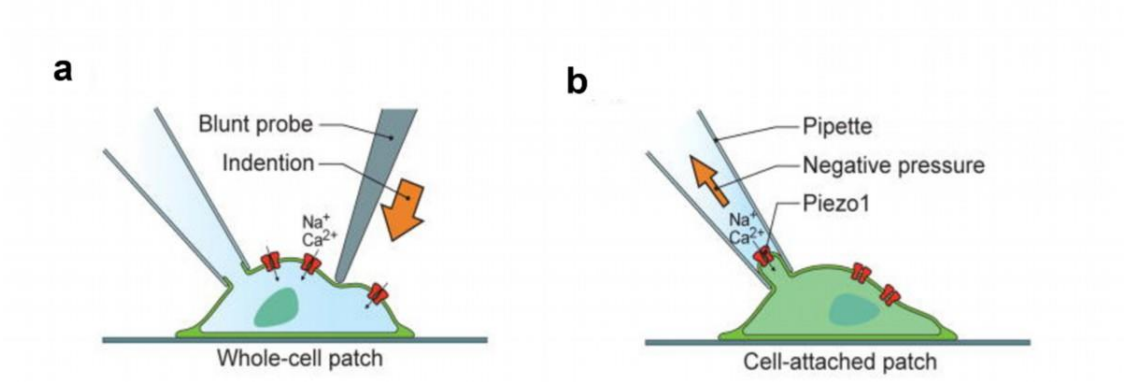

Figure 2.3 **Schematic representation of the *poke* and *stretch* configuration**. (**a**) In *poke* setup a blunt probe (typically a fire-polished glass pipette) mechanically indents the cell, applying a mechanical stimulus. Simultaneously, a glass pipette is used to form a tight seal with the cell membrane; (**b**) In *stretch* configuration, a negative pressure (suction) is applied to a patch of the cell membrane using a glass pipette, activating mechanosensitive ion channels. Image adapted from (Wu et al., 2017)

In both *poking* and *stretching* configurations of patch-clamp experiments, the application of suction or large indentations can potentially compromise cell integrity. For instance, during the aspiration process, the membrane and underlying structures, such as the cytoskeleton, may be mechanically disrupted. This can modify the normal interactions between the cytoskeleton and mechanosensitive ion channels, which can play an important role in how these channels respond to mechanical stimuli. Additionally, large deformations of the membrane during stretching or poking may exceed the physiological range of mechanical stimuli, leading to abnormal channels activation or even irreversible damage to the membrane. Moreover, during poking a double mechanical stimulus is actually applied: the suction to establish the patch-clamp and the indentation. As a result, the

measured responses may be impacted by the set-up configuration, making it difficult to determine the mechanical stimulus to which the channels are responding.

2.3. Optical tweezers

Optical tweezers (OTs) is a biophysical method widely used in the manipulation of the single molecule (Bustamante et al., 2021) which offers also significant advantages as a method for localized mechanical stimulation due to their high precision and non-invasive nature.

The technique uses a focused laser beams to trap and manipulate microscopic particles with nanometer-level accuracy. OTs operate by focusing a laser beam through a high numerical aperture objective onto a dielectric micro-particle. The radiation pressure generates forces, with the dominant component acting along the electric field gradient, which traps the particle at the focal point. The optical trap behaves like a linear Hooke's spring, allowing precise manipulation of the particle by adjusting the focus. OTs can be used for nanoindentation measurements (***Fig. 2.4a***), where force-indentation curves are generated and fitted to the Hertz model to calculate the Young's Modulus. It is also employed to globally stretch cells and study their elastic and viscoelastic properties (***Fig. 2.4b***). The two primary configurations are single- and dual-trap systems. Another important application of this technique is active microrheology (***Fig. 2.4c***), where OTs induce the displacement of beads injected into cells, allowing for the measurement of the shear modulus (G) by applying external forces.

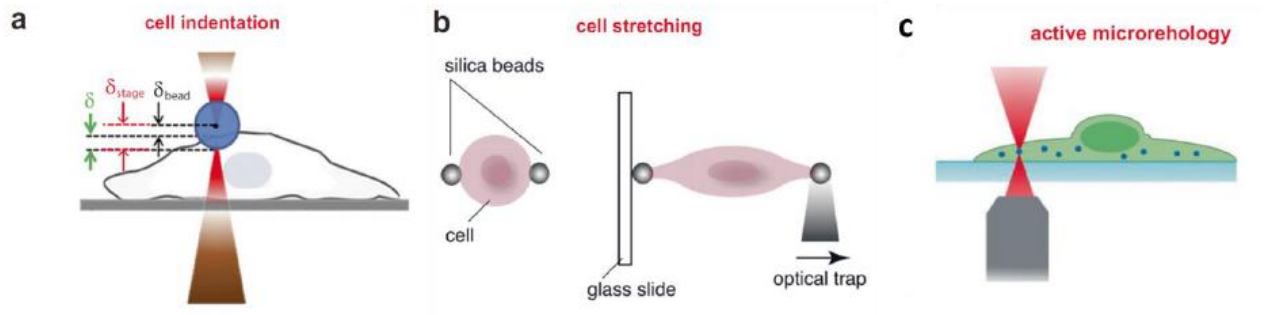

Figure 2.4 **Different operational modes of the OTs**. (**a**) cell indentation in which the stage is displaced upward by δ_{stage}, enabling interaction between the cell and the bead. The bead is moved by a δ_{bead} while it is indenting the cell by $\delta = \delta_{stage} - \delta_{bead}$. (**b**) cell stretching through an anchored bead and an optical trapped movable bead, (**c**) beads moved by OTs that is incorporated inside the cell. Image adapted from (Arbore, 2019)

Optical trapping is particularly effective for applying forces in the range of 0.1 to 100 pN (Sun et al., 2022). Given the variety and wide range of forces to which cells are subjected into the tissue, determining the threshold of mechanosensitivity—the minimum force required to activate mechanosensitive ion channels—is relevant for understanding how cells detect and respond to mechanical cues. OTs mechanical stimulation, in combination with calcium imaging, have shown that low applied forces (20 pN) can elicit localized calcium response in some kind of cells (Falleroni et al., 2022).

2.4. Atomic Force Microscopy

Since its invention in 1986, AFM has been widely applied across various fields, with growing emphasis on biological applications (Binnig et al., 1986). A significant advantage of AFM in this area is its ability to operate under physiological conditions, allowing researchers to explore the biophysical properties of cells in ways that are directly relevant to biological processes.

The working principle of AFM involves a probe, typically conical or pyramidal in shape, with a curvature radius ranging from a few nanometers for sharper tips to as much as 50 nm. This probe is located at the end of a flexible cantilever made of silicon or silicon nitride. Forces exerted between the probe and the sample surface cause slight bending of the cantilever, which is detected by a position-sensitive detector, which measures the deflection of a laser beam focused on the backside of the cantilever (***Fig. 2.5***). The force exerted during cantilever deflection can be measured with piconewton (pN) sensitivity by applying Hooke's law: F=kd, where (*F*) is the force, (*k*) is the spring constant of the cantilever, and (*d*) is the displacement measured by the laser on the photodetector. By multiplying the laser displacement by the cantilever's spring constant, we obtain the force values acting between the AFM tip and the sample.

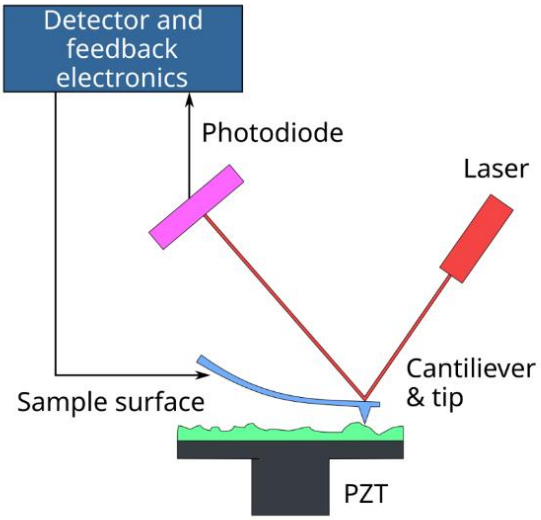

Figure 2.5 **Sketch of AFM.** Cantilever deflection detected by the laser beam that bounces back on the photodiode while the tip moves in x,y and z directions. Image adapted from Wikipedia.org

2.4.1 Imaging

In imaging mode, the cantilever scans the sample in three dimensions (*x*, *y*, *z*) using a computer-controlled piezo actuator, providing topography images with lateral and vertical resolution of <1 nm and <0.1 nm, respectively (Dufrêne et al., 2017). AFM can operate in different imaging modes based on the distance between the AFM tip and the sample, as various forces dominate the interaction at different distances (***Fig. 2.7***). In *non-contact mode*, the tip scans the sample in the long-range attractive forces such as Van der Waals interactions are the primary influence. As the tip moves closer, the force-distance curve shifts, and *contact mode* is activated, where short-range repulsive forces, mainly Coulomb interactions, dominate. An intermediate mode, known as *intermittent or tapping mode*, bridges the gap between these two approaches, enabling the application of a broader range of forces and providing more gentle imaging approach.

The choice of imaging mode depends on several factors, such as the sample's nature, environmental conditions, and the specific biophysical properties being studied. Traditional imaging modes can be challenging to apply to very soft or loosely immobilized biological samples due to their sensitivity and complexity.

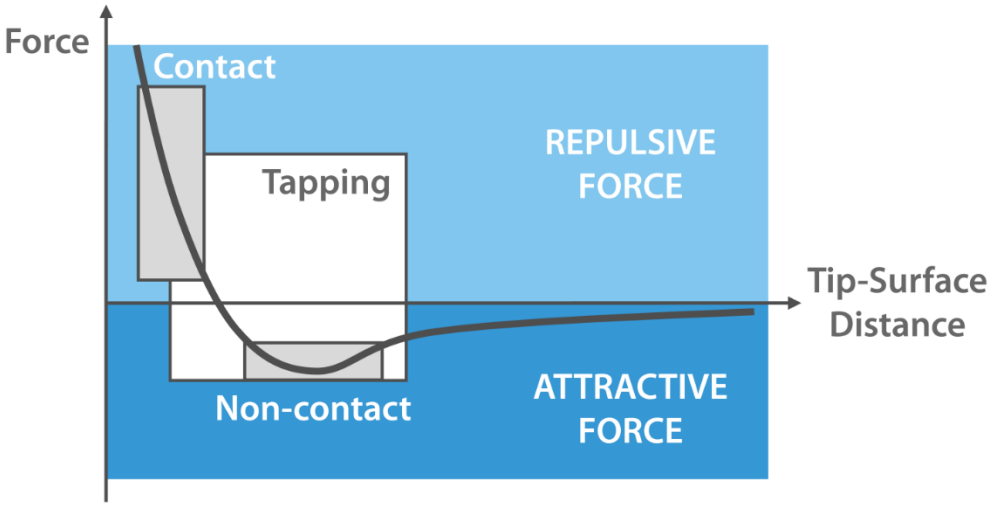

Figure 2.7 **Graphical representation of the traditional AFM imaging modes based on the tip-sample interaction forces as a function of tip-surface distance**. In non-contact mode, long-range attractive forces (e.g., Van der Waals forces) dominate, whereas in contact mode**,** short-range repulsive forces (primarily Coulomb interactions) become dominant. Tapping mode bridges these two extremes, where the tip intermittently makes contact with the surface, allowing for a balanced application of both attractive and repulsive forces. Image from www.nanoandmore.com

In this respect, a less invasive imaging mode is represented by *quantitative imaging* (QI) mode that offers precise control over tip-sample interactions, by recording force-distance curves at each pixel of the scanned image. This enables QI mode to eliminate lateral forces, thus minimizing the risk of damaging delicate or soft samples, such as biological tissues and polymers, which are prone to deformation under conventional AFM modes (Chopinet et al., 2013). As results this modality provides high-resolution mapping of challenging samples such as soft or loosely bound ones.

QI functions effectively in diverse environments, including both ambient air and liquid, enhancing its adaptability across different experimental conditions. A further advantage of this technique is its ability to simultaneously provide information about both the topography and mechanical properties of a sample, including stiffness, adhesion, and elasticity. The detailed mechanical data provided by QI and its ability to investigate complex, sensitive samples without causing damage offers a powerful tool for studying the biophysical properties of cells, viruses, and other delicate materials.

2.4.2 Force Spectroscopy

One of the key advantages of AFM over other microscopy techniques lies in its ability to detect and apply a wide range of forces (from pN up to few μN), which are highly relevant to biological processes, from interactions at the protein level to those involving entire cells (Alsteens et al., 2017). In force spectroscopy mode, cantilever bending is recorded while the tip approaches and retracts from the sample. During the approach, the cantilever bends upwards when pressed against the sample, generating force-indentation curves (***Fig. 2.8a***). By fitting these curves with the Hertz model, the mechanical properties of individual cells, such as cell stiffness, can be assessed. During the retraction, attractive forces between the tip and the sample can be measured (***Fig. 2.8b, c***).Various AFM force spectroscopy modes, including single-molecule force spectroscopy (SMFS) and single-cell force spectroscopy (SCFS), can be used to quantify and localize interaction forces like adhesion and binding/unbinding forces.

These modes make AFM a versatile tool for studying biological processes at the molecular level, and its ability to precisely measure forces at the nanoscale makes it invaluable for cellular biomechanics research (Krieg M. F., 2019).

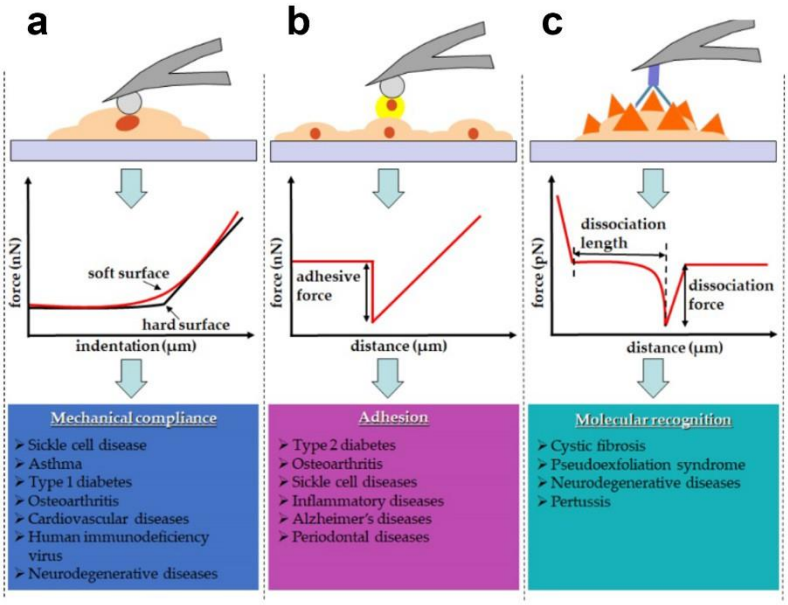

Figure 2.8 **Scheme illustrating principal application of force spectroscopy.** (**a**) Indentation; (**b**) cell-cell force spectroscopy, (**c**) and single molecule interaction forces. Image taken from (Kiio & Park, 2020).

In mechanobiology, AFM can be exploited also in different configurations. For instance, the cantilever can be held in *static contact* with the cell, the forces exerted by the cell—whether due to external (contraction) or physiological stimuli—can be measured through the cantilever's deflection. This method has proven to be crucial for evaluating forces and pressures developped during cell division (Stewart et al., 2011), and the relationship between the actomyosin cytoskeleton and osmotic pressure during mitotic rounding (O'Callaghan et al., 2011). Alternatively, the cantilever can keep *a constant force* over a specified time, allowing researchers to elucidate on the intensity of mechanical stresses that affect cellular processes (e.g. mitosis) (Cattin et al., 2015).

Indeed, AFM can be combined with optical or fluorescence microscopy, allowing for the correlation of mechanical properties with cytoplasmic organelles and the actin cortex, while also facilitating the observation of biological processes triggered by mechanical stimuli.

2.4.3 Calibration of probe

Calibration of the AFM cantilever is a crucial step to ensure accurate force measurements. The process typically involves determining the cantilever's spring constant and the sensitivity that allow to convert the cantilever deflection into force. To evaluate the sensitivity the AFM cantilever is approached against a hard, non-deformable surface (e.g., glass or silicon) and a voltage-piezo displacement is acquired. In the contact region, where the surface is hard, the plot will show a linear relationship. The inverse of the slope of the linear region gives the deflection sensitivity, expressed

in (nm/V). This step converts the photodetector voltage signal into a physical deflection of the cantilever in nanometers. (***Fig. 2.9***).

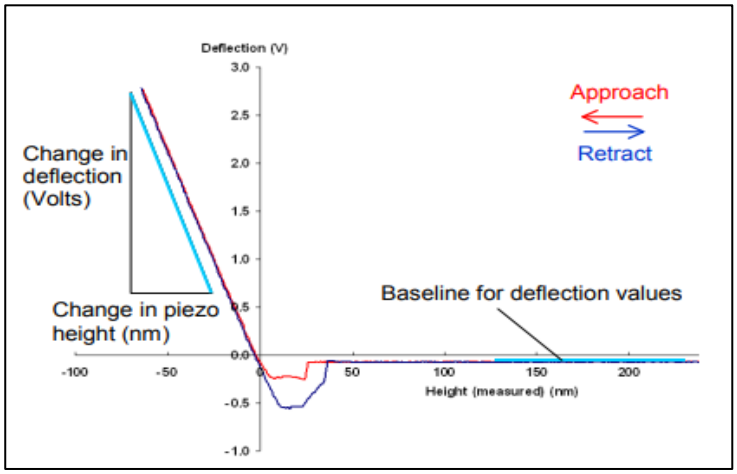

Figure. 2.9 **Sensitivity evaluation.** From the slope of the calibration curve, we can calculate the sensitivity (nm/V). Image from JPK instrument user manual.

Afterward, the spring constant (k) of the cantilever is evaluated by analyzing the free oscillations of the cantilever by the thermal noise method. In this theorem the free oscillations of the cantilever is associated to the k by the following formula:

$$< x > = \sqrt{\frac{k_b T}{k_{cantilever}}}$$

in which (x) is the vibration amplitude, (k_b) is the Boltzmann constant, (T) the temperature.
Once k and sensitivity are evaluated, the deflection of the cantilever recorded as change in the voltage signal on the photodiode (V) can be converted into a force signal by the Hooke's law:

$$F\ (nN) = k\left(\frac{nN}{nm}\right) s\left(\frac{nm}{V}\right) V(V)$$

2.5 Fluidic Force Microscopy

A novel approach in AFM is the Fluidic Force Microscopy (FluidFM), which combines the accurate force-controlled positioning of AFM with the versatility of fluidics. Such approach was demonstrated to be extremely interesting to manipulate biological objects offering an additional tool for single-cell biophysical studies (Meister et al., 2009)
The basic components of FluidFM are the same as AFM, the core innovation lies in the microchanneled cantilever with micrometer or nanometer scale aperture at the free end of the cantilever, which is connected to a pressure controller via tubing (***Fig. 2.10***) (M. Li et al., 2022).

Moreover, the whole system, as AFM, can be combined with optical microscopy enabling to monitor sample during experiments. Furthermore, its compatibility with fluorescence and advanced optical microscopy techniques (e.g., confocal, FLIM, TIRF, FRET, FCS, and super-resolution) allows for analysis also of cellular features or mechanotransduction processes (Lüchtefeld et al., 2024).

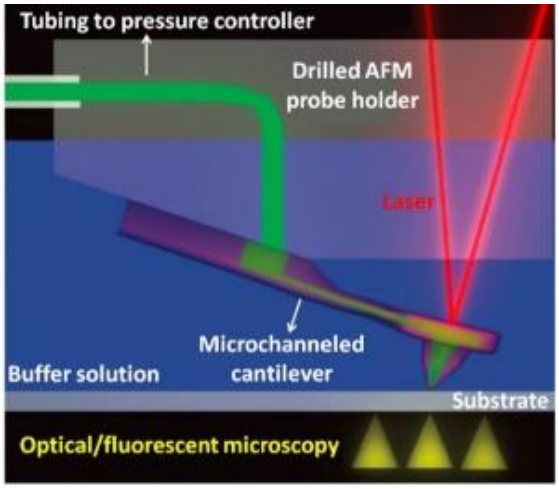

Figure 2.10 **Schematic representation of FluidFM**. The probe is connected to a fluid reservoir and a pressure controller via tubing, allowing precise control of applied pressure. The cantilever can be equipped with a nanoscale aperture at its tip, thus enabling also the delivery or aspiration of liquids. A laser is used to detect the deflection of the cantilever, providing precise force feedback. The whole set-up can be integrated with optical/fluorescence microscopy. Image modified from (M. Li et al., 2022)

The design of FluidFM probes enhances AFM with innovative features, allowing for three-dimensional manipulations on individual living cells, enabling for instance adsorbing, extracting, transporting, placing, delivering, and injecting molecule according to the shape of the probe (Deladi, 2004). Among them, various FluidFM probes have been developed for biological applications, few examples are shown in ***Fig. 2.11*****.**

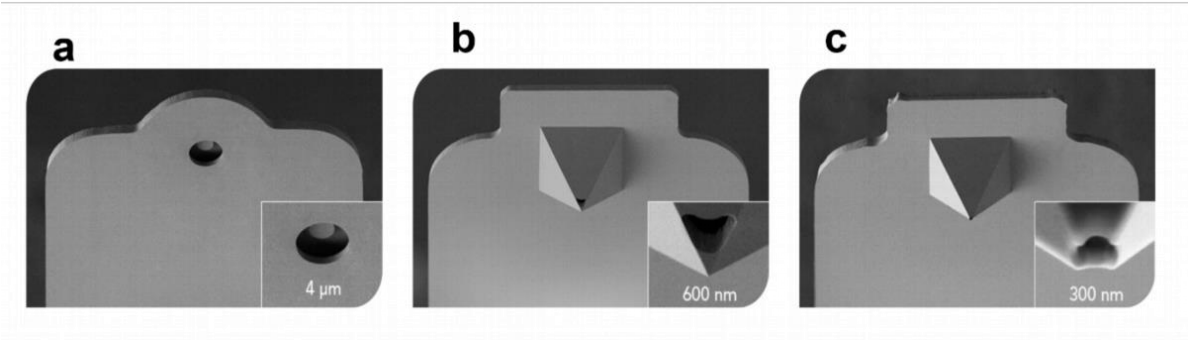

Figure 2.11 **Scanning electron microscopy images of FluidFM probes tailored for various single-cell applications**. (**a**) the FluidFM Micropipette, available with apertures of 2, 4, and 8 µm, is ideal for reversible immobilization of individual cells; (**b**) the FluidFM Nanosyringe, equipped with a 600 nm sharp apex, allows for precise intracellular injection and sampling of materials from the cytoplasm or nucleus; (**c**) the FluidFM Nanopipette, featuring a 300 nm aperture, provides the smallest standard probe aperture, ideal for highly localized dispensing of liquids and nanoprinting. Image from cytosurge.com.

2.5.1 Advantages over traditional AFM

FluidFM technology finds several very interesting applications in mechanobiology field. The measure of adhesion forces is one of them, which can be obtained by capturing a single cell through the use of micropipette cantilevers (Potthoff et al., 2012) **(*Fig. 2.11a***). In this mode, the cell of interest, optically selected, is gently approached in a way that the cantilever aperture aligns on top of the cell (***Fig. 2.12***). Then a gentle contact can be established and maintained by the AFM feedback, while a negative pressure is applied to immobilize the cell, and the following retraction of the cantilever pulls and detaches the cell from the substrate. Recording the cantilevers, deflection allows to determine the force required for this detachment. Alternatively, a floating cell can also be directly trapped from the solution, as in standard SCFS. After completion of adhesion measurements, the immobilized cell can be released by applying positive pressure, making the cantilever ready for immobilization of the next cell. This overcomes important limitations of SCFS in which cantilevers have to be chemically modified to attach a single cell, but cannot be reused for several cells (Angeloni et al., 2023)

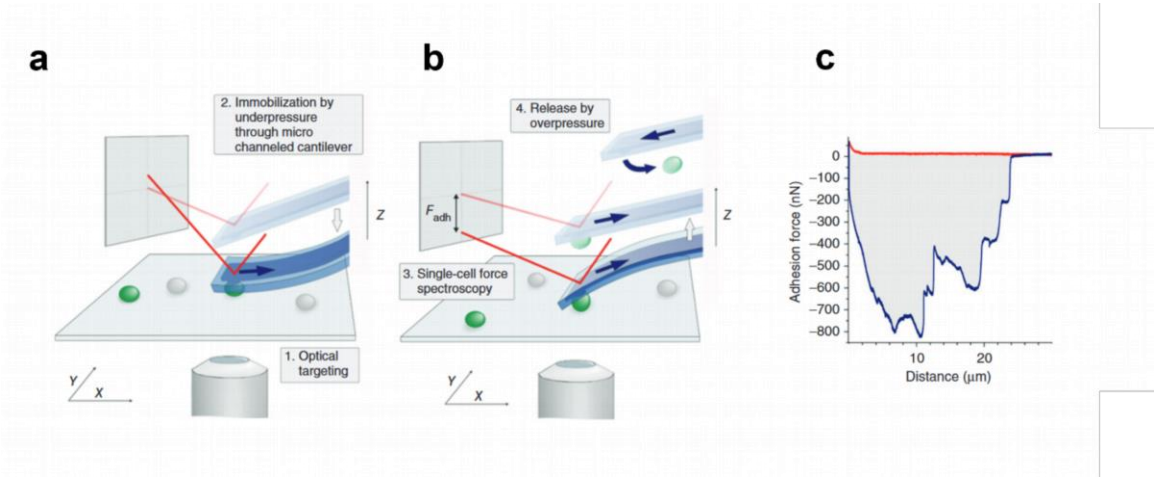

Figure 2.12 **Schematic view of FluidFM-based single-cell force spectroscopy**. (**a**) Optical targeting of cell, followed by approach and immobilization to the cantilever through application of negative pressure; (**b**) Single-cell force spectroscopy during retraction of the cantilever with immobilized cell and subsequent release of the cell by a short pulse of positive pressure; (**c**) resulting force-distance curve obtained that enable to measure adhesion force and adhesion energy (gray area). Image modified from (Potthoff et al., 2012).

In the same configuration, FluidFM is applied to measure forces exerted by motile cells. In these studies, individual sperm cells are captured using negative pressure, allowing the assessment of forces associated with the flagellar beating frequencies in both mouse (Battistella et al., 2023) and human spermatozoa (Tufoni et al., 2024). The captured sperm cells are subsequently released by applying positive pressure.

Another interesting approach utilizes a probe, as shown in ***Figure 2.11c***, to combine FluidFM with patch-clamp techniques, effectively overcoming the traditional limitations of patch-clamp. This approach facilitates gentle and stable contact between the AFM tip and the cell membrane, allowing for sequential patch clamping and injection without visible cell damage (Ossola et al., 2015). Further applications of FluidFM nanosyringes and nanopipettes (***Fig. 2.11b, c***) include temporal single-cell profiling, allowing for precise and repeated analysis of individual cells over time (W. Chen et al., 2022), as well as CRISPR gene editing, which enhances the precision and efficiency of genetic modifications (Antony et al., 2024).

A more recent study by Lüchtefeld et al. (Lüchtefeld et al., 2024) presents a cutting-edge approach for investigating cellular mechanosensitivity using a novel FluidFM-based nanopipette probe. This technique combines fluidic force microscopy with fluorescence imaging to precisely control and measure cellular membrane tension while observing mechanosensitive calcium channel activity in real-time. Through controlled indentation and aspiration, the platform enables separate tuning of mechanical stimuli, allowing researchers to analyze how different forces contribute to membrane tension and its propagation. The addition of fluorescence lifetime imaging with the Flipper-TR probe enhances spatial resolution, offering detailed insights into how tension spreads and interacts with the cytoskeleton. Molecular dynamics simulations further validate these findings, quantifying how localized mechanical cues influence ion channel activation and membrane tension confinement.

2.6 Static and dynamic supports to study mechanosensitive channels

Custom-designed substrates and devices have played a pivotal role in the fields of biomaterials, bioengineering, and developmental biology for many years. These tools provide powerful platforms for studying cellular responses, particularly in areas like mechanotransduction (Xi et al., 2021). The rising cost of animal models, along with their long experimental cycles, ethical concerns, and issues with reproducibility, has emphasized the need for in vitro systems that better mimic in vivo conditions than standard 2D substrates. Micropatterned substrates and cell stretchers, in particular, offer precise control over the mechanical environment, allowing researchers to simulate the static and dynamic forces cells experience within tissues. These systems provide critical insights into the activation of

mechanosensitive channels by replicating key aspects of physiological mechanics in controlled experimental settings.

2.6.1 Micro and nano-structure

Considering that mechanotransduction operates at the nanoscale the use of micro- and nanostructure fabrication offers a powerful method for investigating the molecular mechanisms and pathways involved in this process (Liu & Nakamura, 2021). Typically, the natural extracellular matrix in various tissues such as bone, tooth, nerve, skin, muscle, and heart, exhibits highly oriented, grooved patterns with nanoscale dimensions (***Fig. 2.14***).

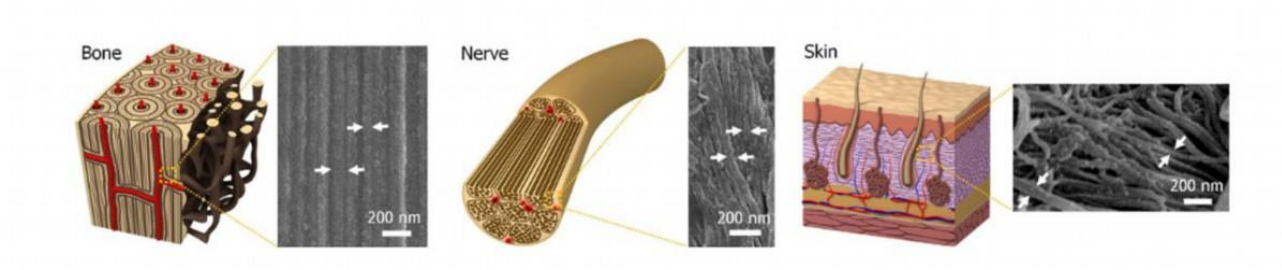

Figure 2.14 **Graphical and SEM images of some *ex vivo* tissues**. Graphical representations and SEM images of *ex vivo* human bone, nerve, and skin tissues, showing the alignment of nanostructures with various nanogrooves. White arrows highlight the varying dimensions of these nanogrooves.. Image adapted from (J. Kim et al., 2013)

To replicate the key characteristics of the cellular microenvironment, extensive research has employed micro- and nano-fabricated substrates made from materials like polydimethylsiloxane (PDMS), poly(methylmethacrylate) (PMMA), and silicon. These engineered surfaces have been used to explore how defined topographical features impact cellular adhesion (Biela et al., 2009), morphology, migration (Bettinger et al., 2009), stem cell differentiation (Oh et al., 2009), and other cellular functions. Structural elements such as grooves, ridges, and wells, fabricated at both cellular and sub-cellular scales, have become instrumental in analyzing cell behavior. Nanogratings and ridges, in particular, have been applied to induce cytoskeletal alignment and direct migration in a wide range of cell types, including smooth muscle cells, macrophages, corneal epithelial cells, fibroblasts, endothelial cells, and neurons (J. M. Corey & Feldman, 2003; Teixeira et al., 2003). Collectively, these studies have demonstrated that cellular activities are significantly influenced by substrates that mimic the topographical features of the extracellular matrix. The fabrication of flexible

microstructures in combination with electrophysiology and calcium imaging provided an extremely useful tool in the investigation of mechanosensitive channels (***Fig. 2.15***).

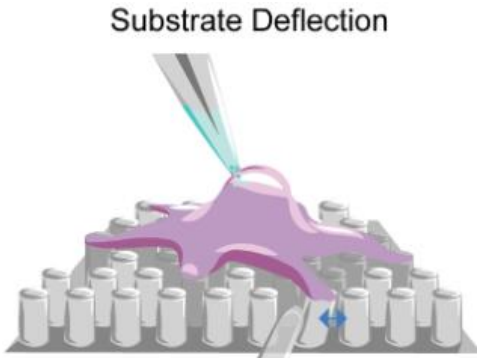

Figure 2.15 **Scheme representing pillar array combined with patch-clam**. recording electrode on top of the cell, stimulating glass probe displacing the flexible pillar below. Image adapted from (Richardson et al., 2022).

Bavi et al explored the role of these micro- and nano-structures in modulating PIEZO1 activity, in response to exogenously applied stimuli (Bavi et al., 2019). Using elastomeric pillar arrays as force transducers, the study demonstrated that mechanical stimuli could be applied at precise cell-substrate contact points by deflecting individual pili. Their results showed that PIEZO1 demonstrated increased sensitivity to substrate deflections when the spacing between pili was wider. However, this heightened sensitivity was not observed on stiffer substrates. Additionally, while cellular contractility was required for the sensitization of PIEZO1, it was not necessary for its activation.

2.6.2 Cell stretcher device

Another important tool in the mechanobiology and in the study of mechanosensitive channels is represented by the cell-stretcher device (Constantinou & Bastounis, 2023). A cell stretcher is a precision-engineered device designed to apply unilateral or uniform mechanical forces to living cells. It consists of a stretchable substrate on which cells are cultured. This substrate can be stretched or compressed by applying mechanical force, either manually or through automated systems, depending on the design. The stretching mechanism is often driven by motors or actuators, this system applies controlled mechanical forces to the substrate, simulating the physical stretching that cells experience in their natural environments, such as in tissues under strain. Cell stretchers can allow precise adjustments of force magnitude, frequency, and duration, giving researchers the ability to fine-tune the mechanical environment. Frequently are compatible with optical microscopy enabling to observe

and record cellular responses in real time. By subjecting cells to mechanical strain, cell stretchers help simulate conditions like tissue expansion, contraction, or pressure changes, making them essential tools in studying mechanosensitive ion channels, cellular mechanics, and tissue engineering.

An example of that is reported by (O. Friedrich et al., 2019), where they described a new iso-stretcher that, can be combined with calcium imaging. The system provided new insight into the mechanosensitivity of adult ventricular cardiomyocytes.

CHAPTER 3

New insights into PIEZO2 mechanosensitivity by Atomic Force Microscopy

3.1 Introduction

The distinct tissue expression of the PIEZO2 channel likely influences its activation mechanisms, sparking significant interest in understanding how mechanical forces interact with cells to activate these channels. However, the complexity of cell membranes and the variety of potential activation pathways present challenges in quantitatively and mechanistically defining how force is transduced to the channel.

Previous studies on PIEZO2 activation were carried out by patch clamp techniques in *stretch* and *poke* configurations in heterologous systems (S.-H. Woo et al., 2015) and cells that naturally express the channel, such as dorsal root ganglion (DRG) neurons (Coste et al., 2010) and Merkel cells (S. H. Woo et al., 2014). While heterologous systems are valuable for exploring the channel's molecular properties, they may not fully replicate the complex environment of sensory neurons. These investigations showed that whole-cell responses activates PIEZO2 currents in DRG neurons (Murthy, 2023), Merkel cells (Ikeda et al., 2014), and heterologous systems (Murthy, 2023; Verkest et al., 2022). Interestingly mutants lacking various intracellular domains evoked poking induced current indistinguishable from the wild type PIEZO2. Moreover, it was also observed that the current amplitudes of PIEZO2 is very sensitive to the stimulation velocity, which is consistent with rapidly adapting low-threshold mechanoreceptor afferent fibers (Verkest et al., 2022). In this set-up configuration, it was not possible to precisely measure the applied pressure. Instead, low positive pressure was observed to activate the PIEZO2 channels in Merkel cells (Shin et al., 2019). Similarly, stretch-activated single-channel events were observed in excised membrane patches in DRG in response to positive pressure stimuli within the range of 20-100 mmHg (Murthy, 2023). Experiments in stretch configuration demonstrated that in Merkel cells the application of negative pressure up to -190 mmHg failed to active PIEZO2 current (Ikeda & Gu, 2014). More recently, Murthy et al. investigated the activation of the channel in PIEZO2-transfected HEK293 and DRG, examining both macroscopic and single-channel currents (Murthy, 2023). Their studies on PIEZO2-transfected HEK293 cells, using the cell-attached stretch configuration, revealed a response to negative pressures ranging from 0 to -80 mmHg, with half-maximal activation of PIEZO2 at approximately P_{50} = (50 ±

4) mmHg. The same work, along with other studies (Moroni et al., 2018; Szczot et al., 2021), highlighted that PIEZO2 is a membrane stretch-activated channel. However, other studies, have shown that PIEZO2-dependent stretch-activated single-channel currents can be altered by mutations of PIEZO2 pore region (Coste et al., 2015; Geng et al., 2020; Verkest et al., 2022). In particular Verkest et al. proposed that PIEZO 2 is activated by cytoskeleton-transmitted forces, although they do not totally reject the stretch-membrane activation. Tension can propagate on short distance so likely this can activate only channel close to the stimulus (Verkest et al., 2022).

Despite the ongoing debate, each study has been crucial in advancing our understanding of PIEZO2 channel function. However, the measurement conditions, including tip diameter, mechanical step increments, the time between steps, probe velocity, and the duration of the applied mechanical stimulus are crucial, since they can all have an impact on the PIEZOs activation.

In this sense, nanotechnological techniques can address certain constrains of patch clamps, including limited spatial resolution (µm range) and force sensitivity, particularly in poking configurations, thereby enhancing our understanding about PIEZO2 channel activation.

In this chapter, PIEZO2 activation was studied by using Atomic Force Microscopy (AFM) combined with calcium imaging. This nanotechnological approach enables to apply a controllable and quantifiable force on a cell, without forming a seal with the membrane, that can induce an additional mechanical stress on the cell. This also prevents disruption of the channel's interactions with the membrane and cytoskeleton, allowing us to study the channel in conditions closer to its physiological state.

3.2 Experimental section

3.2.1 Cell line and PIEZO2 expression

Human embryonic kidney cells (HEK-293) are generally used as heterologous system for transfection. In order to evaluate the PIEZO2 endogeneous expression in this model system, a quantitative PCR (qPCR) was performed. Total RNA from different cell lines was extracted with TRIzol reagent (Invitrogen, 15596026). 1 µg of RNA was reverse and transcribed to cDNA using the PrimeScript RT Reagent Kit (Takara Bio USA Inc., San Jose, CA, USA, RR047A). Quantitative PCR was performed using SsoFast™ EvaGreen® Supermix (Bio-Rad, Hercules, CA, USA) on the CFSX384™ Real-Time PCR Detection System (Bio-Rad, Hercules, CA, USA). Plate was sealed and placed in CFSX384 Real-Time System (Bio-Rad, Hercules, CA, USA). GAPDH was used for normalization. Each sample in each group was detected in triplicate. The following sets of primers (Sigma-Aldrich, St. Louis, MO, USA) were used in the study: PIEZO1 forward primer: 5’ CATCTTGGTGGTCTCCTCTCTGTCT-3; PIEZO1 reverse primer: 5’

CTGGCATCCACATCCCTCTCATC-3; Piezo2 forward primer: 5' TGCACAGTCAAAGGCTATCAA -3; Piezo2 reverse primer:5'- ATGCTGTCCCAAATGATTCC-3'; GAPDH forward primer:5'- GAAGGGCTCATGACCACAGT-3'; GAPDH reverse primer: 5'-TGCAGGGATGATGATGTTCTGGG-3'; TRPV1 reverse primer: 5'-TTCTTGCTCTCCTGTGCGATCTTGT-3'; TRPV1 forward primer: 5' GGCTGTCTTCATCATCCTGCTGCT-3'. Resulting data were visualized with CFSX Manager software.

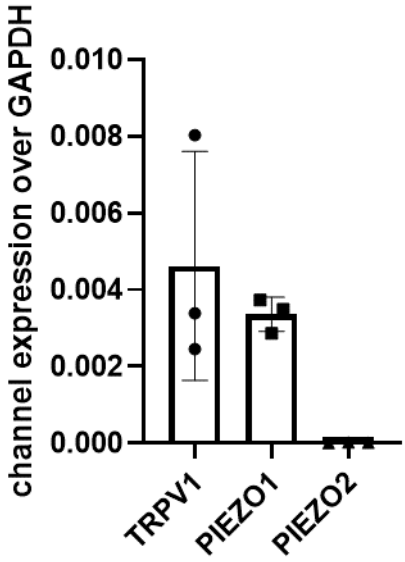

Figure 3.1 **qPCR analysis of mechanosensitive and thermosensitive channels in HEK-293 cells.** Data from triplicate experiments are shown as individual dots, with bars representing the mean ± STD.

The analysis revealed that PIEZO2 is not expressed in this cell line, while showing the presence of the mechanosensitive PIEZO1 channels, together with the thermosensitive channel TRPV1 (***Figure 3.1***).

3.2.2 PIEZO2 transfection

Cells were seeded on 35mm glass-bottom (MatTek) dish coated with poly-L-lysine (100 μg/mL) for 30 min and then with 2% Matrigel (SIAL, #356231) for at least 20 min both at room temperature (RT) to promote cell adhesion. Cells were cultured in DMEM-GlutaMAX™ (Gibco, #31966-047) supplemented with 10% FBS (Euroclone, #ECS0180L) and 1% Penicillin-Streptomycin (Euroclone, #ECB3001D). Cells were maintained at 37 °C and 5% CO_2 in a humidified incubator. Transfection was performed after six hours at a ratio of 750 ng of DNA to 8.25 μL of linear PEI (0.33mg/mL).

Linear PEI solution was added to the DNA one, vortexed and incubated for 15 minutes at room temperature. Afterword, the transfected cells were left over-night (about 14-16 hours) in incubator at 37 °C and 5% CO_2 . Afterward, the cells were used for experiment.
PIEZO2-green lantern DNA construct was kindly provided by Francesco Taberner (Instituto de Neurociencias, Alicante).

3.2.3 AFM combined with calcium imaging

AFM-based indentation on single cell were applied using a NanoWizard II AFM (JPK Instruments, Bruker) integrated with an inverted optical Axiovert 200 microscope (Carl Zeiss AG, Oberkochen, Germany) equipped with an X-cite® 120Q fluorescence illuminator (Excelitas Technologies Corp., Waltham, MA, USA), 40× objective (LD Plan_Neofluar, Carl Zeiss AG, Oberkochen, Germany). An AFM cantilever modified with a micrometer bead (5µm diameter) and with a nominal spring constant of 0.5-9 N/m (CP-FM-BSG-A-5, NanoAndMore GmbH) was used for the mechanical stimulation. Before each measurements the spring constant of the cantilever was calibrated in the fluid chamber of measurements using thermal noise method (te Riet et al., 2011). Based on the assumption that the contact area between the bead and the cell can be considered as half sphere surface of the bead, we can be evaluated the contact area as $A=2\pi r^2$ and, as result the pressure applied can be evaluated as P=F/A (Gaub & Müller, 2017). Hence, with a 5µm bead diameter and force of 50nN we are applying on the whole cell a pressure of about +10mmHg.
AFM stimulation was combined with calcium imaging to monitor the activity of the mechanosensitive channels. As result, two red-fluorescent calcium dyes were used: Rhod-2AM and Rhod-3AM. The cells were loaded with 1mM Rhod-2AM (R1244, Thermofisher) in cell medium for 1 hour at 37°C. After incubation, the samples were washed two times with NPSS (140mM NaCl, 5mM KCl, 2 mM $MgCl_2$, 1mM $CaCl_2$, 10 mM HEPES, 1Mm glucose) and de-esterification in the same solution was performed at 37°C for at least 15 minutes before the experiment. Instead, the cells were labeled with Rhod-3AM (R10145, Thermofisher) for 50 minutes at 37°C in cell medium with Power Load buffer 100x and Probenicid 250mM. After incubation, the samples were washed two times with NPSS solution pH 7.4 (140mM NaCl, 5mM KCl, 2 mM $MgCl_2$, 1mM $CaCl_2$, 10 mM HEPES, 1Mm glucose) and incubated at 37°C in the same medium with Probenicid 250mM for an additional 30 minutes to allow de-esterification of the dye.
Following the calcium dye loading of the cells, the petri dish was placed under the microscope, a cell of interest was chosen, and the AFM probe was positioned on the center of the cell. Mechanical stimulation ramp was programmed using experiment planner option of JPK software. Physical

stimulations were performed with force of 50nN with two different stimulus durations: 0.5s and 10s. The stimulation ramp consists of: (1) approaching the cell at 5µm/s speed, (2) a pause of 0.5s (or 10s) applying 50nN, (3) cantilever retraction from the cell at the same speed. Each cell was stimulated with short stimulus of 0.5s, then, after one minute of recovery, with long stimulus of 10s. All measurements were performed in NPSS at room temperature.

A fluorescence time-lapse movie was recorded, starting 10 seconds before stimulation until the end of measurements (a total duration of 90 seconds). Image acquisition was performed using a 200 ms exposure time per frame, with an interval of 200 ms. The time-lapse was captured using an XM10 monochrome CCD camera (Olympus Corporation, Tokyo, Japan). Time-lapse movies were analyzed by ImageJ with Time Viewer plug-in. The fluorescence signal of images was normalized as follows: $\Delta F/F_0$ with F being fluorescence at time t_i, and F_0 is the mean for the first 5 frames at t_0.

3.3. Results and Discussions

3.3.1 Mechanically activated response of PIEZO2 by controlled AFM indentation

To deliver a localized and controlled mechanical stimulation to the PIEZO2 channel, we used an AFM probe modified with a micrometer bead. Unlike standard patch-clamp experiments, this approach involved applying a single, controlled force step, followed by retraction. Importantly, in AFM, the cell was not connected to a monitoring pipette, which could introduce unintended mechanical stimulation. The bead attached to the AFM probe was used to vertically push on the nuclear region of the cell, thus applying a pressure both on the plasma membrane and the underlying structures, such as the cytoskeleton, nucleus, and organelles, as illustrated in ***Figure 3.2***.

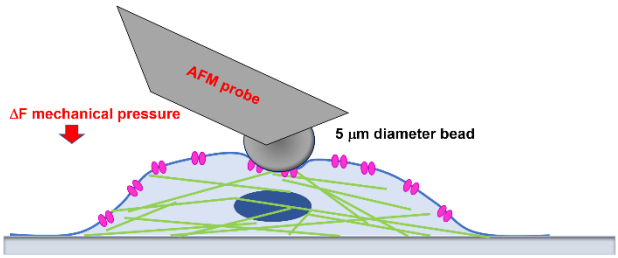

Figure 3.2 **Scheme of a cell subjected to indentation using a cantilever modified with micrometer bead.** The *pink* structures represent the mechanosensitive channels, the *green* lines the cytoskeleton and the *blue* the nucleus. The distribution of the mechanosensitive channels on the plasma membrane is a pure representation.

It is worth to mention that the PIEZO2-Green Lantern construct, that we used, allowed for the localization of PIEZO2 within the cell. As shown in ***Figure 3.3,*** we observed a diffuse signal in the transfected cells, suggesting that the overexpressed PIEZO2 is present not only on the plasma membrane but also at the level of membrane of intracellular compartments.

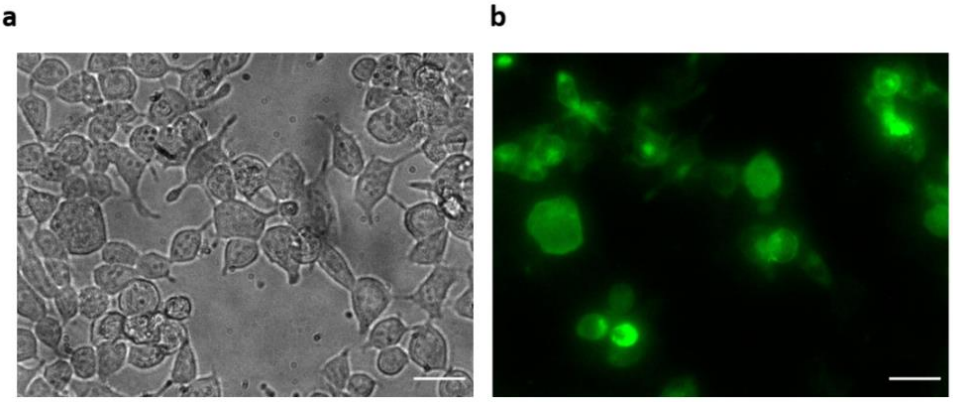

Figure 3.3 **Representative images of HEK 293 cells transfected with PIEZO2 Green Lantern.**
(**a**) Bright field image of HEK 293 cells, and (**b**) fluorescence image showing transfected cells expressing PIEZO2 (green). Scale bar: 50 μm.

To test potential differences on the behavior of PIEZO2 activation when regulating calcium influx between cytosolic calcium and calcium in internal organelles two different dyes were used: Rhod3-AM for which the uptake into organelles has been reduced, and translates into better cytosolic localization, and Rhod-2AM which is localized in all cell compartments (also organelles).
We first investigated the response of the PIEZO2 transfected cells in presence of Rhod-2AM. Once selected the green fluorescent transfected cell, it was indented with 50nN force for 0.5s and 10s stimulus duration, and the same protocol was applied to non-transfected HEK cells (those without green fluorescence) present in the same plate. Upon probe indentation of the PIEZO2-transfected cell loaded with the Rhod-2AM calcium dye, an increase in calcium signal was detected (***Figure 3.4a-c***), while in non-transfected cells a signal increment was not generally observed, as shown in ***Figure 3.4d-f***.

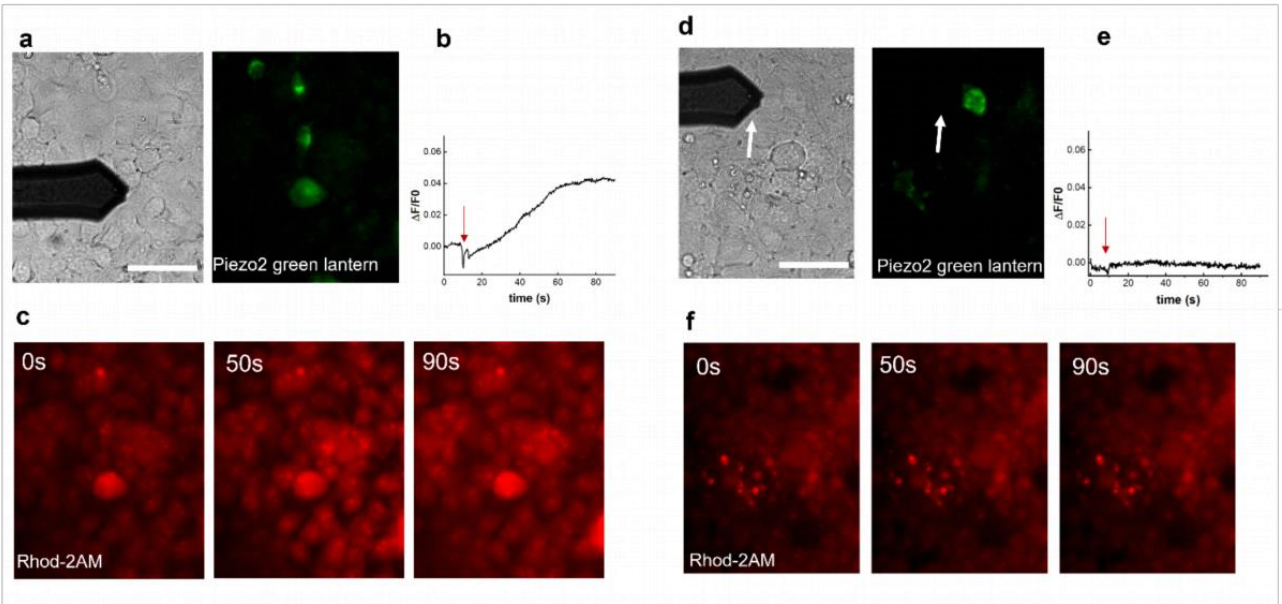

Figure 3.4 **Representative images upon mechanical stimulation in presence of Rhod-2AM calcium dye.** ***(a)*** Bright-field and fluorescence image showing the AFM cantilever in contact with the HEK cells expressing PIEZO2-Green Lantern; (**b**) Calcium trace (ΔF/F0) showing the response upon mechanical stimulation (50 nN) applied at the time indicated by the red arrow. The drop in the calcium trace at 10s is associated with the bead-cell contact; (**c**) time-lapse images showing Rhod-2AM fluorescence at 0, 50, and 90s after stimulation, indicating intracellular calcium increase following mechanical force application. (**d-e**) Same measurements were repeated for non-transfected cells (control) indicated by the white arrow. Scale bar 50 µm.

Similar experiments were repeated with Rhod-3AM. In ***Figure 3.5*** representative images of PIEZO 2-HEK transfected and non-transfected cells (control) in presence of Rhod-3AM calcium dye in response to indentation are shown. Upon stimulation, transfected cells showed an increase in fluorescence intensity (***Figure 3.5a-c***), reflecting a rise in cytosolic calcium levels. In contrast, non-transfected HEK cells (control), when subjected to the same mechanical stimulus, generally did not exhibit any significant increase in fluorescence signal (***Figure 3.5d-f***).

Additionally, we noticed that, especially when utilizing Rhod2-AM, transfected cells typically showed stronger baseline calcium fluorescence than non-transfected cells. This suggests that the overexpressed PIEZO2 channels may facilitate calcium influx into the cytosol even in the absence of mechanical stimulation.

We then analysed the percentage of responding cells in presence of both calcium dyes upon mechanical stimulation as reported in ***Figure 3.6***.

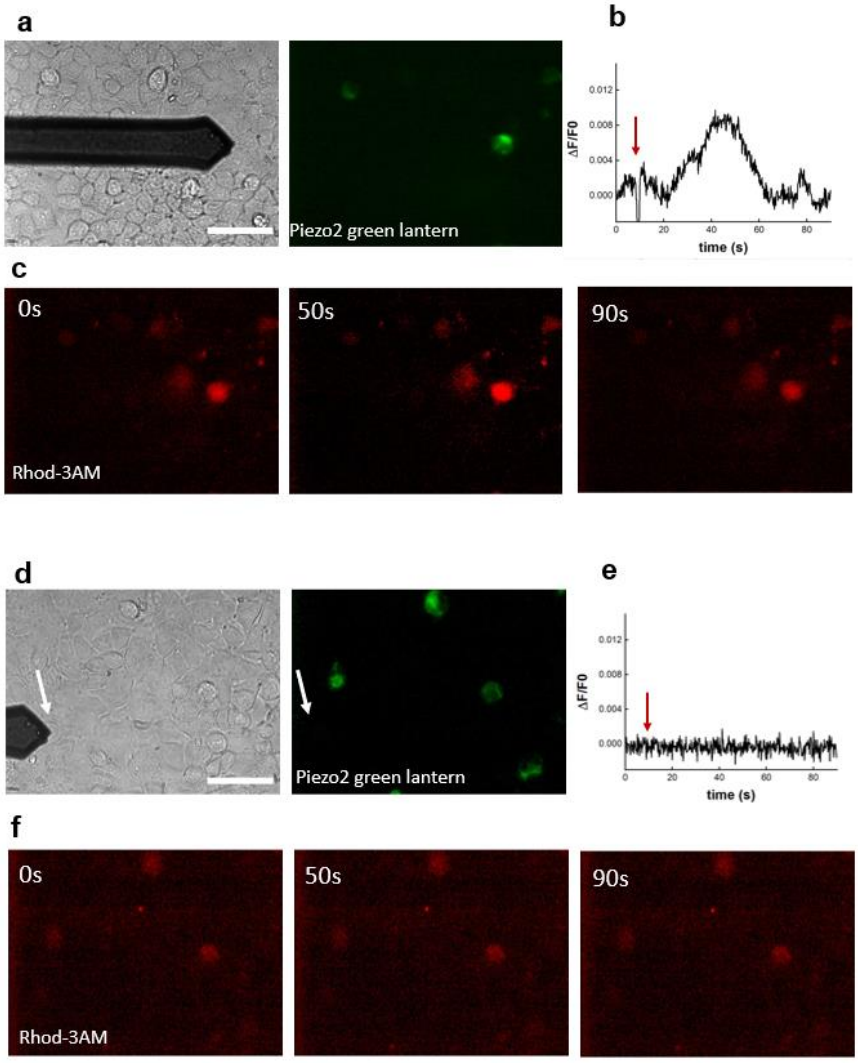

Figure 3.5 **Representative images upon mechanical stimulation in presence of Rhod-3AM calcium dye.** ***(a)*** Bright-field and fluorescence image showing the AFM cantilever in contact with the HEK cells expressing PIEZO2-Green Lantern. (**b**) Calcium trace (ΔF/F0) showing the response upon mechanical stimulation (50 nN) applied at the time indicated by the red arrow; (**c**) time-lapse images showing Rhod-3AM fluorescence at 0, 50, and 90s after stimulation, indicating cytosolic calcium increase upon indentation. (**d-e**) Same measurements were repeated for non-transfected cells indicated by the white arrow. Scale bar 50 µm.

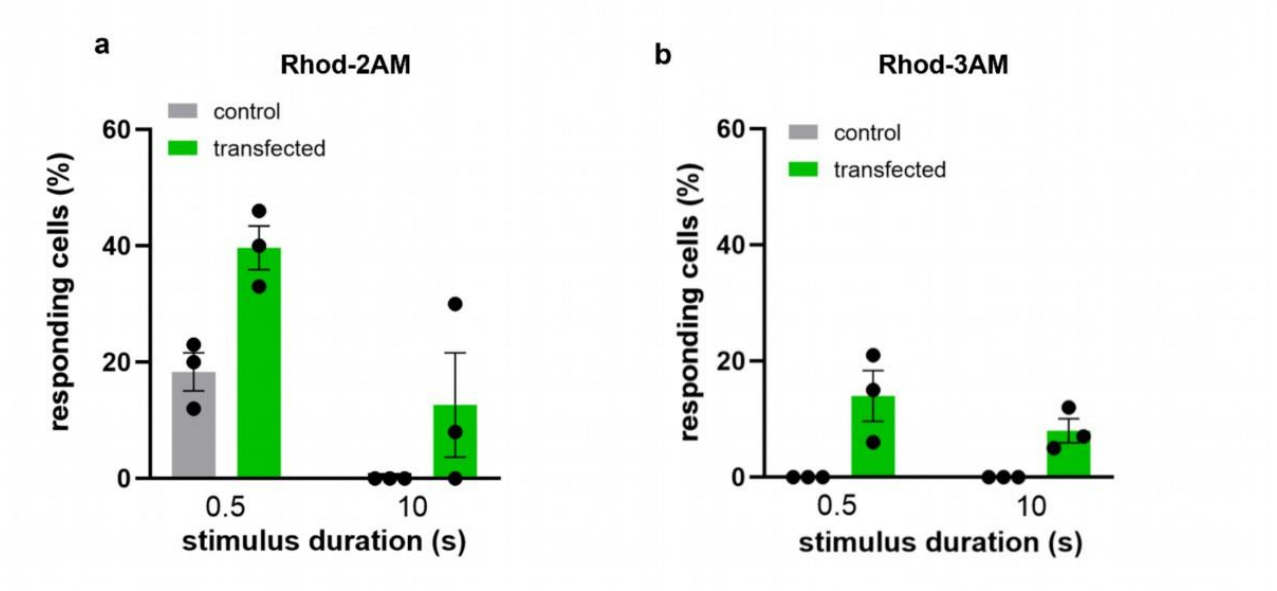

Figure 3.6 **Percentage of responsive cells to short and long mechanical stimuli.** Comparison of percentages of responsive cells for PIEZO2 transfected HEK cells and non-transfected (control) to bead indentation with Rhod-2AM (a) and Rhod-3AM (b). Dots represent three independent experiments. Bar shows mean ± SEM. We analyzed a total number (n) of cells for Rhod-2AM n=31for control, and n=35 for transfected; for Rhod-3AM n=30 for control and n= 30 for transfected.

Using both fluorescent dyes, upon application of 50nN indentation force, PIEZO2-transfected HEK cells showed a higher response compared to non-transfected HEK cells, for both short and long stimulation durations. The enhanced response of the transfected cells indicates that the activation observed is primarily due to PIEZO2. As a result, we found that low-pressure indentation (+10 mmHg) was sufficient to activate PIEZO2 channels, which aligns with previous findings showing that low positive pressures (+10 and +20 mmHg) are sufficient for channel activation (Shin et al., 2019). These confirm the low activation threshold of PIEZO2 channels in response to positive pressure. Moreover, this pressure is lower than the pressure typically required in AFM-based stimulation to activate PIEZO1 channels in both HEK-transfected cells (Gaub & Müller, 2017) and cells endogenously expressing PIEZO1 (Braidotti et al., 2024), as well as in cortical neurons (Gaub et al., 2020), where pressures between 20–75 mmHg were used. These studies demonstrated that PIEZO1 channels required higher forces to induce calcium influx. Despite structural homology between PIEZO1 and PIEZO2, key differences, such as specific charged amino acids, can play a crucial role in their distinct mechanosensitivity. Previous studies showed that neutralizing these charged residues increased the mechanical threshold for PIEZO2 activation, underscoring their importance for the channel's sensitivity to mechanical stimuli and suggesting that PIEZO2 can respond to different mechanical environments (Verkest et al., 2022). A low activation threshold is consistent with PIEZO2's role as a highly sensitive ion channel involved in light-touch sensing (Ranade, Woo, et al., 2014).

Moreover, the high percentage of responsive cells with Rhod-2AM (***Figure 3.6a***) indicates a substantial calcium influx into both the cytoplasm and intracellular compartments, suggesting that at least in transfected cells, PIEZO2 may also be expressed in the membranes of intracellular organelles, particularly mitochondria. Indeed, Rhod-2AM has been recognized as an effective dye for measuring Ca^{2+} dynamics within mitochondria (Babcock et al., 1997; Wadia et al., 1998).

Additionally, with Rhod-2AM a significantly higher percentage of transfected cells responded to the short stimulation (0.5s) compared to long stimulus (10s). This is consistent with PIEZO2's rapid response to brief mechanical stimuli, as it is classified as a rapidly adapting mechanosensitive ion channel (Ranade, Woo, et al., 2014). After the longer stimulation (10s), the percentage of responding transfected cells decreased but remained significantly higher than in control cells. This behavior could also be related to the modulation of PIEZO2 activity due to the sequential application of stimuli, beginning with 0.5s stimulus followed by the 10s stimulus. Despite allowing for recovery time, repetitive stimulation may result in PIEZO2 becoming less efficient during prolonged or repeated exposure (Coste et al., 2010; Lewis et al., 2017)

Using Rhod-3AM, we generally observed a lower percentage of responding cells compared to Rhod-2AM (***Figure 3.6b***). Additionally, the proportion of responsive cells remained consistent regardless of whether the stimulation was short or long, suggesting that the increase in cytoplasmic calcium is not affected by the duration of the stimulus

3.3.2 Mechanical stimulation of single PIEZO2-transfected cell evokes collective cell response

Upon indenting a single cell of PIEZO2 transfected cell, we noticed also a collective cell calcium response from the neighboring cells. This phenomenon was frequently observed with Rhod-2AM, while it was not relevantly detected with Rhod-3AM. An example of such behavior is reported in ***Figure 3.7.*** A single PIEZO2 transfected cell is stimulated (***Figure 3.7a***), and nearly simultaneous activity is observed in neighboring cells (circled in ***Figure 3.7b***), suggesting a coordinated response. To assess whether such behavior is due to spontaneous activity or is evoked by the mechanical stimulation, we recorded the same field in the absence of mechanical stimulation by monitoring the activity of the same cells (***Figure 3.7c)***. In this case, no calcium dynamic was observed for all cells, indicating that the collective cell response is triggered by the mechanical stimulus. We observed this phenomenon regardless of whether the stimulated cell showed a response or not. Same experiment was repeated also for non-transfected HEK cells (control).

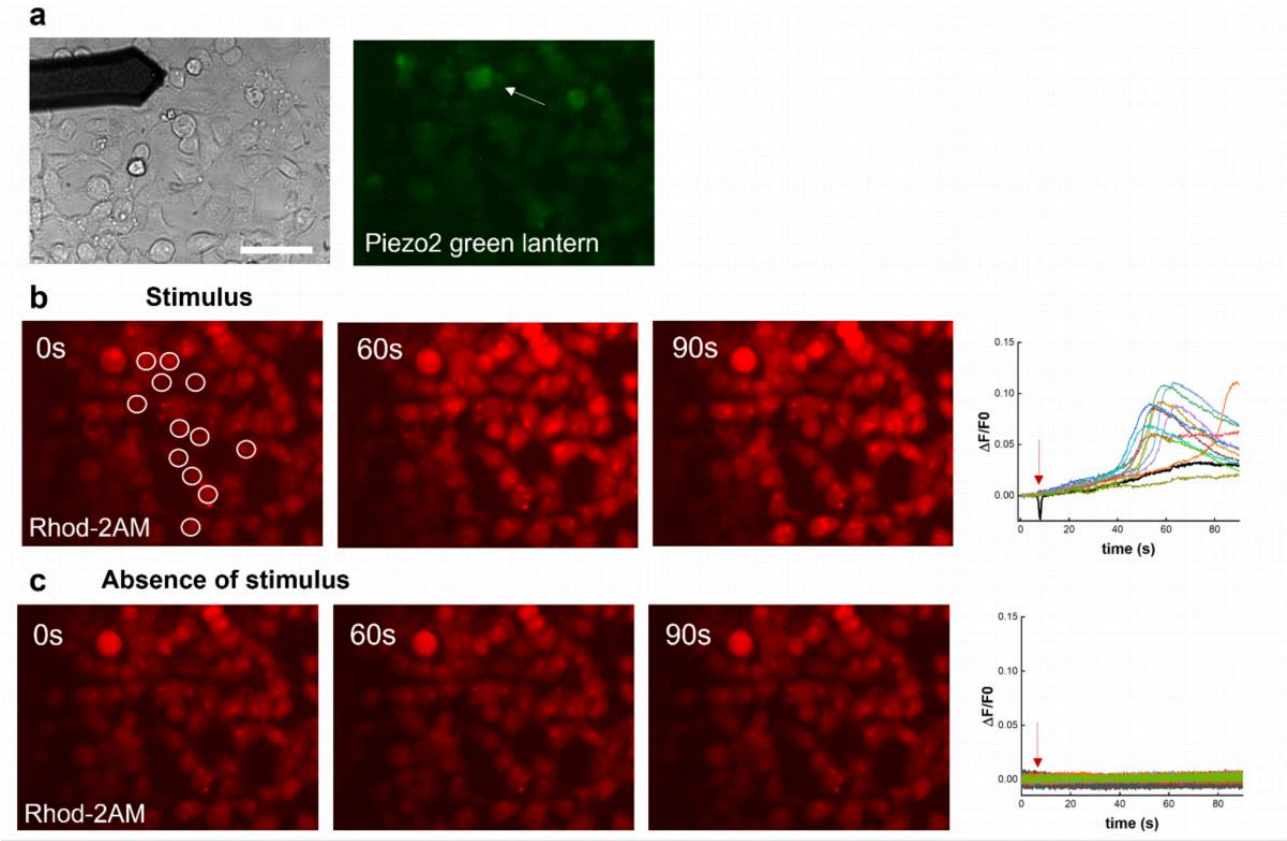

Figure 3.7 **Collective cell response upon mechanical stimulation of single cell loaded with Rhod-2AM.** ***(a)*** Bright-field showing the AFM cantilever in contact with the PIEZO2-Green Lantern transfected cell indicated by the white arrow; (**b**) time-lapse images of Rhod-2AM fluorescence at 0, 50, and 90 seconds and the calcium dynamic (ΔF/F0) of the cells identified by white circles, upon mechanical stimulation (50 nN) applied at the time indicated by the red arrow of the transfected cell. The white circle identified the neighboring cells surrounding the stimulated one. (**c**)Time-lapse images of the same area in (**b**) showing Rhod-2AM fluorescence at 0, 50, and 90 seconds in absence of stimulation and the corresponding calcium dynamic for the same cells analysed in (**b**) identified by the white circle. Scale bar 50 µm.

To quantify the frequency of this behavior, we calculated the percentage of the area exhibiting this response (***Figure 3.8).*** This collective cell response was observed significantly more often in PIEZO2-transfected cells than non-transfected ones. This behavior occurs simultaneously with mechanical stimulation, but appears to be independent of the calcium response in the mechanically stimulated cell. Therefore, we hypothesize that mechanical stimulation may trigger a rapid influx of other cations, initiating a calcium signaling cascade that activates neighboring cells.

The absence of this response when using Rhod-3AM, which only binds to cytosolic calcium, suggests that the collective response might involve mainly calcium influx in intracellular compartments (e.g. endoplasmic reticulum or mitochondria). These findings point out the potential role of PIEZO2 not only in local mechanosensitivity, but also in coordinating broader calcium signaling networks within the cell population.

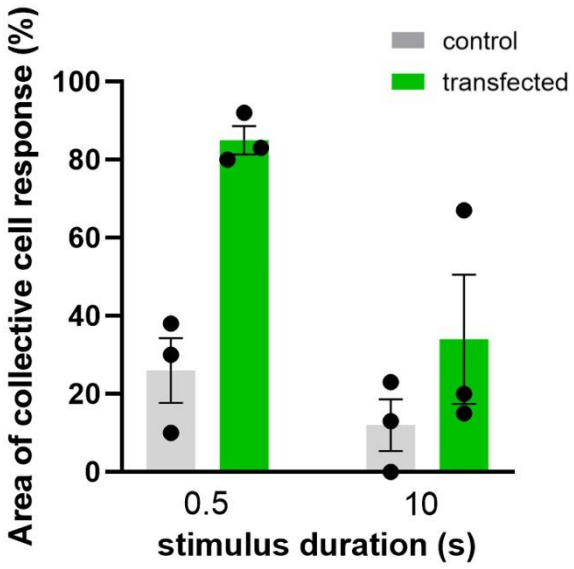

Figure 3.8 **Percentage of area exhibiting collective cell response following single cell mechanical stimulation.** PIEZO2-transfected cells show a higher percentage of response compared to non-transfected (control) cells after both 0.5s or 10s stimulation durations. Dots represent three independent experiments, bars are mean ± SEM. Number of area analysed (n): n=31 for control n= 35 for PIEZO2 transfected cells.

3.4 Conclusions

In summary by using AFM-based mechanical stimulation combined with calcium imaging we demonstrated that PIEZO2 efficiently respond to short-duration stimuli at low indenting pressure (+10mmHg), consistently with physiological mechanical sensitivity, rapid activation and short latency of PIEZO2 channels. Additionally, the differences in response observed between Rhod-2AM and Rhod-3AM, suggest that Rhod-2AM captures calcium activity also within intracellular organelles, indicating that in the heterologous system PIEZO2 may also be expressed in internal compartments with different dynamic in its activation.

Regarding the collective cell response observed for the PIEZO2 transfected cells we do not know yet the reason or the mechanism of this behavior, but we can suppose that the channel is rapidly activated enabling also the influx of other cations, that we were not able to monitor in our configuration, which are able to activate a coordinated cell response. Moreover, we cannot exclude that similar behaviour might be also related to the presence of PIEZO1 channels and possible interactions between the two channels (Dubin et al., 2017). In this regard, silencing of PIEZO1 would be helpful to clarify this issue.

CHAPTER 4

Response of calcium mechanosensitive channels in dorsal root ganglion neurons upon mechanical stimulation of the plasma membrane

4.1 Introduction

The first observation of mechanically activated currents in dorsal root ganglion (DRG) neurons dates back to 1999, when McCarter and colleagues (McCarter et al., 1999) demonstrated that indentation of DRG's soma with a blunt glass probe could elicit a macroscopic current, using the whole-cell patch clamp technique. Since then, the integration of advanced nanotechnological techniques has provided new opportunities for refining traditional methods in studying the behavior of mechanosensitive channels with greater precision. Among them, atomic force microscopy (AFM) and optical tweezers (OT), that allow for more precise control over mechanical stimuli, have been successfully employed to investigate mechanosensitive calcium channels in both neuronal (Falleroni et al., 2022; Gaub et al., 2020) and non-neuronal cells (Braidotti et al., 2024). They enable the application of mechanical forces ranging from piconewtons to hundreds of nanonewtons, targeting specific cellular locations, including the nuclear region, soma, and dendrites. However, when AFM and OT indent the cell, they likely impact the entire plasma membrane and the underlying cytoskeleton, depending on the force applied.

In this framework, Fluidic Force Microscopy (FluidFM), a cutting-edge nanoscale technology that combines the precision of AFM with microfluidic capabilities, can be used to stimulate plasma membrane. This versatile platform allows for the manipulation of single cell to assist in the analysis of their mechanical features or response to mechanical stimulus (Battistella et al., 2023; Dehullu et al., 2019; M. Li et al., 2022; Lüchtefeld et al., 2024; Tufoni et al., 2024). A significant advantage of FluidFM, over traditional patch-clamp, is its ability to modulate the cellular environment dynamically with high spatial resolution. In this case the FluidFM probe, a microchanneled tipless cantilever, is brought into contact with the cell at a controlled force by using a force feedback control system of AFM that ensures a stable and gentle contact between the probe and the cell membrane (as in standard contact-AFM). Afterward, a pump system can inject or aspirate, as result positive or negative pressure at the end of the channel can push or pull the cell membrane. This can be used to locally deform plasma membrane, enabling also to explore the response of a cell to the two different stimuli (pressure

and aspiration) within a single experiment. Very recently, FluidFM combined with a newly designed cylindrical probe demonstrated the potential of this approach for investigating the membrane tension generated in the vicinity of the probe and its effect on PIEZO1 behavior (Lüchtefeld et al., 2024).
In this chapter, FluidFM is exploited to investigate the response of mouse mechanosensory neurons at different culture time (24h and 48h) upon application of positive or negative pressure at the level of plasma membrane of soma.

4.2 Experimental section

4.2.1 Animals and DRG culture

Animals were housed with ad libitum food and water and subjected to a controlled 12-hours light-dark cycle. All animal procedures were performed in accordance with European Union (EU) guidelines (2010/63/UE) and Italian law (decree 26/14) and the ethical committee from SISSA. Animal use was approved by the Italian Ministry of Health, in agreement with the EU Recommendation 2007/526/CE.
Adult C57/Bl6 mice (more than 6 weeks old) were euthanized in a CO_2 chamber and DRG neurons extracted and collected in sucrose-based artificial cerebrospinal fluid (ACSF; 234 mM Sucrose, 2.5 mM KCl, 0.5 mM $CaCl_2$, 10 mM $MgSO_4$, 1.25 mM NaH_2PO_4, 26 mM $NaHCO_3$, 11 mM Glucose). DRG neurons were enzymatically digested in collagenase type IV (10ng/µL, Sigma-Aldrich #C5138) for 26 minutes at 37°C, followed by centrifugation at 700*g* for 3 minutes and remotion of the supernatant. The pellet was then resuspended and incubated with 0.05% Trypsin EDTA (Gibco, #25300-054), for 26 minutes at 37°C and mechanically isolated by repeated pipetting. Cell debris was removed by passing cell suspension through a 100 µm filter (BD™, #340632). The cell suspension was pelleted and resuspended in DMEM-GlutaMAX™ (Gibco, #31966-047) supplemented with 10% FBS (Euroclone, #ECS0180L) and 1% Penicillin-Streptomycin (Euroclone, ECB3001D) and plated in 35mm glass-bottom (MatTek) dish coated with poly-L-lysine (100µg/mL) and 2% Matrigel (SIAL, #356231). Cells were maintained at 37 °C and 5% CO_2 in a humidified incubator.

4.2.2 Quantitative-PCR

Total RNA from DRG neurons was extracted with TRIzol reagent (Invitrogen, 15596026). 1 µg of RNA was reverse and transcribed to cDNA using the PrimeScript RT Reagent Kit (Takara Bio USA Inc., San Jose, CA, USA, RR047A). Quantitative-PCR (qPCR) was performed using SsoFast™ EvaGreen® Supermix (Bio-Rad, Hercules, CA, USA) on the CFSX384™ Real-Time PCR Detection

System (Bio-Rad, Hercules, CA, USA). Plate was sealed and placed in CFSX384 Real-Time System (Bio-Rad, Hercules, CA, USA). GAPDH was used for normalization. Each sample in each group was detected in triplicate. The following sets of primers (Sigma-Aldrich, St. Louis, MO, USA) were used in the study: PIEZO1 forward primer 5' – GCGCTTGCTAGAACT -3'; PIEZO1 reverse primer 5' – ATTGTTGGGGAAGGG -3'; PIEZO2 forward primer 5' – CGTCTGCATCCTACA-3'; PIEZO2 reverse primer 5'- CATTGACTTTGCCAT- 3'; GAPDH forward primer 5'- GAAGGGCTCATGACCACAGT-3'; GAPDH reverse primer 5'- TGCAGGGATGATGATGTTCTGGG-3';TRPV1 forward primer 5'- GTTTACCTCGTCCACCCTGA 3'; TRPV1 reverse primer: 5' –AGAGAGCCATCACCATCCTG-3'. Resulting data were visualized with CFSX Manager software.

4.2.3 Immunofluorescence assay

For immunofluoresce experiments, the cells were fixed with 4% paraformaldehyde (PFA) for 15 minutes at room temperature (RT). After fixation and four washes with PBS, DRG were incubated for 20 minutes in the blocking solution, composed by 0.3% Triton X-100 and 2% serum (generally from the specie on which the secondary antibodies were harvested) in PBS at RT. Then, neurons were incubated with primary antibodies for Neurofilament 200 (NF-200) and Tyrosine Hydroxilase (TH) diluted in blocking solution for 1 hour at RT. After extensive rinses with 0.3% Triton X-100 in PBS, DRG were incubated with secondary antibodies diluted in blocking solution for 1 hour at RT. DRG were extensively rinsed with 0.3% Triton X-100 in PBS, mounted on glass slides with ProLong Diamond Antifade Mountant (ThermoFisher, #P36970) and imaged using a Nikon A1R confocal microscope. In ***table 1*** are reported the antibody used in the procedure described above:

Table 1**:** Antibody used to identify DRG neurons with different functionality.

Reactivity	Dilution	Host	Company, #
Primary Antibody			
Anti NF-200	1:200	mouse	Sigma- Aldrich, #MAB5266
Anti-Tyrosine Hydroxylase	1:200	rabbit	Sigma-Aldrich, #AB152
Secondary Antibody			
Anti-Mouse 488	1:500	Donkey	Invitrogen, #A21202
Anti- Rabbit 596	1:500	Donkey	Invitrogen, #A21206

4.2.4 FM styryl dye labeling

Neuronal plasma membranes were stained using FM 4-64FX (Invitrogen, #F34653). Cells were incubated with 10 μM of FM4-64 in Hanks' Balanced Salt Solution (HBSS) without magnesium or calcium for 20 minutes at 37°C in a humidified atmosphere of 5% CO_2. After incubation, cells were washed three times with NPSS saline solution at pH 7.4 (140 mM NaCl, 5 mM KCl, 2 mM $MgCl_2$, 10 mM Glucose, 1 mM $CaCl_2$, and 10 mM HEPES).

4.2.5 FluidFM coupled with calcium imaging

The mechanical stimulation of single cells was performed by using a FluidFM instrument (Cytosurge) working with a NanoWizard II AFM instrument (JPK Instruments, Berlin, Germany), integrated with inverted microscope Axiovert 200 (Carl Zeiss, Jena, Germany).

The mechanical stimulation was applied by using a FluidFM probes connected to a pressure pump controller. We used FluidFM probes which consist of microchannel cantilevers with at the apex an aperture of 4μm diameter and nominal spring constant of 0.3N/m (Cytosurge). Before experiments, each probe was immersed in the experimental solution and then calibrated using the thermal noise method (te Riet et al., 2011)

FluidFM stimulation was combined with calcium imaging. Hence, before mechanical stimulation, the DRGs were loaded with calcium sensitive 5 μM Fluo-8 dye (Abcam) for 40 min at 37 °C 5% CO_2. After incubation, the medium was replaced with NPSS saline solution pH 7.4 (140 mM NaCl, 5 mM, KCl, 2 mM $MgCl_2$, 10 mM Glucose and 1 mM $CaCl_2$, 10 mM HEPES).

Calcium activity was monitored by using a mercury lamp as light source and an CCD Camera (Olympus XM10) and 40X objective lens. For the total duration of measure (90s), a time lapse movie is recorded, with 200ms exposure time for a single image acquisition and interval of 200 ms.

A cell of interest was selected and the FluidFM probe was positioned on the central area of soma. Mechanical stimulation protocols were programmed using experiment planner options of the JPK software. The cantilever was lowered on the central area of soma with a speed of 5 μm/s until a force set point of 1 nN is reached; the force set point was held constant by the AFM controller operating in contact mode. After 10s a positive or negative pressure was applied (+/- 40mbar and +/- 80mbar) for 5s to mechanically stimulate the cell. Afterward the pressure was lowered to +2mbar for 2s and then further lowered to 0 mbar up to the end of the measure. After 45s from the end of the stimulation, the probe is then retracted from the cell at a speed of 5 μm/s. All experiments were done at room temperature.

During the experiments we periodically checked the leakage pressure of the FluidFM probe and cleaned the probe. After stimulating approximately 2-3 cells, we moved the probe from petri dish and

immersed sequentially in a warm milliQ solution (50–60 ◦C), a warm bleach 5 % solution and again in Milli-Q water. Every step takes more or less 2 min, each time a positive and negative pressure is applied to remove any cell debris attached to the probe (Battistella et al., 2023; Tufoni et al., 2024). Time lapse fluorescence images were analyzed by ImageJ, plug-in Time Viewer. To evaluate the variation of fluorescence intensity in time, the ROI was drawn including the whole cell. The fluoresce signal of images was normalized as follows: ΔF/F0 with F being fluorescence at time t*i*, and F*0* is the mean for the first 5 frames at t*0*.

4.3 Results and discussions

4.3.1 Selecting mechanosensory DRG

From mouse ganglion a heterogeneous population is generally extracted, which includes sensory neurons, (e.g. nociceptors, thermal and mechanosensory neurons) and non-sensory cells (e.g. fibroblasts, macrophages, and Schwann cells) (Qi et al., 2024). To assess the expression of mechanosensitive channels within this population, we conducted quantitative PCR (qPCR) for PIEZOs and TRPV1 channels. The qPCR data showed that PIEZO2, together with TRPV1, are more expressed than PIEZO1 (***Fig. 4.1***). TPPV1 is a thermosensitive channel (Cao et al., 2013), while only PIEZOs are definitively shown to be mechanically gated (Coste et al., 2010). The higher expression of PIEZO2 is known to be mainly associated with DRG neurons (Coste et al., 2010), while other channels can be located both on sensory neurons and non-sensory cells.

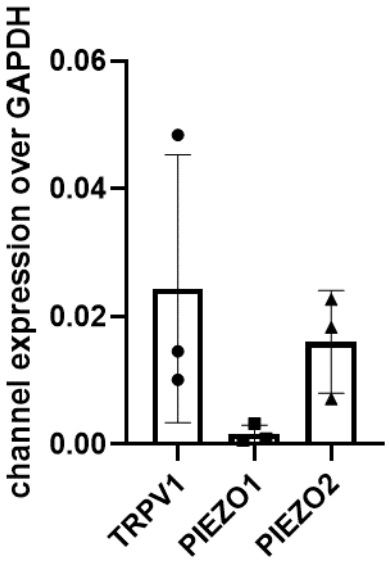

Figure 4.1 **qPCR analysis of mechanosensitive and thermosensitive channels in DRG samples.** Data from triplicate experiments are shown as individual dots, with bars representing the mean ± STD.

Moreover, we intended to determine the proportion of mechanosensory neurons because our objective was to stimulate them specifically. In this sense, a PIEZO2 antibody could be used for this, but presently, commercially available PIEZO2 antibodies are reported to lack sufficient sensitivity and specificity for reliable detection(Acheta et al., 2022; Dalghi et al., 2019). Hence to evaluate the percentage of mechanosensory neurons in our culture, we stained DRG neurons with NF-200 that labels mechanosensitive neurons (Lawson, 2002; Sann et al., 1995), and TH that labels C-Low threshold mechanoreceptor (C-LTMR) characterized by small diameter and unmyelinated afferents that innervate the trunk hairy skin. (Noble et al., 2022). By analyzing these images, we observed that in our sample 40% of neurons are mechanoreceptors and proprioception (NF) and 15% are low threshold mechanoreceptors (TH) (***Fig. 4.2***). These data demonstrated that in our sample about 55% of DRG neurons are mechanoreceptors.

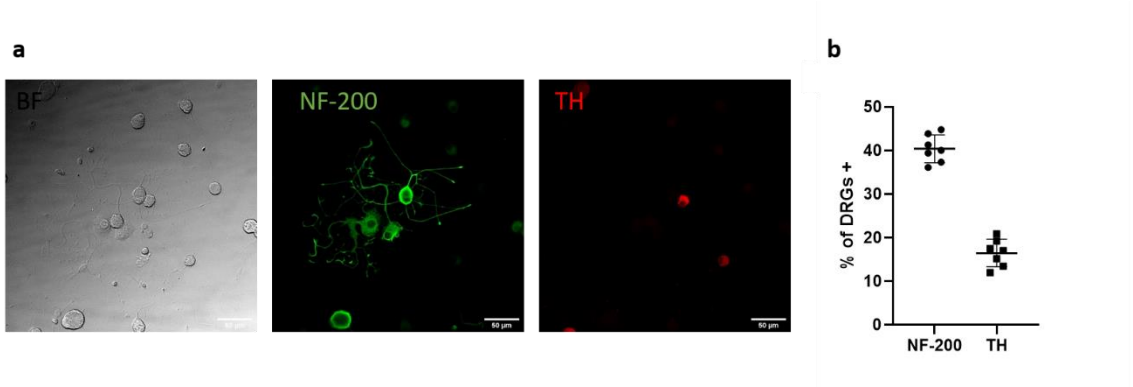

Figure 4.2 **Evaluation of NF-200 and TH positive neurons**. (**a**) Representative bright field (BF) and confocal fluorescence images of DRG neurons upon staining with NF-200 and TH after 24h in culture (**b**) percentage of DRG neurons NF-200 positive compared to TH-positive neurons. Bars represent the mean ± SD. Data are from at least three sample areas from two independent experiments. Number of areas evaluated n= 7 for NF-200 and n= 8 for TH.

To identify these mechanosensory neurons in living cells for mechanical stimulation, it would be helpful to incorporate an additional parameter related to their morphology. According to the literature, PIEZO2 transcripts are expressed across DRG neurons of all sizes, but with particularly high levels in the largest diameter neurons, which are associated with touch and proprioception (Wang et al., 2019). In contrast, PIEZO1 transcripts are more selectively and highly expressed in smaller neurons, which are recognized to be nociceptors (S. M. Shin et al., 2023).

To focus on a more homogeneous population of mechanosensory neurons, we therefore chose to stimulate only the larger neurons. In ***Fig. 4.3*** is reported an evaluation of the size of soma of DRG neurons total population and those stimulated. Here it is possible to see that, for stimulation, only very large cells have been chosen as respect to the size of soma of others DRG neurons present in the samples investigated. This selective stimulation can help to minimize variability that could arise from

stimulating different DRG neurons populations, which might otherwise have different mechanosensitive properties.

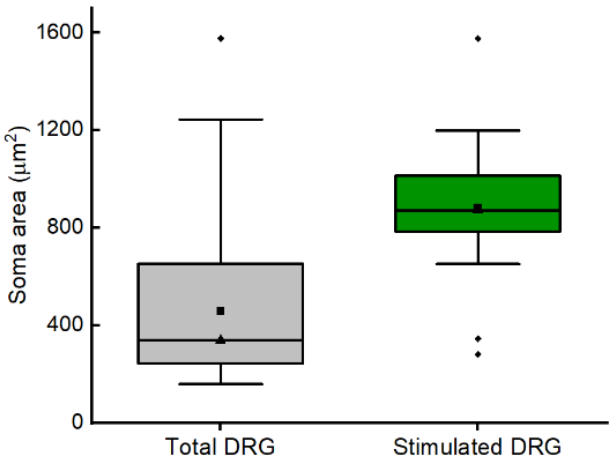

***Figure 4.3* Area of DRG soma**.
The area of all soma of DRG neurons in a sample as compared with that of the neurons chosen for the mechanical stimulation. Data are reported in box plots, middle bar indicates the median value.

4.3.2 The activation of calcium mechanosensitive channels in response to membrane deformation

To selectively stimulate the plasma membrane, the FluidFM probe aperture was placed in contact with the soma of DRG neurons with controlled force, thanks to the AFM feedback. Once positioned, positive or negative pressure was delivered by micrometer-sized aperture in contact with the cell surface. This enabled to push or pull the plasma membrane, depending on whether positive (***Fig. 4.4a***) or negative pressure (***Fig. 4.4b***) is applied. Additionally, repeated stimulation using both positive and negative pressures provide insight into the membrane's dynamic response and the behavior of mechanosensitive ion channels under various mechanical stresses.

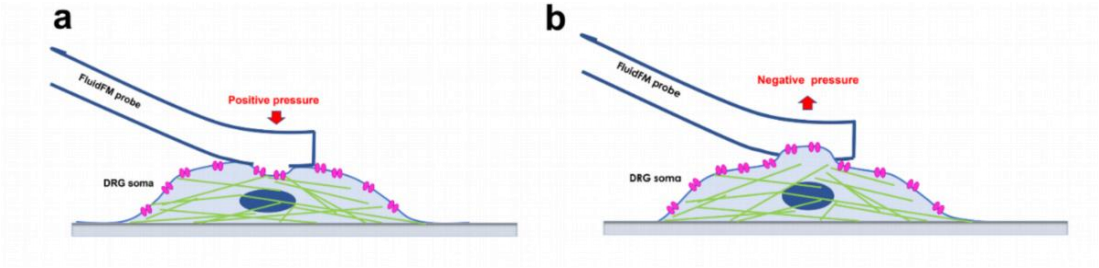

***Figure 4.4* Schematic representation of mechanical stimulation on the plasma membrane via FluidFM.**
Scheme illustrating how positive (**a**) or negative (**b**) pressure applied through FluidFM are expected to stimulate the plasma membrane, allowing to investigate mechanical effects in both directions. The pink structures represent the mechanosensitive channels, the green lines the cytoskeleton and the blue the nuclei.

The distribution of the mechanosensitive channels on the plasma membrane reported in the scheme is a pure representation, as well as the number of channels included or surrounding the region stimulated by the probe. *In vivo* PIEZO 2 is known to be located at the end of fibers (Villarino et al., 2023), but *in vitro,* when they are cultured on standard culture supports, DRG neurons lose their physiological polarization and, in such conditions, the organization and localization of PIEZO2 channels, or other mechanically activated channels, within the cell and on the plasma membrane is unclear. Nevertheless, the presence and the response of mechanosensitive channels including PIEZO2 in DRG neurons was successfully investigated at the level of soma (Murthy, 2023; Sann et al., 1995; S.-H. Woo et al., 2015).

Hence, we stimulated the soma of DRG neurons, which was contacted with 1nN force, to minimize the mechanical stimulation by the probe itself. The large DRG soma examined had a height exceeding 20 µm, thus enabling us to easily position the aperture of the tipless FluidFM probe in contact with plasma membrane. Afterward a pressure (+/- 40mbar and +/- 80mbar) for 5 min was applied, as described in details in the experimental section. The positive and negative pressures were applied sequentially first negative and subsequently, after more than 1 min recovery, positive pressure.

We noticed that a fluorescence signal having the characteristics shown in ***Figure 4.5(a)*** is correlated with the movement of the cantilever, as it comes in and out of contact, as indicated by the time scale. All fluorescence traces with this form were categorized as cells that did not respond. Instead, when an increase in the fluorescence signal is observed in the entire soma almost instantly after the pressure is applied (Fig. 5b) or after 2 and 20s after the mechanical stimulation (Fig. 5c), these were considered responding cells. The sudden jump in the fluorescence signal at 60s (traces in ***Fig. 4.5b, c***) is associated with probe retraction, which however, was not observed to influence the dynamic of calcium signal.

When replacing the experimental solution with a calcium-free NPPS, we did not observe any changes in fluorescence signal, suggesting that the rise of fluorescence signal detected is related to mechanically evoked calcium response, such as the activation of mechanosensitive ion channels located on the plasma membrane in response to the mechanical pressure.

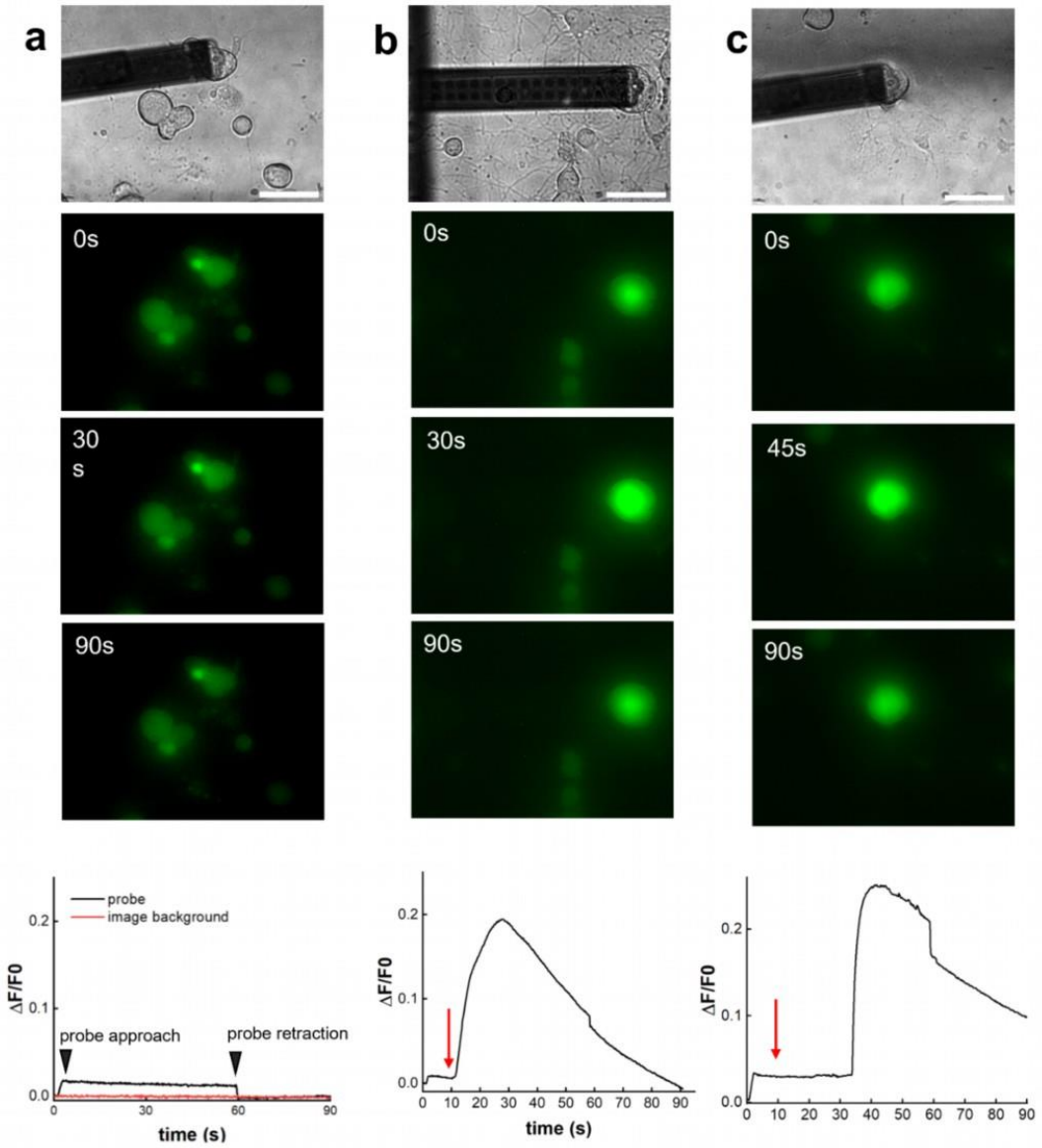

Figure 4.5 **Representative fluorescence signal traces in the absence and presence of cellular response.** (**a**) Bright field and fluorescence signal in absence of a detectable cellular response, time-lapse images showing fluorescence signal at 0, 30, and 90s together with corresponding calcium dynamics; black arrows indicate the approach and retraction times. (**b**) Bright field and rapid increase in fluorescence immediately after mechanical stimulation, time-lapse images showing fluorescence signal at 0, 30, and 90s together with corresponding calcium dynamics. (**c**) Bright field and fluorescence signal of delayed fluorescence after 20 seconds post-stimulation, time-lapse images showing fluorescence at 0,45, and 90s together with corresponding calcium dynamics. Calcium dye: Fluo 8AM; the red arrows indicate the stimulation event. Scale bar: 50 µm

The analysis of the responsive cells demonstrated that the proportion of responding cells at (+/- 40 mbar) is relatively low, but still comparable with the response observed in literature (Verkest et al., 2022). At these pressures, the percentage of responsive cells was observed to be similar for both 24 and 48h culture times (***Fig. 4.6a***), with also comparable signal intensity (***Fig. 4.6c***). This suggests that low-pressure activation remains stable over time, and that mechanically activated calcium

channels in DRG neurons are consistently responsive to mild mechanical stimuli across these culture time.

By increasing the applied pressure at 80mbar, the percentage of responsive cells does not significantly change at 24h for +/-80 mbar, while increases at 48h, mainly for +80mbar (***Fig. 4.6b***). The intensity of signal at -80mbar increases as respect to +40 mbar consistently, for both 24h and 48h. Instead, at +80mbar, the intensity of the signal is overall lower (***Fig. 4.6d***).

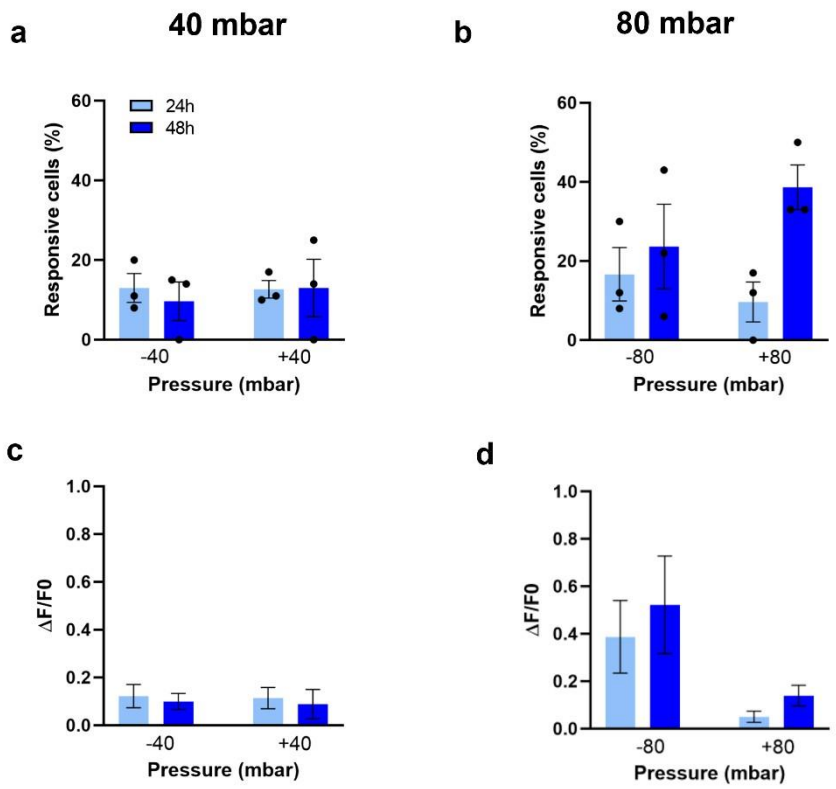

Figure 4.6 **DRG neurons response at different culture time to increasing pressures.** (**a**) percentage of responsive DRG neurons at +/- 40mbar and (**b**) +/-80mbar at 24h or 48h culture time. Fluorescence intensity for (**c**) +/- 40mbar and (**d**) +/- 80mbar. Dots represent three independent experiments, for each pressure a total of cells *n*=30-40 were analyzed. The data are shown as mean ± sem.

The increment of responding cells at 48h for both +80and -80mbar indicates that with prolonged culture more cells become sensitive to stronger pressures. This behavior suggests that culture time plays a crucial role in enhancing DRG mechanosensitivity, which could be associated with cellular adaptations, such as increased expression of mechanosensitive channels, or changes in channels availability. However, at +80mbar, even if the number of responsive cells increases as respect to -80mbar, a lower signal intensity is observed. This behavior is challenging to explain definitively, but we can speculate that it may be linked to the cell's higher calcium conduction in response to negative pressure, which appears to be more effective than positive pressure. Notably, we have also to consider

that the measurements were performed by applying first -80mbar (or -40mbar) and then +80mbar (or +40mbar). The way in which negative and positive pressure are applied can be also a key factor that can affect the efficiency of the mechanosensitive channels. Similarly, negative pressure combined with repeated applied pressure, could prime or alter the mechanosensitive pathways in a way that changes the cell ability to respond robustly to subsequent positive pressure, leading to lower signal intensity at +80 mbar. In other words, mechanically stimulated channels may initially exhibit high conductance under negative pressure, allowing for a significant influx of calcium upon activation, but they tend to quickly desensitize, reducing calcium flow after repeated high-pressure stimulation. A similar behavior has been observed when applying negative voltage or repetitive mechanical stimuli, as demonstrated by other studies (Hao & Delmas, 2010).

Similarly, we observed that prolonged localized mechanical stimulation reduced the cell response in PIEZO2-transfected HEK cells (see *Chapter 3*). The membrane tension, which may have been altered by the previously applied negative pressure, could also play a significant role in modulating the calcium conductance. For example, in the case of PIEZO1, it was found that resting membrane tension significantly influenced the gating of the channel, and it may be important in regulating the conductance of the channels (Lewis & Grandl, 2015).

4.3.3 The response of calcium mechanosensitive channels at the membrane stretching

Additionally, we noticed also that some DRG neurons responded during probe retraction, upon detachment from the plasma membrane, about 45s after the mechanical stimulation (***Fig. 4.7***). This response, generally, was not correlated with the response observed during the pressure stimulus; in other words, neurons either responded to the pressure stimulus or to the detachment, but not both.

To exclude that the rise of calcium signal at the probe retraction could be due to the extraction of a plasma membrane patch, we repeated the experiment in presence of a membrane marker. After observing the cell response at the probe detachment (***Fig. 4.8a, b***), we moved the tip away from the stimulated cell and we did not detect any membrane fluorescence in the probe aperture or in its proximity (***Fig. 4.8c***), even when the probe was positioned in areas of the sample devoid of cells (***Fig. 4.8d***). This suggests that the observed cell response is not associated with the detachment of a plasma membrane patch or membrane damage that could result in massive calcium influx.

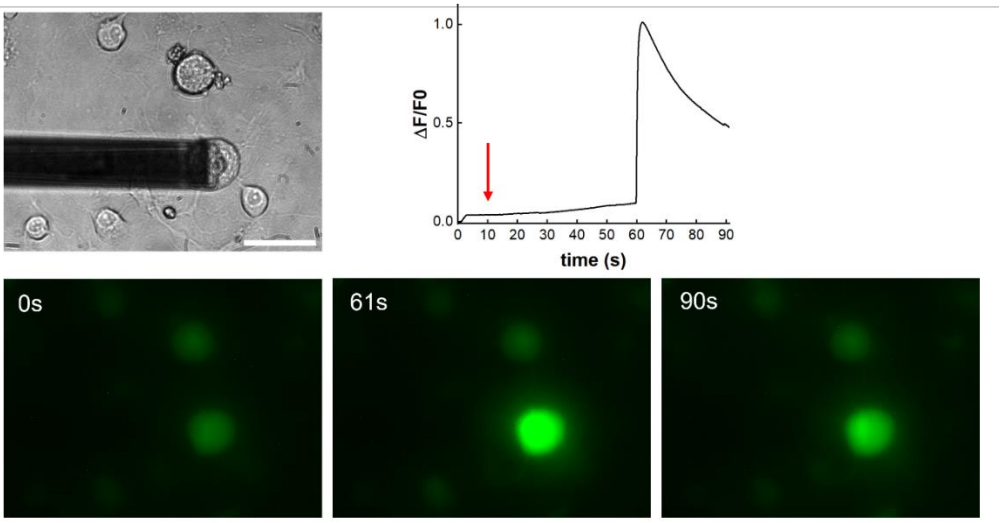

Figure 4.7 **Cell response at the probe detachment.** Bright field and time-lapse images of fluorescence after probe detachment at 0, 61, and 90s, together with corresponding calcium dynamics. The red arrow indicates the stimulation time. Scale bar 50 µm.

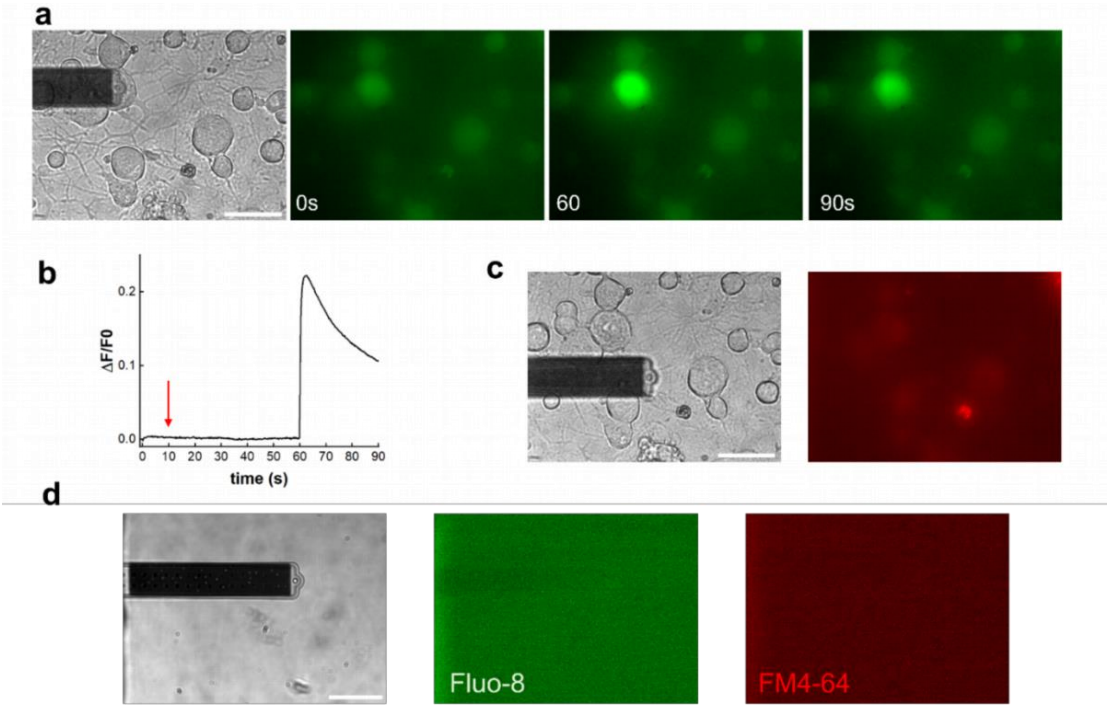

Figure 4.8 **Cell response at the probe detachment in presence of FM4-64 membrane marker. (a)** Bright field and time-lapse images of fluorescence after probe detachment at 0, 60, and 90s, and (**b**) calcium dynamics in which the red arrow indicates the stimulation time, (**c**) the probe is moved out of the stimulated cell and a fluorescence image for FM4-64FX (red signal) is acquired to monitor the membrane presence. (**d**) The probe was also moved in an area in absence of cell and both channel for Fluo-8 (green signal) and FM4-64FX (red signal) were acquired. Scale bar 50 µm.

To quantify these events, we evaluate the percentage of responding cells and the intensity of fluorescence signal (***Fig. 4.9***). Both at 24h and 48 h culture, this type of response appears to be more frequent for negative pressure (-40 and -80 mbar), with an increment at -80 mbar (***Fig. 4.9a, b***), while the signal intensity remains relatively consistent at both pressures (***Fig. 4.9a, c***). This effect is remarkably reduced for positive pressures.

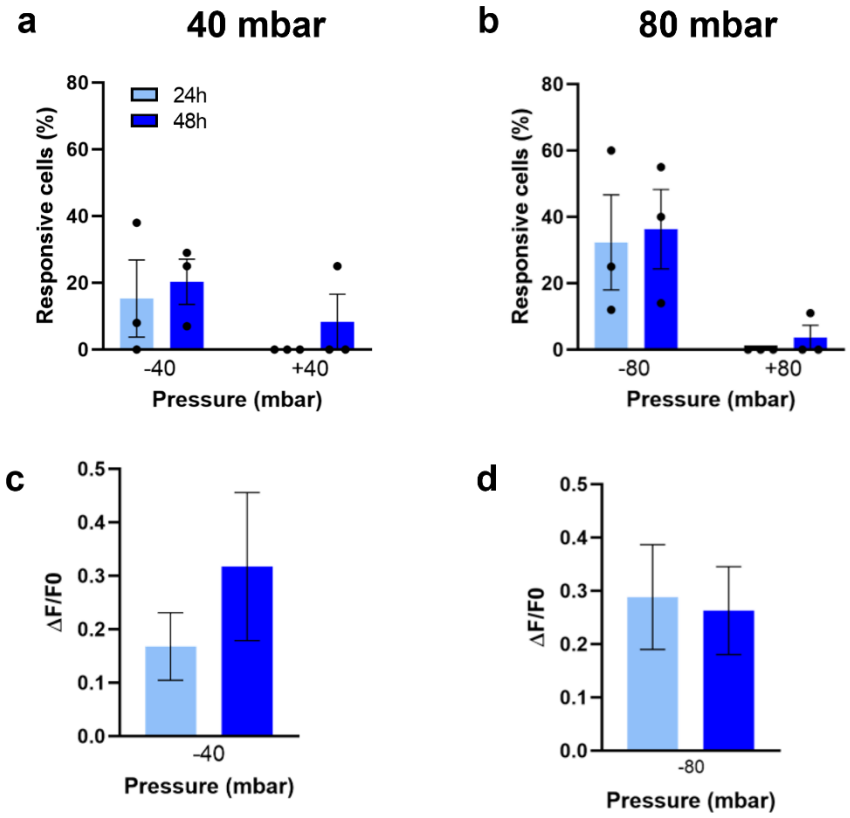

Figure 4.9 **DRG neurons response at different culture time at probe detachment. (a)** percentage of DRG neurons exhibiting increase in calcium signal response at the probe retraction for +/- 40mbar (**b**) or +/-80mbar at 24h or 48h culture time. (**c**) Intensity of the signal for +/- 40mbar (**d**) and +/- 80mbar. The data are shown as mean ± sem. Intensity for positive value was not reported since it was not observed at 24h. For each pressure a total of cells *n*=30-40 were analyzed.

In a very recent study by using a novel FluidFM probe with cylindrical tip, Lüchtefeld et al. (Lüchtefeld et al., 2024) demonstrated that membrane tension remains highly localized at the probe area and that only, in the absence of cytoskeletal elements, tension was able to propagate over longer distances. In our configuration, we can assume that the plasma membrane is deformed primarily at the point where pressure is applied, meaning that the mechanical stimulus remains confined to this

region. As a consequence, only mechanosensitive calcium channels located within or immediately surrounding the area of probe contact area are activated.

Instead, in the case of the response observed during probe retraction, we can hypothesize that during negative pressure stimulation, even after the pressure is released, the membrane remains slightly curved and trapped in the cantilever aperture. As the probe is retracted, the surrounding membrane is pulled, causing further membrane stretching. Presently, we lack precise information about the extent of membrane stretching during this retraction, but we can envisage two scenarios: (i) the increased membrane tension propagates, leading to the activation of additional mechanosensitive channels; or (ii) some channels in the area subjected to pressure, which were not initially activated, could be stimulated upon probe detachment. Without specific data to differentiate between these scenarios, it remains challenging to determine whether new channels are involved or if the same channels within the membrane patch are being activated.

4.4 Conclusions

In conclusion, FluidFM technique revealed that mechanosensitive calcium channels at the plasma membrane in DRG neurons respond to increased higher pressure +/-80 mbar, with higher conductance at negative pressures, especially after 48 hours of culture. This might indicate changing in mechanosensitive expression on glass or even different relocation of channels in the membrane after long culturing on flat rigid substrate. To confirm it, we should combine FluidFM with better ability to localize mechanosensitive channels, as for instance PIEZO2, highly involved in the transmission of the mechanical signal in these neurons.

CHAPTER 5

The impact of mechanical cues on dorsal root ganglion neurons polarization and PIEZO2 cellular localization

5.1 Introduction

The function of DRG neurons is strictly linked to their unique morphology, characterized by a single, bifurcating process that gives rise to both a peripheral and a central axonal branch (Nascimento et al., 2018). This structural arrangement is key to their ability to transmit sensory information. The peripheral branch primarily interfaces with target tissues such as skin and muscle, where it detects and relays sensory stimuli. In contrast, the central branch projects into the spinal cord, conveying processed signals to higher neural circuits. *In vivo*, the presence and activity of PIEZO2 channels have been observed at the peripheral sensory neuron endings (Villarino et al., 2023). However, on standard supports for in vitro culture, the polarization of DRG is lost and, as result, also PIEZO2 is likely redistributed within the DRG neuron.

External cues from the microenvironment significantly influence DRG morphology and, as a result, its functionality in physiological and pathological conditions (Koser et al., 2016; Pillai & Franze, 2024). This means that also the spatial distribution of PIEZO2 across the DRG can be affected by the mechanical stimuli from the microenvironment, including stiffness or anisotropy. Despite significant interest in the field, how physical signals determine DRG neuron morphology and functionality, and, in particular, the localization and organization of PIEZO2 remains unclear.

The fundamental role of mechanical forces in morphogenesis, and cell differentiation is widely demonstrated and described (Alvarez & Smutny, 2022). Similarly, mechanosensing of microenvironmental biophysical cues and subsequent mechanotransduction are strongly involved in the regulation of neuronal cell development and function in central and peripheral nervous system (Chighizola et al., 2019; Franze, 2013; Pillai & Franze, 2024). The axonal growth and elongation are guided and modulated by external applied forces(de Vincentiis et al., 2020; Franze & Guck, 2010; Kilinc et al., 2015, Sauter and Miller, 2020). As results substrate stiffness and topography emerged as potential features to manipulate neuronal organization and growth (Sirkkunan et al., 2022). In particular, the use of nano and micro-patterned substrates, including grooves and pillars, provides a controlled and reproducible tool for inducing neural cell polarization and axonal guidance (Repic et al., 2016; Sunnerberg et al., 2021; Tonazzini et al., 2013).

The ability to control and direct neuronal growth *in vitro* has important consequences not only for applications in tissue engineering, neural repair, but also for uncovering the mechanisms that underlie sensory perception and neuropathic conditions.

In this chapter, we exploited directional micro-patterned gratings to investigate how topographical stimuli can promote directional axonal elongation and the PIEZO2 channels' organization within cells. Polydimethylsiloxane micro-grooved substrates, with gratings' pattern with period of 2 μm and 20 μm (period= ridge + groove width) were fabricated by solvent casting, and used as culture supports for mouse DRG neurons or HEK cells. The transfection of HEK cells with PIEZO2-green lantern, a fluorescent chimera protein, enables us to localize the PIEZO2 channel within the cells.

The impact of the topographical features on DRG/ HEK morphology, mechanics and PIEZO2 arrangement within HEK transfected cells was investigated by confocal microscopy and atomic force microscopy (AFM).

5.2 Experimental section

5.2.1 Fabrication of aligned micro-patterned substrates

By using solvent casting, polydimethylsiloxane (PDMS) micro-grooved substrates with gratings' pattern were fabricated, as described in (Tonazzini et al., 2015). They have gratings (GRs) with a period of 2 μm or 20 μm (period= ridge + groove width). Flat PDMS regions of the same substrates were used as control.

5.2.2 Culture preparation of DRG neurons

The culture of DRG neurons was prepared as described in *Chapter 4*. GRs substrates were treated using an oxygen plasma process for 30 seconds at 40 W to ensure surface activation. After treatment, the substrates were coated with poly-L-lysine (100 μg/mL) for 30 min and then with 2% Matrigel (SIAL, #356231) for at least 20 min both at room temperature (RT) to promote cell adhesion. Subsequently, DRG neurons were seeded on the coated substrates and maintained in a humidified incubator at 37°C with 5% CO_2 for 24h.

5.2.3 Immunofluorescence staining of DRGs

After 24-48h culture DRG were fixed with 4% paraformaldehyde (PFA) for 15 minutes at 4°C. After fixation and 4 rounds of PBS 1X washes DRG were incubated for 20 minutes in the blocking solution, composed by 0.3% Triton X-100 and 2% serum (generally from the specie on which the secondary antibodies were harvested) in PBS 1X at RT. Then, neurons were incubated with primary antibodies

Anti- β3 Tubulin in rabbit (abT2200, Sigma-Aldrich,1:500) diluted in blocking solution for 1h at RT. After extensive rinses with 0.3% Triton X-100 in PBS, DRGs were incubated with secondary antibody Anti-Rabbit 488 (abA21206, Invitrogen, 1:250) diluted in blocking solution for 1h at RT. DRGs were extensively rinsed with 0.3% Triton X-100 in PBS, mounted on glass slides with ProLong Diamond Antifade Mountant (ThermoFisher, #P36970).

5.2.4 HEK-293 cells transfection and staining

Human embryonic kidney (HEK-293) cells were seeded on GRs, previously coated with poly-L-lysine (100μg/mL), with a 20.000 cells/cm^2. Cells were cultured in DMEM-GlutaMAX™ (Gibco, #31966-047) supplemented with 10% FBS (Euroclone, #ECS0180L) and 1% Penicillin-Streptomycin (Euroclone, #ECB3001D). Cells were maintained at 37 °C and 5% CO_2 in a humidified incubator. Transfection was performed after 24 horus,at a ratio of 650 ng of DNA to 7.2 μL of linear PEI (0.33mg/mL). Linear PEI solution was added to the DNA one, vortexed and incubated for 15 minutes at room temperature.

Then, the transfected cells were left over-night (about 14-16 hours) in incubator at 37 °C and 5% CO_2 . Afterward, the cells were used for experiments.

HEK cells were stained with CellMask-deep red (ThermoFisher, C10045) to label plasma membrane. Then, the cells were incubated for 15 minutes at 37°C in a humidified incubator with 5% CO_2. After being adequately rinsed, the cells were fixed for 15 min in 4% paraformaldehyde in PBS at RT. After washing, samples were mounted using Fluoroshield histology mounting medium with 4′,6-diamidino-2-phenylindole (DAPI) (SigmaAldrich, F6182).

5.2.5 Confocal imaging

The samples were imaged using a Zeiss LSM 800 (Jena, 439 Germany) inverted confocal microscope with a 40 × 1.5 numerical aperture oil immersion objective using 3 laser lines (405, 488, and 647 nm). The pinhole aperture was set at 1.0 airy. Each reported confocal image was obtained from a z-series (total stack-depth was within 10 μm; steps = 1 μm). The resulting z-stack was processed by ImageJ software (NIH, USA) into a single image using ‘z-project’ and ‘Max intensity’ options.

5.2.6 Cell morphological analysis

DRGs orientation was quantified by analyzing the β3 Tubulin fluorescence signal with the “Directionality” tool of the software FIJI (http://fiji.sc/Fiji), as described in (Tonazzini et al., 2015). This plug-in returned a directionality histogram by exploiting image fast Fourier transform (FFT) algorithms: isotropic images generate a flat histogram, whereas oriented images give a peaked histogram. These histograms were finally fitted by Gaussian curves, whose centre provided the center

of the Gaussian curve, which represents the direction in which the image is oriented (here normalized to the GR pattern orientation direction). We analysed at least 4 fields per sample, with image dimensions kept fixed to 320x320 µm2. We performed n ≥ 3 independent experiments for each condition.

The confocal images of HEK cells were also used to evaluate single-cell morphology and PIEZO2 intracellular distribution, by ImageJ (NIH). Single cell contours were drawn by the “Polygon selection” tool on the z-stacks (Cell mask + GFP channels) and processed by the "Measurement" tool (with the options "Area", “Fit ellipse”, and "Feret's diameter"). The parameters measured in this analysis were: cell area (µm^2); cell aspect ratio (AR): the ratio between the length of the major axis and the minor axis for the best-fitted ellipse of the cell. The orientation of the patterns was measured by the “Angle tool” of ImageJ; for FLAT membranes, a random direction was chosen.

5.2.7 Quantification of PIEZO2 signal localization in HEK cells

To localize the signal of PIEZO2, the confocal images of HEK-PIEZO2 transfected cells were processed with ImageJ. All PIEZO2-positive cells’ images were rotated to have the cell main axis on the vertical direction and then processed. On each single cell, two plot profiles along the major axis of PIEZO2-fluorescent signal (P1 and P2) were traced from the nucleus’ center up to the cell’ boundary, as schematically shown in ***Figure. 1.*** The resulting profiles were then plotted and analysed by Origin-Pro software. The distance profile and the fluorescence intensity were normalized for the maximum values: (dmax) for the distance nucleus-end cell profile, and (Imax) for fluorescence intensity.

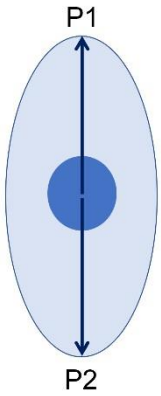

Figure 5.1 **Scheme of simplified cell to illustrate the traces of the plot profiles evaluated along the major axis**: P1 and P2 from the nucleus (*dark blue*) to the end of the cell (*arrow*).

5.2.8 Quantitative imaging by Atomic Force Microscopy

Quantitative imaging (QI) by atomic force microscopy (AFM) was performed by a NanoWizard III AFM (JPK Instruments, Bruker) integrated with an inverted optical microscope Olympus IX71.
QI-AFM of DRGs was performed on living cells in culture medium and fixed cells in PBS. Such AFM imaging modality is more appropriate for highly corrugated sample that can be now easily and non-destructively imaged because of the large Z-range. QI mode delivers real force curves for each pixel and therefore provide also the possibility to get reliable quantitative data with highest resolution. A major advantage of this modality is, that no lateral forces act on the sample during scanning. This preserves the sample and the tip from destructive interaction. Cantilever with nominal k= 0.07 N/m (MLCT -Bruker) were used for imaging. Imaging parameters were adjusted to obtain stable force-indentation curve. In general, a force of 0.5nN, pixel time 6-10 ms and Z length 600-800 nm were used for imaging. Resulting topographical images were processed and analysed by Gwyddion free software.

5.2.9 AFM-indentation measurements

AFM-based indentation measurements were performed using a NanoWizard III AFM (JPK Instruments, Bruker) integrated with an inverted optical microscope (Olympus IX71) for sample observation. DRG neurons were analysed in petri-dish and in culture medium at room temperature. The status of cells was constantly monitored by optical microscope. MLCT-SPH probes (Bruker), 20µm tall cylindrical tip shank with a spherical tip radius of 5 µm, were used as indenters.
Using the optical microscope, the probe was brought over the soma of single DRG and pressed down to indent the cell. The motion of the z-PIEZO and the force were recorded. On each cell three to five force–displacement curves were acquired with a force load of 1nN and at a rate of at 5µm/s in closed-loop feedback mode. Cell elastic properties can be assessed by determining the young's modulus (E), which can be evaluated by fitting the force-indentation curves with the Hertz model:

$$F = \frac{4}{3}\frac{E}{(1-\nu^2)}\sqrt{R}\delta^{3/2}$$

where (F) is the force, (R) is the radius of the spherical indenter and (ν) is the sample's Poisson ratio (set to 0.5 for the cell) and (δ) is the indentation depth.
Data fitting was performed on the approaching part of the recorded force-distance curves. JPK Data Processing software was used to convert the force-distance curve into the force–indentation curve by

subtracting the cantilever bending from the signal height to calculate indentation. Fitting with the Hertz model was performed by a Matlab routine for indentation of 2 µm.

5.2.10 Statistical Analysis

All the experiments were repeated at least three times independently for each condition. Data are reported as the average value ± the standard error of the mean (mean ± SEM), unless differently stated. For statistical analysis One-Way ANOVA test (Bonferroni Multiple Comparison test was performed to compare multiple conditions) or Student's t-test (when comparing two different conditions) were used. Results are considered statistically significant for $p < 0.05$.

5.3 Results and Discussions

5.3.1 Aligned micro-patterned substrates guide axonal growth of DRG neurons

Before experiments with cells, the micropattern substrates' gratings (GRs) were characterized by QI-AFM imaging (***Fig. 5.2***), which confirmed that they have a period of 2.0 ± 0.1µm for T2, and 19.4 ± 0.3 µm for T20, with a depth of 180 ± 9 nm for T2 and 327 ± 18 nm for T20, as evaluated by cross section profile.

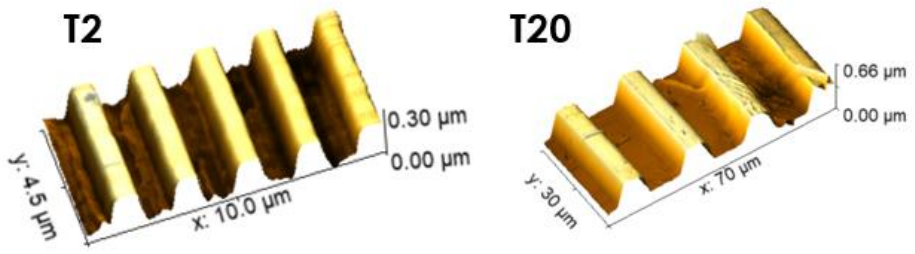

Figure 5.2 **Gratings characterization by QI-AFM imaging**. 3D representation of topography images of T2 and T20 GRs acquired in PBS solution after Matrigel coating by QI-AFM modality.

To test DRG neurons behavior and their ability to polarize on micropatterned substrates, dissociated DRG cell suspensions were seeded onto GRs with 2µm and 20µm periodicity and on flat PDMS substrates, both uniformly coated as described in the experimental section.

To investigate axonal directionality, we analyzed the organization of β3-tubulin signal. Already after 24h culture, DRG neurons soma were surrounded by extended axonal processes. These axonal processes grew without specific orientation on standard flat coverslips, while on GRs we observed

that they are efficiently oriented along the pattern both on T20 and on T2 (***Fig. 5.3a***). DRG interacting with GRs extended their axonal protrusions aligned to the pattern direction (β-tubulin directionality = 12 ± 3° on T20 and, 5 ± 1° on T2), while a random alignment was observed, as expected, on flat PDMS (β-tubulin directionality = 45 ± 4°) (***Fig. 5.3b***).

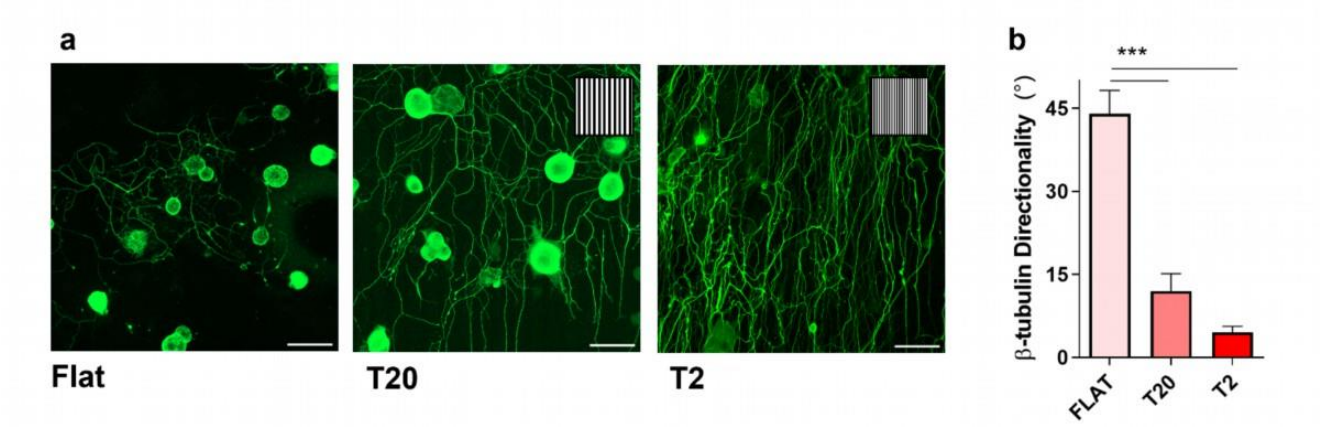

Figure 5.3 **Representative confocal images of DRG stained with ß3-tubulin on different patterned substrates and directionality analysis. (a)** Drg neurons were stained with ß3-tubulin after 24-48 hours on PDMS flat and micropatterned T20 and T2 GRs**.** In the inset is schematically reported the grating orientation.(**b**) Process-tubulin directionality data are reported as (mean ± SEM), number of samples n= 5 for flat, n=3 on T20, and n=7 for T2. *** ($p<0.001$). Scale bar 50µm.

These results, in agreement with literature data (Repic et al., 2016; Sunnerberg et al., 2021; Tonazzini et al., 2013), indicate that axonal guidance in DRG neurons is strongly sensitive to linearized micro-patterns, which represent physical constrains similar to that encountered *in situ* in the extracellular environment. We noticed that DRG neurons respond efficiently in terms of contact guidance to GRs, particularly on the smaller ones (i.e. T2).

5.3.2 Topography of the oriented axon on aligned micro-patterned substrates

To visualize whether the axon growth on top of the ridges or into the grooves we analysed the their morphology by using QI-AFM imaging. We focused on DRGs on T2 GRs, which appear to be particularly efficient for contact guidance of DRGs. We generally observed that when the size of axonal processes is smaller than or comparable to the groove width, they can grow linearly into the grooves (***Fig. 5.4b, c, e),*** whereas in other cases they align along the ridges following the pattern direction (***Fig.5.4d*****).** Moreover, we noticed also that when these axonal processes grow into the groove, they can grasp the lateral border of ridges suggesting a strong interaction with them (***Fig. 5.4e, f*** blue arrow). We can hypothesis that they represent anchoring points, where the axon senses

environmental cues and remains stably anchored to the micropattern guide. On the contrary, on flat substrates (***Fig.5.5***), DRGs display random axonal processes that in some cases cross large fibroblasts as shown in ***Figure 5.5b-d***. In general, these topographical images suggest that the axonal processes, irrespectively of their size and location, orient themselves according to the gratings' topographical pattern both along the ridges or into the grooves.

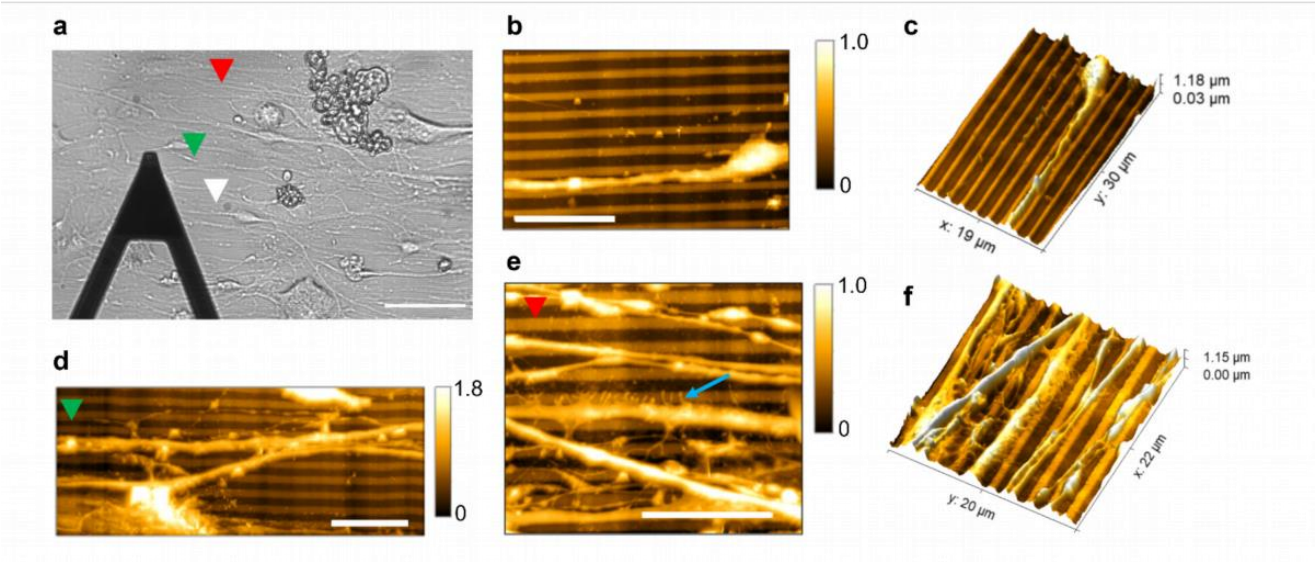

Figure 5.4 **Representative QI-AFM images of DRG axonal processes on GRs**. (**a**) Bright field image of a sample area, (**b**) axonal process aligned into the grooves of T2-GR, and (**c**) corresponding 3D representation; (**d**) axonal process on the ridges; (**e**) an example of axonal process into the groove with lateral cell anchoring point as indicated by the blue arrow, (**f**) corresponding 3D representation. The colored triangles indicated scanned areas. Scale bar of bright field image 50µm. Scale bar for all QI images 10µm.

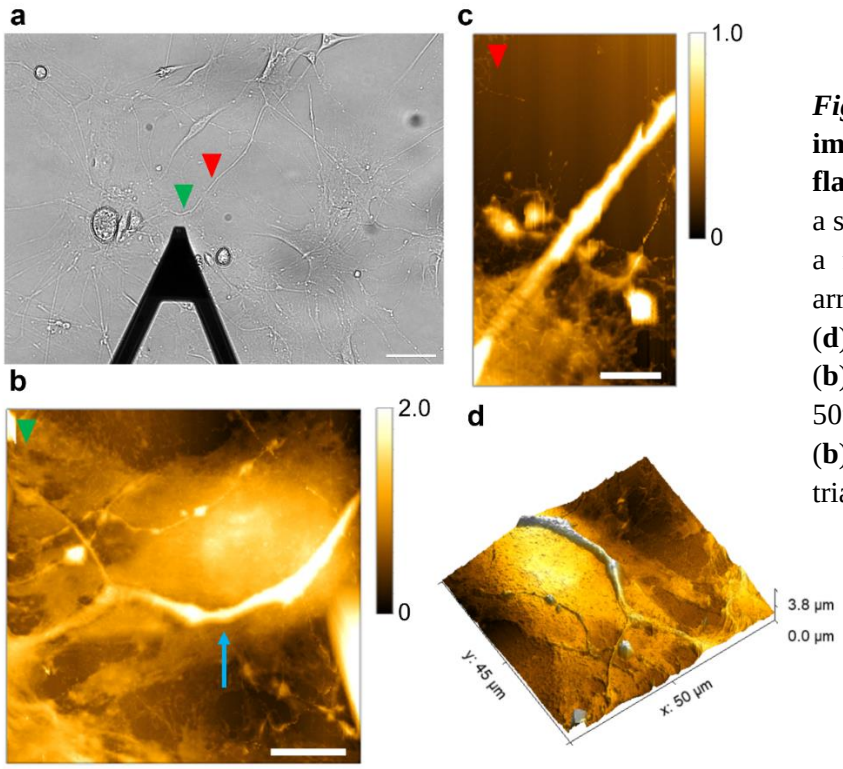

***Figure 5.5* Representative QI-AFM images of DRG axonal processes on flat substrates.** (**a**) Bright field image of a sample area, (**b**) axonal process across a fibroblast as indicated by the blue arrow, (**c**) the rest of the same process: (**d**) 3D view of topography reported in (**b**). Scale bar in bright field image 50µm. Scale bar for QI images 5µm in (**b**) and 10µm in (**c**). The colored triangles indicated scanned area.

5.3.3 The elasticity of DRG's soma is not affected by surface topography

Variation in cell stiffness in response to substrate mechanics is widely observed in different cell type, which is frequently correlated to their cytoskeleton reorganization (Doss et al., 2020). To test the potential impact of T2-GR topography on DRG elasticity, we assessed the mechanical properties of DRG neurons using AFM-based indentation measurements. These measurements were performed on the soma of neurons cultured on glass (stiffness in the GPa range), on flat PDMS (stiffness in the MPa range), and on T2-GR (with a stiffness comparable with that of flat PDMS but with a distinct topography). As shown in ***Figure 5.6a***, once selected the soma is indented by the AFM-probe.

The Young's modulus (*E)* values obtained for the DRG's soma on flat PDMS and T2-GR substrates do not change significantly as respect to glass substrates (***Fig. 5.6b***).

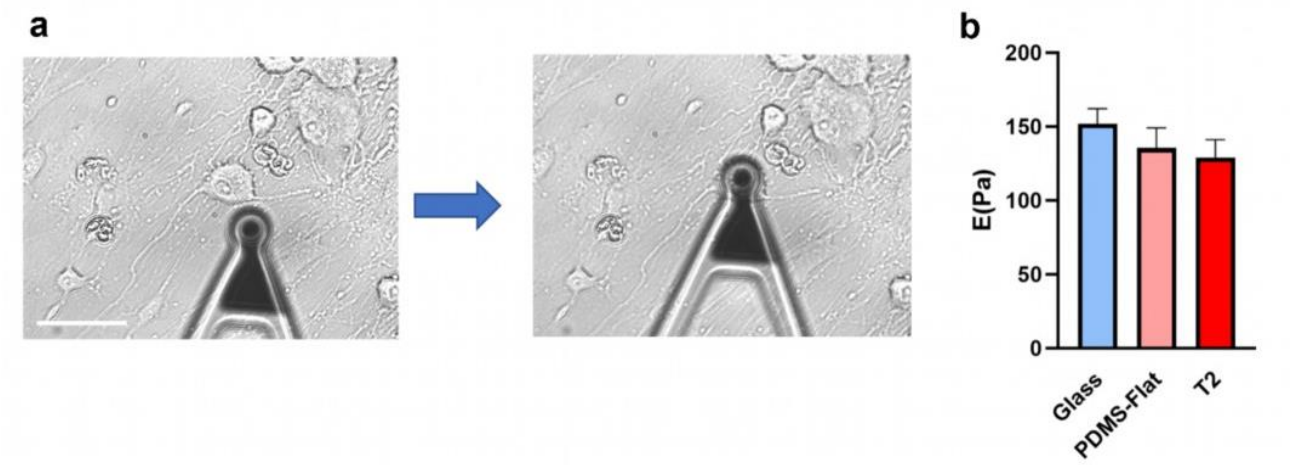

Figure 5.6 **Representative AFM images of indentation measurements of DRGs and cell elasticity.** (**a**) Bright field image of a selected soma of mouse DRG neuron on T2-GRs and AFM probe positioning at the centre of soma for indentation measurements; Scale bar 50 µm. (**b**) The *E* values of soma obtained for the DRGs cultured on glass standard petri dish, flat PDMS and T2-GRs; Number of cells analysed: n =45 for glass; n=29 on PDMS flat and n=41 on T2-GR. Data are reported as (mean±SEM).

These findings indicate that substrate geometry has no effect on the stiffness of DRG' soma. Hence, while the PDMS micro-patterns strongly influences the DRG neurons' polarization, their topography has neglectable effects on soma mechanics.

5.3.4 Aligned micro-patterned can orient PIEZO2 expression

After observing that GRs efficiently induce DRG polarization, we exploited them to polarize HEK cells and to investigate the impact on PIEZO2 cellular distribution. To achieve this, we used HEK cells transfected with PIEZO2-Green Lantern plasmid. In this configuration, the GFP-like protein is fused to the PIEZO2 channel, allowing for easier and undoubtedly identification of PIEZO2 location within the cell. This approach enables to overcome the problem of identifying PIEZO2 via immunostaining *in vitro*. Commercially available antibodies for PIEZO2 often are observed to be not sensitive or not specific enough to detect PIEZO2 (Zhu et al., 2023), as we also observed in preliminary experiments. Therefore, using a fluorescent protein-tagged PIEZO2 fusion offers a more reliable approach for studying the channel's localization in cells.

HEK cells were seeded on GRs and flat substrates and transfected with PIEZO2-Green Lantern. After fixation and additional staining for nuclei and cell membranes, the cells were imaged using confocal microscopy. The morphology of HEK cells was analyzed, by evaluating their aspect ratio. The data

demonstrated that the cells are more elongated on GRs as respect to flat substrates, used as control condition (***Fig.5.7***). Hence, GRs are effective in inducing HEK cell polarization along the pattern.

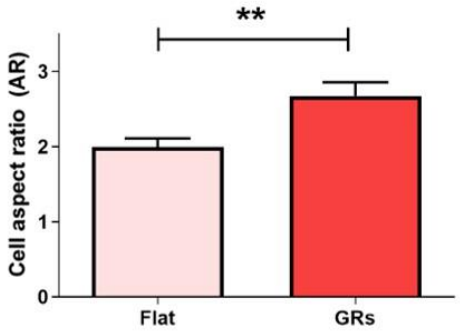

Figure 5.7 **HEK Cell morphology analysis on flat vs. GRs via aspect ratio.** HEK cell morphology analysis on flat substrates (Flat) and on grating (GRs), by using cellular aspect ratio. Cell analyzed in total n= 30 for GRs and n=37 for flat substrates. Data are reported as (mean±SD); ** ($p < 0.0022$).

By comparing the confocal images, we noticed that on flat substrates, the PIEZO2 signal is uniformly expressed in the cytoplasm (***Fig. 5.8a***), whereas when cells are more elongated/polarized, as it is on GRs, it seems to be mainly located at the periphery of the cell (***Fig. 5.8b***).

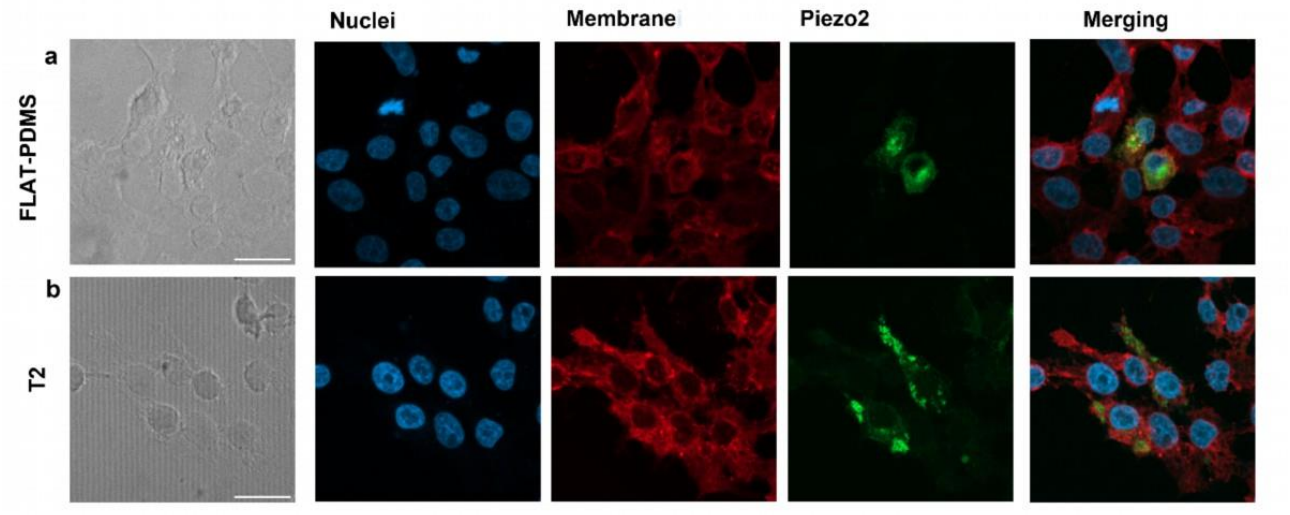

Figure 5.8 **Confocal images of transfected HEK cells on flat vs GRs**. (**a**) Representative confocal images of HEK cells transfected PIEZO2-green lantern on flat PDMS (**b**) and on T2-GRs; from left to right: bright field image, dapi (*blue signal*), cell plasma membrane (*red signal*), PIEZO2 (*green*) and merged image. Scale bar 20 µm.

This behavior can be better visualized by a plot profile traced from the nucleus's centre up to the end of the cell (***Fig 5..9*)**. In the case of cells on GRs, it is possible to see that the PIEZO2 signal appears to be mainly located at the edge of the cell, often along the major axis (***Fig. 5.9a***), whereas on flat substrates the signal appears to be more uniformly distributed in the whole cell (***Fig. 5.9b***).

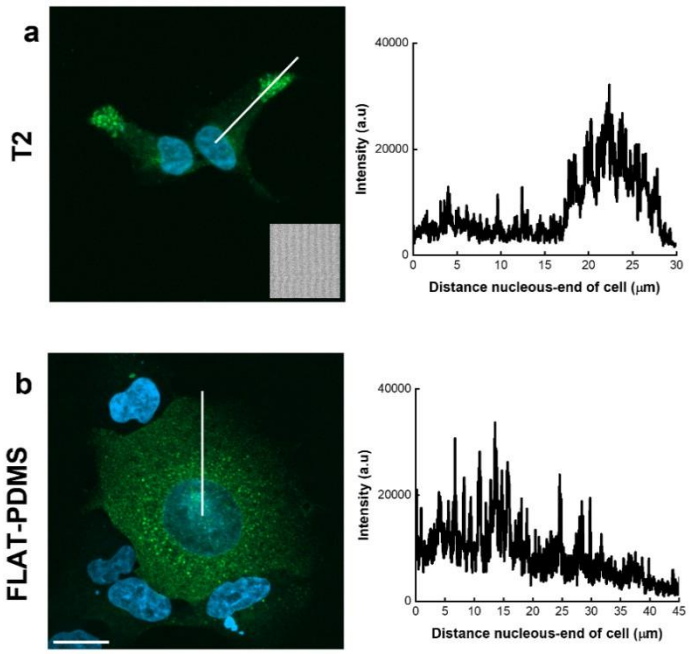

***Figure 5.9* Confocal images of transfected HEK cells on GRs vs flat.** (**a**) Representative confocal images of HEK cells transfected with PIEZO2-green lantern on T2-GRs (**b**) and on flat PDMS substrates. For both panel (a and b) from left to right: merged image of nucleus (*blue signal*) and PIEZO2 (*green signal*), profile obtained along the white line. Scale bar 20 μm.

To quantitatively describe this behavior, the plot profiles of Piezo2 signal intensity along the major axis (P1+P2, obtained as described in experimental section) of all PIEZO2-trasfected cells were normalized and averaged ***(Fig. 5.10)***. The results showed that, in general, for PIEZO2-transfected cells the fluorescence signal raises at the cell edges on GRs (***Fig. 5.10a***), while it is quite uniform within the cells on flat substrates (***Fig. 5.10b***). Being the cells more elongated on GRs, we envision a link between cell elongation and Piezo2 intracellular localization.

To focus the analysis on more elongated cells, we selected the cells with an AR ≥2. The profiles of these cells were then averaged and replotted. This data refinement confirmed that, for cells on GRs (***Fig. 5.10c***), the fluoresce signal increases with the distance from the center of the nucleus, at the cell ends, whereas this trend is not observed on flat substrates (***Fig. 5.10d***).

Overall, this analysis reinforces the initial observations, suggesting that in polarized or elongated cells on GRs, PIEZO2 channels are predominantly localized at the cell periphery along the major axis.

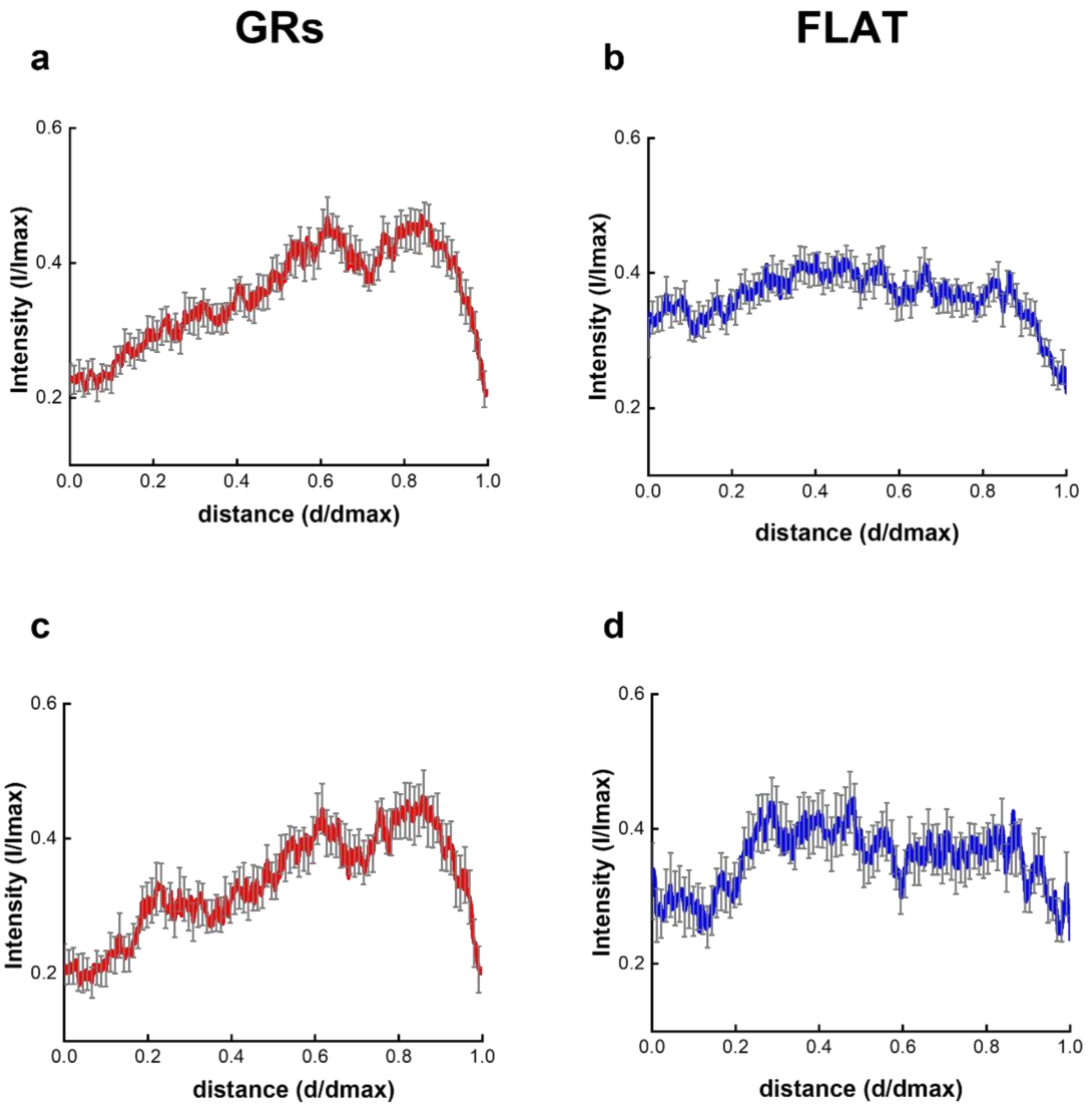

Figure 5.10 **Plot profiles along major axis of transfected HEK cells on flat vs GRs substrates**. (**a**) average of plot profiles obtained for all cells on GRs (*red curve*) and (**b**) on Flat substrates (*blue curve*). Cell analyzed in total n= 29 for GRs and n=31 for flat substrates. (**c**) average of plot profiles obtained for cells with AR > 2 for GRs and (**d**) flat substrates. For AR>2 number of cells on GRs n=19 and on Flat substrate n=12. Data are shown as (mean ± sem). Independent experiments for GRs n=3 and n=4 for Flat substrates.

5.4 Conclusions

These results show that micropatterned PDMS substrates with different periodicities (2 µm and 20 µm) promote DRG polarization and axonal alignment along the grating patterns, as demonstrated by confocal imaging and QI-AFM. The topography images show that these axonal processes can either grew along the ridges or aligned within the grooves.

Mechanical measurements indicate that the micro-patterned topography does not significantly change the stiffness of the DRG soma, suggesting that these features do not impact soma mechanics.

Micropatterned substrates induce cell polarization also in HEK cells, though to a smaller extend. HEK cells on GRs show increased elongation and higher aspect ratio. Since micropatterns facilitate cell elongation, they were exploited to study intracellular PIEZO2 expression in HEK-PIEZO2 transfected cells. Here HEK cells, grown on GRs substrates, display a more localized distribution of the PIEZO2 signal at the cell's periphery, while such distribution was less common on flat substrates where cells are mainly rounded and less polarized. These findings indicate that microstructural cues can influence cell polarization and distribution of PIEZO2 channels in cells.

CHAPTER 6

Final conclusion and future prospects

The ability of cells to sense and respond to mechanical forces from their environment is a fundamental biological process conserved throughout evolution. In somatosensory system, mechanotransduction pathways enable organisms to perceive tactile stimuli, process auditory signals, and regulate proprioception. The discovery of PIEZO channels has marked a new era in understanding mechanotransduction in mammals. In general, PIEZO1 participates in a wide range of physiological processes, while PIEZO2 mainly acts in somatosensation. Despite significant progresses, several fundamental questions about their gating mechanism remain still unresolved.

This thesis is particularly focused on PIEZO2, about the effect of intensity of applied forces, stimulus duration, directionality on the channel activation, and the influence of geometrical cues on its localization. Since PIEZOs discovery, electrophysiology, using stretch and poke stimulation methods, has been the golden tool for exploring these channels. However, these approaches have some limitations: in the poke configuration, precise control of applied forces is challenging, and the measurement pipette itself may introduce additional mechanical stimulation. In other configurations, such as the stretching method, the membrane-cytoskeleton interaction can be altered.

To address these issues, we employed Atomic Force Microscopy (AFM) based approach combined with calcium imaging. This nanotechnological approach enabled the application of controlled force, vertical pressure and localized stimulus on PIEZO2 transfected HEK cells without disrupting the membrane-cytoskeleton interface, offering insights into PIEZO2 function in near-physiological conditions. PIEZO2, known for mediating rapidly adapting mechanically activated currents in DRG neurons, was analyzed under two different stimulus durations: a short stimulus and a longer one. Our results demonstrated that at low indenting pressure (+10mmgH), HEK cells overexpressing PIEZO2 responded more efficiently to shorter stimuli, in line with its established physiological function of the channel. Additionally, the use of dual calcium dyes, targeting different cellular compartments, suggested the possibility that transfection may extend to organelles. The data further revealed that calcium influx through ion channels, sourced from both extracellular and intracellular compartments, varied depending on the duration of the mechanical stimulus. AFM in combination with calcium imaging, provided an additional advantage by enabling us to visualize not only the response of the stimulated cell, but also of neighboring ones. This revealed a collective response to mechanical stimulation, highly pronounced when stimulating overexpressing PIEZO2 transfected cells in presence of calcium dye able to access all cellular compartments. However, a key limitation emerged: we could only track calcium ion, limiting the ability to capture simultaneous the dynamics of other

cations that may be responsible of this collective cell response. This issue could be addressed by integrating AFM with patch-clamp electrophysiology, which can monitor multiple ion currents simultaneously.

Despite the precision in force, pressure application and stimulus positioning provided by AFM, another possible limitation arises: mechanical stimulation of the bead modified cantilever can activate mechanosensitive channels on both the plasma and intracellular membranes. To overcome this issue and target specifically the plasma membrane channels, advanced methodologies such as Fluidic Force Microscopy (FluidFM) can be utilized, offering modulation of cellular environment dynamically with high spatial resolution. This technique was used to deform DRG neuron plasma membrane enabling the exploration of the cell's response to pressure and aspiration in a single experiment. By using quantitative PCR (qPCR), we analyze the expression of mechanosensitive channels in mouse DRG, which, as expected, confirmed the higher expression of PIEZO2. However, it is important to note that dorsal root ganglion neuron cultures consist of a heterogeneous mix of sensory neurons: mechanosensory, nociceptors and thermal neurons. To enhance the specificity of our analysis, we conducted immunofluorescence experiments by using antibodies targeting mechanosensory neurons (NF-200). This approach provided a quantitative estimatation, indicating that in our sample 40% of neurons are mechanosensitive and proprioceptive, while 15% are low threshold mechanoreceptors. Furthermore, in order to limit the stimulation to mechanosensory neuron, we selectively stimulated DRGs with large soma, which are typically identified as mechanosensory, while smaller neurons are classified as nociceptors. Concerning results obtained from FluidFM, they revealed differential responses to lower (40mbar) and higher (80mbar) pressures depending on the culture time. In general, we noticed that a higher response is observed at 48h culture time, in particular with higher conductance at negative pressures (-80 mbar). This could suggest alterations in the expression of mechanosensitive channels on glass surfaces or changes in their membrane localization following prolonged culturing on flat, rigid substrates. Moreover, we detected a calcium signal also upon probe detachment, suggesting an important role of further stretching the plasma membrane in the activation of mechanosensitive channels included or adjacent to the stretched membrane. We do not yet know which channels—those in the region at the probe aperture or the surrounding area—were activated, so it would be useful to combine FluidFM with super-resolution microscopy to investigate this further. This would allow us to directly visualize the channels involved in the cell response by visualizing for instance the green lantern PIEZO2 channel in vitro. In FluidFM experiments, we focused on stimulating the soma of DRG neurons, as their physiological polarization is typically lost when cultured on flat surfaces. To investigate the effect of geometrical cues on DRG morphology, we utilized micropatterned substrates with specific periodicity, which effectively restored DRG polarization. The possibility to localize the PIEZO2 position in the DRG would be crucial at this point. However, up to now commercially available antibodies for PIEZO2 provide unreliable results,

as also we observed in testing experiments. Hence, we tested the PIEZO2 tagged with a green fluorescent protein transfected in HEK cells, and we observed that passive geometric cues can influence the localization of mechanosensitive channels. These findings suggest that a static mechanical stimulus from cell microenvironment can determine not only cellular orientation, but may also play an important role in the cellular distribution of mechanosensitive ion channels. In future, additional investigations can provide a deeper understanding about the precise localization of PIEZO2 channels. As for instance, using DRG neurons, where PIEZO2 channels can be clearly identified, would provide definitive insights into their localization in response to mechanical cues from the cellular microenvironment.

This study employed a multidisciplinary approach, integrating various nanotechnological techniques and methodologies, that enabled to highlight several characteristics of PIEZO2 channels behavior and activation. From these findings, as also from present literature, it emerges that the integration of multiple methodologies (e.g. AFM, FluidFM, micro and nanostructure substrate, electrophysiology, and super-resolution microscopy) represents a powerful approach to unveil how dynamic and static forces affect the behavior and function of PIEZO channels. Advancing our understanding in mechanotransduction in neurons hold significant potential for innovative therapeutic applications in conditions related to mechanosensitive channel dysfunctions, such as neurodegenerative diseases, cancer, and pain.

REFERENCES

Abd-Elsayed, A., Vardhan, S., Aggarwal, A., Vardhan, M., & Diwan, S. A. (2024). Mechanisms of Action of Dorsal Root Ganglion Stimulation. *International Journal of Molecular Sciences*, *25*(7), 1–17. https://doi.org/10.3390/ijms25073591

Acheta, J., Bhatia, U., Haley, J., Hong, J., Rich, K., Close, R., Bechler, M. E., Belin, S., & Poitelon, Y. (2022). Piezo channels contribute to the regulation of myelination in Schwann cells. *Glia*, *70*(12), 2276–2289. https://doi.org/10.1002/glia.24251

Afzal, J., Chang, H., Goyal, R., & Levchenko, A. (2016). *Mechanics of Microenvironment as Instructive Cues Guiding Stem Cell Behavior*. 62–72. https://doi.org/10.1007/s40778-016-0033-9

Al-Lazikani, B., Hill, E. E., & Morea, V. (2008). Protein structure prediction. *Methods in Molecular Biology*, *453*, 33–85. https://doi.org/10.1007/978-1-60327-429-6_2

Albuisson, J., Murthy, S. E., Bandell, M., Coste, B., Louis-Dit-Picard, H., Mathur, J., Fénéant-Thibault, M., Tertian, G., De Jaureguiberry, J. P., Syfuss, P. Y., Cahalan, S., Garçon, L., Toutain, F., Simon Rohrlich, P., Delaunay, J., Picard, V., Jeunemaitre, X., & Patapoutian, A. (2013). Dehydrated hereditary stomatocytosis linked to gain-of-function mutations in mechanically activated PIEZO1 ion channels. *Nature Communications*, *4*(May). https://doi.org/10.1038/ncomms2899

Alsteens, D., Gaub, H. E., Newton, R., Pfreundschuh, M., Gerber, C., & Müller, D. J. (2017). Atomic force microscopy-based characterization and design of biointerfaces. *Nature Reviews Materials*, *2*(5). https://doi.org/10.1038/natrevmats.2017.8

Alvarez, Y., & Smutny, M. (2022). Emerging Role of Mechanical Forces in Cell Fate Acquisition. *Frontiers in Cell and Developmental Biology*, *10*(May), 1–7. https://doi.org/10.3389/fcell.2022.864522

Anderson, E. O., Schneider, E. R., & Bagriantsev, S. N. (2017). Piezo2 in Cutaneous and Proprioceptive Mechanotransduction in Vertebrates. In *Current Topics in Membranes* (Vol. 79). Elsevier Ltd. https://doi.org/10.1016/bs.ctm.2016.11.002

Angeloni, L., Popa, B., Nouri-Goushki, M., Minneboo, M., Zadpoor, A. A., Ghatkesar, M. K., & Fratila-Apachitei, L. E. (2023). Fluidic Force Microscopy and Atomic Force Microscopy Unveil New Insights into the Interactions of Preosteoblasts with 3D-Printed Submicron Patterns. *Small*, *19*(2). https://doi.org/10.1002/smll.202204662

Antony, J. S., Herranz, A. M., Mohammadian Gol, T., Mailand, S., Monnier, P., Rottenberger, J., Roig-Merino, A., Keller, B., Gowin, C., Milla, M., Beyer, T. A., & Mezger, M. (2024).

Accelerated generation of gene-engineered monoclonal CHO cell lines using FluidFM nanoinjection and CRISPR/Cas9. *Biotechnology Journal*, *19*(4), 1–6. https://doi.org/10.1002/biot.202300505

Árnadóttir, J., & Chalfie, M. (2010). Eukaryotic mechanosensitive channels. *Annual Review of Biophysics*, *39*(1), 111–137. https://doi.org/10.1146/annurev.biophys.37.032807.125836

Babcock, D. F., Herrington, J., Goodwin, P. C., Park, Y. B., & Hille, B. (1997). Mitochondrial participation in the intracellular Ca2+ network. *Journal of Cell Biology*, *136*(4), 833–844. https://doi.org/10.1083/jcb.136.4.833

Bae, C., Sachs, F., & Gottlieb, P. A. (2011). The mechanosensitive ion channel Piezo1 is inhibited by the peptide GsMTx4. *Biochemistry*, *50*(29), 6295–6300. https://doi.org/10.1021/bi200770q

Battistella, A., Andolfi, L., Stebel, M., Ciubotaru, C., & Lazzarino, M. (2023). Investigation on the change of spermatozoa flagellar beating forces before and after capacitation. *Biomaterials Advances*, *145*(December 2022), 213242. https://doi.org/10.1016/j.bioadv.2022.213242

Bavi, N., Richardson, J., Heu, C., Martinac, B., & Poole, K. (2019). PIEZO1-Mediated Currents Are Modulated by Substrate Mechanics. *ACS Nano*, *13*(11), 13545–13559. https://doi.org/10.1021/acsnano.9b07499

Beča, K. I. K., Girard, B. M., Heppner, T. J., Hennig, G. W., Herrera, G. M., Nelson, M. T., & Vizzard, M. A. (2021). The Role of PIEZO1 in Urinary Bladder Function and Dysfunction in a Rodent Model of Cyclophosphamide-Induced Cystitis. *Frontiers in Pain Research*, *2*(October), 1–12. https://doi.org/10.3389/fpain.2021.748385

Bettinger, C. J., Langer, R., & Borenstein, J. T. (2009). Engineering substrate topography at the Micro- and nanoscale to control cell function. *Angewandte Chemie - International Edition*, *48*(30), 5406–5415. https://doi.org/10.1002/anie.200805179

Beverley, K. M., & Levitan, I. (2024). Cholesterol regulation of mechanosensitive ion channels. *Frontiers in Cell and Developmental Biology*, *12*(January), 1–9. https://doi.org/10.3389/fcell.2024.1352259

Biela, S. A., Su, Y., Spatz, J. P., & Kemkemer, R. (2009). Different sensitivity of human endothelial cells, smooth muscle cells and fibroblasts to topography in the nano-micro range. *Acta Biomaterialia*, *5*(7), 2460–2466. https://doi.org/10.1016/j.actbio.2009.04.003

Binnig, G., Quate, C. F., & Gerber, C. (1986). Atomic force microscope. *Physical Review Letters*, *56*(9), 930–933. https://doi.org/10.1103/PhysRevLett.56.930

Botello-Smith, W. M., Jiang, W., Zhang, H., Ozkan, A. D., Lin, Y. C., Pham, C. N., Lacroix, J. J., & Luo, Y. (2019). A mechanism for the activation of the mechanosensitive Piezo1 channel by

the small molecule Yoda1. *Nature Communications*, *10*(1). https://doi.org/10.1038/s41467-019-12501-1

Braidotti, N., Demontis, G., Conti, M., Andolfi, L., Ciubotaru, C. D., Sbaizero, O., & Cojoc, D. (2024). The local mechanosensitive response of primary cardiac fibroblasts is influenced by the microenvironment mechanics. *Scientific Reports*, *14*(1), 1–14. https://doi.org/10.1038/s41598-024-60685-4

Brylka, L. J., Alimy, A. R., Tschaffon-Müller, M. E. A., Jiang, S., Ballhause, T. M., Baranowsky, A., von Kroge, S., Delsmann, J., Pawlus, E., Eghbalian, K., Püschel, K., Schoppa, A., Haffner-Luntzer, M., Beech, D. J., Beil, F. T., Amling, M., Keller, J., Ignatius, A., Yorgan, T. A., … Schinke, T. (2024). Piezo1 expression in chondrocytes controls endochondral ossification and osteoarthritis development. *Bone Research*, *12*(1), 1–16. https://doi.org/10.1038/s41413-024-00315-x

Bustamante, C. J., Chemla, Y. R., Liu, S., & Wang, M. D. (2021). Optical tweezers in single-molecule biophysics. *Nature Reviews Methods Primers*, *1*(1). https://doi.org/10.1038/s43586-021-00021-6

Cahalan, S. M., Lukacs, V., Ranade, S. S., Chien, S., Bandell, M., & Patapoutian, A. (2015). Piezo1 links mechanical forces to red blood cell volume. *ELife*, *4*(MAY), 1–12. https://doi.org/10.7554/eLife.07370

Cao, E., Liao, M., Cheng, Y., & Julius, D. (2013). TRPV1 structures in distinct conformations reveal activation mechanisms. *Nature*, *504*(7478), 113–118. https://doi.org/10.1038/nature12823

Cattin, C. J., Düggelin, M., Martinez-Martin, D., Gerber, C., Müller, D. J., & Stewart, M. P. (2015). Mechanical control of mitotic progression in single animal cells. *Proceedings of the National Academy of Sciences of the United States of America*, *112*(36), 11258–11263. https://doi.org/10.1073/pnas.1502029112

Chalfie, M. (2009). Neurosensory mechanotransduction. *Nature Reviews Molecular Cell Biology*, *10*(1), 44–52. https://doi.org/10.1038/nrm2595

Chaudhuri, O., Parekh, S. H., & Fletcher, D. A. (2007). *Reversible stress softening of actin networks*. *445*(January), 20–22. https://doi.org/10.1038/nature05459

Chen, C. S. (2008). *Mechanotransduction – a field pulling together ?* https://doi.org/10.1242/jcs.023507

Chen, C. S., Alonso, J. L., Ostuni, E., Whitesides, G. M., & Ingber, D. E. (2003). Cell shape provides global control of focal adhesion assembly. *Biochemical and Biophysical Research*

Communications, *307*(2), 355–361. https://doi.org/10.1016/S0006-291X(03)01165-3

Chen, W., Guillaume-Gentil, O., Rainer, P. Y., Gäbelein, C. G., Saelens, W., Gardeux, V., Klaeger, A., Dainese, R., Zachara, M., Zambelli, T., Vorholt, J. A., & Deplancke, B. (2022). Live-seq enables temporal transcriptomic recording of single cells. *Nature*, *608*(7924), 733–740. https://doi.org/10.1038/s41586-022-05046-9

Chighizola, M., Dini, T., Lenardi, C., Milani, P., Podestà, A., & Schulte, C. (2019). Mechanotransduction in neuronal cell development and functioning. *Biophysical Reviews*, *11*(5), 701–720. https://doi.org/10.1007/s12551-019-00587-2

Chopinet, L., Formosa, C., Rols, M. P., Duval, R. E., & Dague, E. (2013). Imaging living cells surface and quantifying its properties at high resolution using AFM in QI™ mode. *Micron*, *48*, 26–33. https://doi.org/10.1016/j.micron.2013.02.003

Constantinou, I., & Bastounis, E. E. (2023). Cell-stretching devices: advances and challenges in biomedical research and live-cell imaging. *Trends in Biotechnology*, *41*(7), 939–950. https://doi.org/10.1016/j.tibtech.2022.12.009

Cook, J. R., Carta, L., Bénard, L., Chemaly, E. R., Chiu, E., Rao, S. K., Hampton, T. G., Yurchenco, P., Costa, K. D., Hajjar, R. J., & Ramirez, F. (2014). Abnormal muscle mechanosignaling triggers cardiomyopathy in mice with Marfan syndrome. *Journal of Clinical Investigation*, *124*(3), 1329–1339. https://doi.org/10.1172/JCI71059

Corey, D. P., & Hudspeth, A. J. (1979). Response latency of vertebrate hair cells. *Biophysical Journal*, *26*(3), 499–506. https://doi.org/10.1016/S0006-3495(79)85267-4

Corey, J. M., & Feldman, E. L. (2003). Substrate patterning: An emerging technology for the study of neuronal behavior. *Experimental Neurology*, *184*(SUPPL. 1), 89–96. https://doi.org/10.1016/S0014-4886(03)00392-3

Coste, B., Houge, G., Murray, M. F., Stitziel, N., Bandell, M., Giovanni, M. A., Philippakis, A., Hoischen, A., Riemer, G., Steen, U., Steen, V. M., Mathur, J., Cox, J., Lebo, M., Rehm, H., Weiss, S. T., Wood, J. N., Maas, R. L., Sunyaev, S. R., & Patapoutian, A. (2013). Gain-of-function mutations in the mechanically activated ion channel PIEZO2 cause a subtype of Distal Arthrogryposis. *Proceedings of the National Academy of Sciences of the United States of America*, *110*(12), 4667–4672. https://doi.org/10.1073/pnas.1221400110

Coste, B., Mathur, J., Schmidt, M., Earley, T. J., Ranade, S., Petrus, M. J., Dubin, A. E., & Patapoutian, A. (2010). Piezo1 and Piezo2 are essential components of distinct mechanically activated cation channels. *Science*, *330*(6000), 55–60. https://doi.org/10.1126/science.1193270

Coste, B., Murthy, S. E., Mathur, J., Schmidt, M., Mechioukhi, Y., Delmas, P., & Patapoutian, A.

(2015). Piezo1 ion channel pore properties are dictated by C-terminal region. *Nature Communications*, *6*(May). https://doi.org/10.1038/ncomms8223

Coste, B., Xiao, B., Santos, J. S., Syeda, R., Grandl, J., Spencer, K. S., Kim, S. E., Schmidt, M., Mathur, J., Dubin, A. E., Montal, M., & Patapoutian, A. (2012). Piezo proteins are pore-forming subunits of mechanically activated channels. *Nature*, *483*(7388), 176–181. https://doi.org/10.1038/nature10812

Cox, C. D., Bavi, N., & Martinac, B. (2017). Origin of the Force: The Force-From-Lipids Principle Applied to Piezo Channels. In *Current Topics in Membranes* (Vol. 79). Elsevier Ltd. https://doi.org/10.1016/bs.ctm.2016.09.001

Cox, Charles D., Bae, C., Ziegler, L., Hartley, S., Nikolova-Krstevski, V., Rohde, P. R., Ng, C. A., Sachs, F., Gottlieb, P. A., & Martinac, B. (2016). Removal of the mechanoprotective influence of the cytoskeleton reveals PIEZO1 is gated by bilayer tension. *Nature Communications*, *7*, 1–13. https://doi.org/10.1038/ncomms10366

Cukierman, E., Pankov, R., Stevens, D. R., & Yamada, K. M. (2001). Taking cell-matrix adhesions to the third dimension. *Science*, *294*(5547), 1708–1712. https://doi.org/10.1126/science.1064829

Dalghi, M. G., Clayton, D. R., Ruiz, W. G., Al-Bataineh, M. M., Satlin, L. M., Kleyman, T. R., Ricke, W. A., Carattino, M. D., & Apodaca, G. (2019). Expression and distribution of PIEZO1 in the mouse urinary tract. *American Journal of Physiology - Renal Physiology*, *317*(2), F303–F321. https://doi.org/10.1152/ajprenal.00214.2019

De Luca, M., Mandala, M., & Rose, G. (2021). Towards an understanding of the mechanoreciprocity process in adipocytes and its perturbation with aging. *Mechanisms of Ageing and Development*, *197*, 1–28. https://doi.org/10.1016/j.mad.2021.111522

de Vincentiis, S., Falconieri, A., Mainardi, M., Cappello, V., Scribano, V., Bizzarri, R., Storti, B., Dente, L., Costa, M., & Raffa, V. (2020). Extremely Low Forces Induce Extreme Axon Growth. *Journal of Neuroscience*, *40*(26), 4997–5007. https://doi.org/10.1523/JNEUROSCI.3075-19.2020

Dehullu, J., Valotteau, C., Herman-Bausier, P., Garcia-Sherman, M., Mittelviefhaus, M., Vorholt, J. A., Lipke, P. N., & Dufrêne, Y. F. (2019). Fluidic Force Microscopy Demonstrates That Homophilic Adhesion by Candida albicans Als Proteins Is Mediated by Amyloid Bonds between Cells. *Nano Letters*, *19*(6), 3846–3853. https://doi.org/10.1021/acs.nanolett.9b01010

Di, X., Gao, X., Peng, L., Ai, J., Jin, X., Qi, S., Li, H., Wang, K., & Luo, D. (2023). Cellular mechanotransduction in health and diseases: from molecular mechanism to therapeutic targets.

Signal Transduction and Targeted Therapy, *8*(1). https://doi.org/10.1038/s41392-023-01501-9

Doss, B. L., Pan, M., Gupta, M., Grenci, G., Mège, R. M., Lim, C. T., Sheetz, M. P., Voituriez, R., & Ladoux, B. (2020). Cell response to substrate rigidity is regulated by active and passive cytoskeletal stress. *Proceedings of the National Academy of Sciences of the United States of America*, *117*(23), 12817–12825. https://doi.org/10.1073/pnas.1917555117

Du, Y., Xu, B., Li, Q., Peng, C., & Yang, K. (2024). *The role of mechanically sensitive ion channel Piezo1 in bone remodeling*. *February*, 1–18. https://doi.org/10.3389/fbioe.2024.1342149

Dubin, A. E., Murthy, S., Lewis, A. H., Brosse, L., Cahalan, S. M., Grandl, J., Coste, B., & Patapoutian, A. (2017). Endogenous Piezo1 Can Confound Mechanically Activated Channel Identification and Characterization. *Neuron*, *94*(2), 266-270.e3. https://doi.org/10.1016/j.neuron.2017.03.039

Dufrêne, Y. F., Ando, T., Garcia, R., Alsteens, D., Martinez-Martin, D., Engel, A., Gerber, C., & Müller, D. J. (2017). Imaging modes of atomic force microscopy for application in molecular and cell biology. *Nature Nanotechnology*, *12*(4), 295–307. https://doi.org/10.1038/nnano.2017.45

Eichinger, J. F., Haeusel, L. J., Paukner, D., Aydin, R. C., Humphrey, J. D., & Cyron, C. J. (2021). Mechanical homeostasis in tissue equivalents: a review. *Biomechanics and Modeling in Mechanobiology*, *20*(3), 833–850. https://doi.org/10.1007/s10237-021-01433-9

Evans, E. L., Cuthbertson, K., Endesh, N., Rode, B., Blythe, N. M., Hyman, A. J., Hall, S. J., Gaunt, H. J., Ludlow, M. J., Foster, R., & Beech, D. J. (2018). Yoda1 analogue (Dooku1) which antagonizes Yoda1-evoked activation of Piezo1 and aortic relaxation. *British Journal of Pharmacology*, *175*(10), 1744–1759. https://doi.org/10.1111/bph.14188

Falleroni, F., Bocchero, U., Mortal, S., Li, Y., Ye, Z., Cojoc, D., & Torre, V. (2022). Mechanotransduction in hippocampal neurons operates under localized low picoNewton forces. *IScience*, *25*(2), 103807. https://doi.org/10.1016/j.isci.2022.103807

Fang, X. Z., Zhou, T., Xu, J. Q., Wang, Y. X., Sun, M. M., He, Y. J., Pan, S. W., Xiong, W., Peng, Z. K., Gao, X. H., & Shang, Y. (2021). Structure, kinetic properties and biological function of mechanosensitive Piezo channels. *Cell and Bioscience*, *11*(1), 1–20. https://doi.org/10.1186/s13578-020-00522-z

Faucherre, A., Kissa, K., Nargeot, J., Mangoni, M. E., & Jopling, C. (2014). Piezo1 plays a role in erythrocyte volume homeostasis. *Haematologica*, *99*(1), 70–75. https://doi.org/10.3324/haematol.2013.086090

Fletcher, D. A., & Mullins, R. D. (2010). Cell mechanics and the cytoskeleton. *Nature*, *463*(7280),

485–492. https://doi.org/10.1038/nature08908

Florez-Paz, D., Bali, K. K., Kuner, R., & Gomis, A. (2016). A critical role for Piezo2 channels in the mechanotransduction of mouse proprioceptive neurons. *Scientific Reports*, *6*, 1–9. https://doi.org/10.1038/srep25923

Fotiou, E., Martin-Almedina, S., Simpson, M. A., Lin, S., Gordon, K., Brice, G., Atton, G., Jeffery, I., Rees, D. C., Mignot, C., Vogt, J., Homfray, T., Snyder, M. P., Rockson, S. G., Jeffery, S., Mortimer, P. S., Mansour, S., & Ostergaard, P. (2015). Novel mutations in PIEZO1 cause an autosomal recessive generalized lymphatic dysplasia with non-immune hydrops fetalis. *Nature Communications*, *6*. https://doi.org/10.1038/ncomms9085

Franze, K. (2013). The mechanical control of nervous system development. *Development (Cambridge)*, *140*(15), 3069–3077. https://doi.org/10.1242/dev.079145

Franze, K., & Guck, J. (2010). The biophysics of neuronal growth. *Reports on Progress in Physics*, *73*(9). https://doi.org/10.1088/0034-4885/73/9/094601

Friedrich, E. E., Hong, Z., Xiong, S., Zhong, M., Di, A., Rehman, J., Komarova, Y. A., & Malik, A. B. (2019). Endothelial cell Piezo1 mediates pressure-induced lung vascular hyperpermeability via disruption of adherens junctions. *Proceedings of the National Academy of Sciences of the United States of America*, *116*(26), 12980–12985. https://doi.org/10.1073/pnas.1902165116

Friedrich, O., Merten, A. L., Schneidereit, D., Guo, Y., Schürmann, S., & Martinac, B. (2019). Stretch in focus: 2D inplane cell stretch systems for studies of cardiac mechano-signaling. *Frontiers in Bioengineering and Biotechnology*, *7*(MAR), 1–9. https://doi.org/10.3389/fbioe.2019.00055

Gargalionis, A. N., Basdra, E. K., & Papavassiliou, A. G. (2018). Tumor mechanosensing and its therapeutic potential. *Journal of Cellular Biochemistry*, *119*(6), 4304–4308. https://doi.org/10.1002/jcb.26786

Gaub, B. M., Kasuba, K. C., Mace, E., Strittmatter, T., Laskowski, P. R., Geissler, S. A., Hierlemann, A., Fussenegger, M., Roska, B., & Müller, D. J. (2020). Neurons differentiate magnitude and location of mechanical stimuli. *Proceedings of the National Academy of Sciences of the United States of America*, *117*(2), 848–856. https://doi.org/10.1073/pnas.1909933117

Gaub, B. M., & Müller, D. J. (2017). Mechanical Stimulation of Piezo1 Receptors Depends on Extracellular Matrix Proteins and Directionality of Force. *Nano Letters*, *17*(3), 2064–2072. https://doi.org/10.1021/acs.nanolett.7b00177

Ge, J., Li, W., Zhao, Q., Li, N., Chen, M., Zhi, P., Li, R., Gao, N., Xiao, B., & Yang, M. (2015).

Architecture of the mammalian mechanosensitive Piezo1 channel. *Nature*, *527*(7576), 64–69. https://doi.org/10.1038/nature15247

Geiger, B., & Bershadsky, A. (2002). Exploring the neighborhood: Adhesion-coupled cell mechanosensors. *Cell*, *110*(2), 139–142. https://doi.org/10.1016/S0092-8674(02)00831-0

Geng, J., Liu, W., Zhou, H., Zhang, T., Wang, L., Zhang, M., Li, Y., Shen, B., Li, X., & Xiao, B. (2020). A Plug-and-Latch Mechanism for Gating the Mechanosensitive Piezo Channel. *Neuron*, *106*(3), 438-451.e6. https://doi.org/10.1016/j.neuron.2020.02.010

Grolleman, J., van Engeland, N. C. A., Raza, M., Azimi, S., Conte, V., Sahlgren, C. M., & Bouten, C. V. C. (2023). Environmental stiffness restores mechanical homeostasis in vimentin-depleted cells. *Scientific Reports*, *13*(1), 1–12. https://doi.org/10.1038/s41598-023-44835-8

Guharay, F., & Sachs, F. (1984). Stretch-activated single ion channel currents in tissue-cultured embryonic chick skeletal muscle. *The Journal of Physiology*, *352*(1), 685–701. https://doi.org/10.1113/jphysiol.1984.sp015317

Guo, Y. R., & MacKinnon, R. (2017). Structure-based membrane dome mechanism for piezo mechanosensitivity. *ELife*, *6*, 1–19. https://doi.org/10.7554/eLife.33660

Hampoelz, B., & Lecuit, T. (2011). Nuclear mechanics in differentiation and development. *Current Opinion in Cell Biology*, *23*(6), 668–675. https://doi.org/10.1016/j.ceb.2011.10.001

Hao, J., & Delmas, P. (2010). Multiple desensitization mechanisms of mechanotransducer channels shape firing of mechanosensory neurons. *Journal of Neuroscience*, *30*(40), 13384–13395. https://doi.org/10.1523/JNEUROSCI.2926-10.2010

Haselwandter, C. A., & Mackinnon, R. (2018). Piezo's membrane footprint and its contribution to mechanosensitivity. *ELife*, *7*, 1–29. https://doi.org/10.7554/eLife.41968

Haswell, E. S., Phillips, R., & Rees, D. C. (2011). Mechanosensitive Channels : What Can They Do and How Do They Do It ? *Structure/Folding and Design*, *19*(10), 1356–1369. https://doi.org/10.1016/j.str.2011.09.005

Humphrey, J. D., Dufresne, E. R., & Schwartz, M. A. (2014). Mechanotransduction and extracellular matrix homeostasis. *Nature Reviews Molecular Cell Biology*, *15*(12), 802–812. https://doi.org/10.1038/nrm3896

Ikeda, R., Cha, M., Ling, J., Jia, Z., Coyle, D., & Gu, J. G. (2014). Merkel cells transduce and encode tactile stimuli to drive aβ-Afferent impulses. *Cell*, *157*(3), 664–675. https://doi.org/10.1016/j.cell.2014.02.026

Ikeda, R., & Gu, J. G. (2014). Piezo2 channel conductance and localization domains in Merkel cells of rat whisker hair follicles. *Neuroscience Letters*, *583*, 210–215.

https://doi.org/10.1016/j.neulet.2014.05.055

Jahin, I., Phillips, T., Marcotti, S., Gorey, M. A., Cox, S., & Parsons, M. (2023). Extracellular matrix stiffness activates mechanosensitive signals but limits breast cancer cell spheroid proliferation and invasion. *Frontiers in Cell and Developmental Biology*, *11*(December), 1–16. https://doi.org/10.3389/fcell.2023.1292775

Jiang, Y., Yang, X., Jiang, J., & Xiao, B. (2021). Structural Designs and Mechanogating Mechanisms of the Mechanosensitive Piezo Channels. *Trends in Biochemical Sciences*, *46*(6), 472–488. https://doi.org/10.1016/j.tibs.2021.01.008

Jin, P., Jan, L. Y., & Jan, Y. N. (2020). Mechanosensitive Ion Channels: Structural Features Relevant to Mechanotransduction Mechanisms. *Annual Review of Neuroscience*, *43*, 207–229. https://doi.org/10.1146/annurev-neuro-070918-050509

Jung, Y. L., & Donahue, H. J. (2007). Cell sensing and response to micro- and nanostructured surfaces produced by chemical and topographic patterning. *Tissue Engineering*, *13*(8), 1879–1891. https://doi.org/10.1089/ten.2006.0154

Katsuta, E., Takabe, K., Vujcic, M., Gottlieb, P. A., Dai, T., Mercado-Perez, A., Beyder, A., Wang, Q., & Opyrchal, M. (2022). Mechano-Sensing Channel PIEZO2 Enhances Invasive Phenotype in Triple-Negative Breast Cancer. *International Journal of Molecular Sciences*, *23*(17). https://doi.org/10.3390/ijms23179909

Katta, S., Krieg, M., & Goodman, M. B. (2015). Feeling Force: Physical and Physiological Principles Enabling Sensory Mechanotransduction. *Annual Review of Cell and Developmental Biology*, *31*, 347–371. https://doi.org/10.1146/annurev-cellbio-100913-013426

Kiio, T. M., & Park, S. (2020). Nano-scientific application of atomic force microscopy in pathology: From molecules to tissues. *International Journal of Medical Sciences*, *17*(7), 844–858. https://doi.org/10.7150/ijms.41805

Kilinc, D., Blasiak, A., & Lee, G. U. (2015). Microtechnologies for studying the role of mechanics in axon growth and guidance. *Frontiers in Cellular Neuroscience*, *9*(JULY), 1–8. https://doi.org/10.3389/fncel.2015.00282

Kim, J., Kim, H. N., Lim, K. T., Kim, Y., Seonwoo, H., Park, S. H., Lim, H. J., Kim, D. H., Suh, K. Y., Choung, P. H., Choung, Y. H., & Chung, J. H. (2013). Designing nanotopographical density of extracellular matrix for controlled morphology and function of human mesenchymal stem cells. *Scientific Reports*, *3*, 1–11. https://doi.org/10.1038/srep03552

Kim, S. E., Coste, B., Chadha, A., Cook, B., & Patapoutian, A. (2012). The role of Drosophila Piezo in mechanical nociception. *Nature*, *483*(7388), 209–212.

https://doi.org/10.1038/nature10801

Kirby, T. J., & Lammerding, J. (2018). mechanosensor. *Nature Cell Biology*, *20*(April). https://doi.org/10.1038/s41556-018-0038-y

Koll, R., Ribera, J. M., Brunner, R. M., Rebl, A., & Goldammer, T. (2020). Gene profiling in the adipose fin of salmonid fishes supports its function as a flow sensor. *Genes*, *11*(1). https://doi.org/10.3390/genes11010021

Koser, D. E., Thompson, A. J., Foster, S. K., Dwivedy, A., Pillai, E. K., Sheridan, G. K., Svoboda, H., Viana, M., Costa, L. D. F., Guck, J., Holt, C. E., & Franze, K. (2016). Mechanosensing is critical for axon growth in the developing brain. *Nature Neuroscience*, *19*(12), 1592–1598. https://doi.org/10.1038/nn.4394

Kung, C. (2005). A possible unifying principle for mechanosensation. *Nature*, *436*(7051), 647–654. https://doi.org/10.1038/nature03896

Lammerding, J., & Kirby, T. J. (2018). Emerging views of the nucleus as a cellular mechanosensor. *Nature Cell Biology*, *20*(4), 373–381. https://doi.org/10.1038/s41556-018-0038-y.Emerging

Lawson, S. N. (2002). Phenotype and function of somatic primary afferent nociceptive neurones with C-, Aδ- or Aα/β-fibres. *Experimental Physiology*, *87*(2), 239–244. https://doi.org/10.1113/eph8702350

Lessey, E. C., Guilluy, C., & Burridge, K. (2012). From mechanical force to RhoA activation. *Biochemistry*, *51*(38), 7420–7432. https://doi.org/10.1021/bi300758e

Lewis, A. H., Cui, A. F., McDonald, M. F., & Grandl, J. (2017). Transduction of Repetitive Mechanical Stimuli by Piezo1 and Piezo2 Ion Channels. *Cell Reports*, *19*(12), 2572–2585. https://doi.org/10.1016/j.celrep.2017.05.079

Lewis, A. H., & Grandl, J. (2015). Mechanical sensitivity of Piezo1 ion channels can be tuned by cellular membrane tension. *ELife*, *4*(December2015), 1–17. https://doi.org/10.7554/eLife.12088

Li, M., Liu, L., & Zambelli, T. (2022). FluidFM for single-cell biophysics. *Nano Research*, *15*(2), 773–786. https://doi.org/10.1007/s12274-021-3573-y

Li, Xu, Hu, J., Zhao, X., Li, J., & Chen, Y. (2022). Piezo channels in the urinary system. *Experimental and Molecular Medicine*, *54*(6), 697–710. https://doi.org/10.1038/s12276-022-00777-1

Li, Xuehua, Han, L., Nookaew, I., Mannen, E., Silva, M. J., Almeida, M., & Xiong, J. (2019). Stimulation of piezo1 by mechanical signals promotes bone anabolism. *ELife*, *8*, 1–22. https://doi.org/10.7554/eLife.49631

Li, Y., Tang, W., & Guo, M. (2021). The cell as matter: Connecting molecular biology to cellular functions. *Matter*, *4*(6), 1863–1891. https://doi.org/10.1016/j.matt.2021.03.013

Lin, Y. C., Guo, Y. R., Miyagi, A., Levring, J., MacKinnon, R., & Scheuring, S. (2019). Force-induced conformational changes in PIEZO1. *Nature*, *573*(7773), 230–234. https://doi.org/10.1038/s41586-019-1499-2

Liu, X., & Nakamura, F. (2021). Mechanotransduction, nanotechnology, and nanomedicine. *Journal of Biomedical Research*, *35*(4), 284–293. https://doi.org/10.7555/JBR.34.20200063

Lüchtefeld, I., Pivkin, I. V., Gardini, L., Zare-Eelanjegh, E., Gäbelein, C., Ihle, S. J., Reichmuth, A. M., Capitanio, M., Martinac, B., Zambelli, T., & Vassalli, M. (2024). Dissecting cell membrane tension dynamics and its effect on Piezo1-mediated cellular mechanosensitivity using force-controlled nanopipettes. *Nature Methods*, *21*(6), 1063–1073. https://doi.org/10.1038/s41592-024-02277-8

Marshall, K. L., Saade, D., Ghitani, N., Coombs, A. M., Szczot, M., Keller, J., Ogata, T., Daou, I., Stowers, L. T., Bönnemann, C. G., Chesler, A. T., & Patapoutian, A. (2020). PIEZO2 in sensory neurons and urothelial cells coordinates urination. *Nature*, *588*(7837), 290–295. https://doi.org/10.1038/s41586-020-2830-7

Martinac, B. (2004). Mechanosensitive ion channels: Molecules of mechanotransduction. *Journal of Cell Science*, *117*(12), 2449–2460. https://doi.org/10.1242/jcs.01232

Martinac, B., Adler, J., & Kung, C. (1990). Mechanosensitive ion channels of E. coli activated by amphipaths. In *Nature* (Vol. 348, Issue 6298, pp. 261–263). https://doi.org/10.1038/348261a0

Martinac, B., & Poole, K. (2018). Mechanically activated ion channels. *International Journal of Biochemistry and Cell Biology*, *97*(January), 104–107. https://doi.org/10.1016/j.biocel.2018.02.011

McCarter, G. C., Reichling, D. B., & Levine, J. D. (1999). Mechanical transduction by rat dorsal root ganglion neurons in vitro. *Neuroscience Letters*, *273*(3), 179–182. https://doi.org/10.1016/S0304-3940(99)00665-5

McMillin, M. J., Beck, A. E., Chong, J. X., Shively, K. M., Buckingham, K. J., Gildersleeve, H. I. S., Aracena, M. I., Aylsworth, A. S., Bitoun, P., Carey, J. C., Clericuzio, C. L., Crow, Y. J., Curry, C. J., Devriendt, K., Everman, D. B., Fryer, A., Gibson, K., Giovannucci Uzielli, M. L., Graham, J. M., … Bamshad, M. J. (2014). Mutations in PIEZO2 cause Gordon syndrome, Marden-Walker Syndrome, and distal arthrogryposis type 5. *American Journal of Human Genetics*, *94*(5), 734–744. https://doi.org/10.1016/j.ajhg.2014.03.015

Meister, A., Gabi, M., Behr, P., Studer, P., Vörös, J., Niedermann, P., Bitterli, J., Polesel-Maris, J.,

Liley, M., Heinzelmann, H., & Zambelli, T. (2009). FluidFM: Combining atomic force microscopy and nanofluidics in a universal liquid delivery system for single cell applications and beyond. *Nano Letters*, *9*(6), 2501–2507. https://doi.org/10.1021/nl901384x

Mierke, C. T. (2024). Extracellular Matrix Cues Regulate Mechanosensing and Mechanotransduction of Cancer Cells. *Cells*, *13*(1). https://doi.org/10.3390/cells13010096

Mikhailov, N., Leskinen, J., Fagerlund, I., Poguzhelskaya, E., Giniatullina, R., Gafurov, O., Malm, T., Karjalainen, T., Gröhn, O., & Giniatullin, R. (2019). Mechanosensitive meningeal nociception via Piezo channels: Implications for pulsatile pain in migraine? *Neuropharmacology*, *149*(October 2018), 113–123. https://doi.org/10.1016/j.neuropharm.2019.02.015

Mirzoev, T. M. (2023). The emerging role of Piezo1 channels in skeletal muscle physiology. *Biophysical Reviews*, *15*(5), 1171–1184. https://doi.org/10.1007/s12551-023-01154-6

Miyamoto, T., Mochizuki, T., Nakagomi, H., Kira, S., Watanabe, M., Takayama, Y., Suzuki, Y., Koizumi, S., Takeda, M., & Tominaga, M. (2014). Functional role for Piezo1 in stretch-evoked Ca2+ influx and ATP release in Urothelial cell cultures. *Journal of Biological Chemistry*, *289*(23), 16565–16575. https://doi.org/10.1074/jbc.M113.528638

Moroni, M., Servin-Vences, M. R., Fleischer, R., Sánchez-Carranza, O., & Lewin, G. R. (2018). Voltage gating of mechanosensitive PIEZO channels. *Nature Communications*, *9*(1), 1–15. https://doi.org/10.1038/s41467-018-03502-7

Murthy, S. E. (2023). Deciphering mechanically activated ion channels at the single-channel level in dorsal root ganglion neurons. *Journal of General Physiology*, *155*(6). https://doi.org/10.1085/jgp.202213099

Murthy, S. E., Dubin, A. E., & Patapoutian, A. (2017). Piezos thrive under pressure: Mechanically activated ion channels in health and disease. *Nature Reviews Molecular Cell Biology*, *18*(12), 771–783. https://doi.org/10.1038/nrm.2017.92

Murthy, S. E., Loud, M. C., Daou, I., Marshall, K. L., Schwaller, F., Kühnemund, J., Francisco, A. G., Keenan, W. T., Dubin, A. E., Lewin, G. R., & Patapoutian, A. (2018). The mechanosensitive ion channel Piezo2 mediates sensitivity to mechanical pain in mice. *Science Translational Medicine*, *10*(462). https://doi.org/10.1126/scitranslmed.aat9897

Nagel, M., & Chesler, A. T. (2022). Neurobiology PIEZO2 ion channels in proprioception. *Current Opinion in Neurobiology*, *75*, 102572. https://doi.org/10.1016/j.conb.2022.102572

Nascimento, A. I., Mar, F. M., & Sousa, M. M. (2018). The intriguing nature of dorsal root ganglion neurons: Linking structure with polarity and function. *Progress in Neurobiology*,

168(December 2017), 86–103. https://doi.org/10.1016/j.pneurobio.2018.05.002

Noble, D. J., Dongmo, R., Parvin, S., Martin, K. K., & Garraway, S. M. (2022). C-low threshold mechanoreceptor activation becomes sufficient to trigger affective pain in spinal cord-injured mice in association with increased respiratory rates. *Frontiers in Integrative Neuroscience*, *16*(December), 1–16. https://doi.org/10.3389/fnint.2022.1081172

Nonomura, K., Woo, S. H., Chang, R. B., Gillich, A., Qiu, Z., Francisco, A. G., Ranade, S. S., Liberles, S. D., & Patapoutian, A. (2017). Piezo2 senses airway stretch and mediates lung inflation-induced apnoea. *Nature*, *541*(7636), 176–181. https://doi.org/10.1038/nature20793

O'Callaghan, R., Job, K. M., Dull, R. O., & Hlady, V. (2011). Stiffness and heterogeneity of the pulmonary endothelial glycocalyx measured by atomic force microscopy. *American Journal of Physiology - Lung Cellular and Molecular Physiology*, *301*(3), 353–360. https://doi.org/10.1152/ajplung.00342.2010

Oh, S., Brammer, K. S., Li, Y. S. J., Teng, D., Engler, A. J., Chien, S., & Jin, S. (2009). Stem cell fate dictated solely by altered nanotube dimension. *Proceedings of the National Academy of Sciences of the United States of America*, *106*(7), 2130–2135. https://doi.org/10.1073/pnas.0813200106

Ossola, D., Amarouch, M. Y., Behr, P., Vörös, J., Abriel, H., & Zambelli, T. (2015). Force-controlled patch clamp of beating cardiac cells. *Nano Letters*, *15*(3), 1743–1750. https://doi.org/10.1021/nl504438z

Pathak, M. M., Nourse, J. L., Tran, T., Hwe, J., Arulmoli, J., Trang, D., & Le, T. (2014). *Stretch-activated ion channel Piezo1 directs lineage choice in human neural stem cells*. *111*(45), 1–6. https://doi.org/10.1073/pnas.1409802111

Peyronnet, R., Martins, J. R., Duprat, F., Demolombe, S., Arhatte, M., Jodar, M., Tauc, M., Duranton, C., Paulais, M., Teulon, J., Honoré, E., & Patel, A. (2013). Piezo1-dependent stretch-activated channels are inhibited by Polycystin-2 in renal tubular epithelial cells. *EMBO Reports*, *14*(12), 1143–1148. https://doi.org/10.1038/embor.2013.170

Pillai, E. K., & Franze, K. (2024). Mechanics in the nervous system: From development to disease. *Neuron*, *112*(3), 342–361. https://doi.org/10.1016/j.neuron.2023.10.005

Potthoff, E., Guillaume-Gentil, O., Ossola, D., Polesel-Maris, J., LeibundGut-Landmann, S., Zambelli, T., & Vorholt, J. A. (2012). Rapid and Serial Quantification of Adhesion Forces of Yeast and Mammalian Cells. *PLoS ONE*, *7*(12). https://doi.org/10.1371/journal.pone.0052712

Qi, L., Iskols, M., Shi, D., Reddy, P., Walker, C., Lezgiyeva, K., Voisin, T., Pawlak, M., Kuchroo, V. K., Chiu, I. M., Ginty, D. D., & Sharma, N. (2024). A mouse DRG genetic toolkit reveals

morphological and physiological diversity of somatosensory neuron subtypes. *Cell*, *187*(6), 1508-1526.e16. https://doi.org/10.1016/j.cell.2024.02.006

Qin, L., He, T., Chen, S., Yang, D., Yi, W., Cao, H., & Xiao, G. (2021). Roles of mechanosensitive channel Piezo1/2 proteins in skeleton and other tissues. *Bone Research*, *9*(1). https://doi.org/10.1038/s41413-021-00168-8

Ranade, S. S., Qiu, Z., Woo, S. H., Hur, S. S., Murthy, S. E., Cahalan, S. M., Xu, J., Mathur, J., Bandell, M., Coste, B., Li, Y. S. J., Chien, S., & Patapoutian, A. (2014). Piezo1, a mechanically activated ion channel, is required for vascular development in mice. *Proceedings of the National Academy of Sciences of the United States of America*, *111*(28), 10347–10352. https://doi.org/10.1073/pnas.1409233111

Ranade, S. S., Woo, S. H., Dubin, A. E., Moshourab, R. A., Wetzel, C., Petrus, M., Mathur, J., Bégay, V., Coste, B., Mainquist, J., Wilson, A. J., Francisco, A. G., Reddy, K., Qiu, Z., Wood, J. N., Lewin, G. R., & Patapoutian, A. (2014). Piezo2 is the major transducer of mechanical forces for touch sensation in mice. *Nature*, *516*(729), 121–125. https://doi.org/10.1038/nature13980

Repic, T., Madirazza, K., Bektur, E., & Sapunar, D. (2016). Characterization of dorsal root ganglion neurons cultured on silicon micro-pillar substrates. *Scientific Reports*, *6*, 1–10. https://doi.org/10.1038/srep39560

Retailleau, K., Duprat, F., Arhatte, M., Ranade, S. S., Peyronnet, R., Martins, J. R., Jodar, M., Moro, C., Offermanns, S., Feng, Y., Demolombe, S., Patel, A., & Honoré, E. (2015). Piezo1 in Smooth Muscle Cells Is Involved in Hypertension-Dependent Arterial Remodeling. *Cell Reports*, *13*(6), 1161–1171. https://doi.org/10.1016/j.celrep.2015.09.072

Rezaei, N., & Saghazadeh, A. (2017). The role of PIEZO2 in human mechanosensation. *Acta Medica Iranica*, *55*(10), 1355–1364. https://doi.org/10.1056/nejmoa1602812

Richardson, J., Kotevski, A., & Poole, K. (2022). From stretch to deflection: the importance of context in the activation of mammalian, mechanically activated ion channels. *FEBS Journal*, *289*(15), 4447–4469. https://doi.org/10.1111/febs.16041

Ridone, P., Pandzic, E., Vassalli, M., Cox, C. D., Macmillan, A., Gottlieb, P. A., & Martinac, B. (2020). *Disruption of membrane cholesterol organization impairs the activity of PIEZO1 channel clusters*. *152*(8).

Ridone, P., Vassalli, M., & Martinac, B. (2019). Piezo1 mechanosensitive channels: what are they and why are they important. *Biophysical Reviews*, *11*(5), 795–805. https://doi.org/10.1007/s12551-019-00584-5

Sann, H., McCarthy, P. W., Jancsó, G., & Pierau, F. K. (1995). RT97: a marker for capsaicin-insensitive sensory endings in the rat skin. *Cell & Tissue Research*, *282*(1), 155–161. https://doi.org/10.1007/BF00319142

Saotome, K., Murthy, S. E., Kefauver, J. M., Whitwam, T., Patapoutian, A., & Ward, A. B. (2018). Structure of the mechanically activated ion channel Piezo1. *Nature*, *554*(7693), 481–486. https://doi.org/10.1038/nature25453

Saotome, K., Singh, A. K., Yelshanskaya, M. V., & Sobolevsky, A. I. (2016). Crystal structure of the epithelial calcium channel TRPV6. *Nature*, *534*(7608), 506–511. https://doi.org/10.1038/nature17975

Servin-Vences, M. R., Moroni, M., Lewin, G. R., & Poole, K. (2017). Direct measurement of TRPV4 and PIEZO1 activity reveals multiple mechanotransduction pathways in chondrocytes. *ELife*, *6*, 1–24. https://doi.org/10.7554/eLife.21074

Sforna, L., Michelucci, A., Morena, F., Argentati, C., Franciolini, F., Vassalli, M., Martino, S., & Catacuzzeno, L. (2022). Piezo1 controls cell volume and migration by modulating swelling-activated chloride current through Ca2+ influx. *Journal of Cellular Physiology*, *237*(3), 1857–1870. https://doi.org/10.1002/jcp.30656

Shin, K. C., Park, H. J., Kim, J. G., Lee, I. H., Cho, H., Park, C., Sung, T. S., Koh, S. D., Park, S. W., & Bae, Y. M. (2019). The Piezo2 ion channel is mechanically activated by low-threshold positive pressure. *Scientific Reports*, *9*(1), 1–9. https://doi.org/10.1038/s41598-019-42492-4

Sirkkunan, D., Pingguan-Murphy, B., & Muhamad, F. (2022). Directing Axonal Growth: A Review on the Fabrication of Fibrous Scaffolds That Promotes the Orientation of Axons. *Gels*, *8*(1). https://doi.org/10.3390/gels8010025

Stewart, M. P., Toyoda, Y., Hyman, A. A., & Muller, D. J. (2011). Force probing cell shape changes to molecular resolution. *Trends in Biochemical Sciences*, *36*(8), 444–450. https://doi.org/10.1016/j.tibs.2011.05.001

Strotmann, R., Harteneck, C., Nunnenmacher, K., Schultz, G., & Plant, T. D. (2000). OTRPC4, a nonselective cation channel that confers sensivity to extracellular osmolarity. *Nature Cell Biology*, *2*(10), 695–702. https://doi.org/10.1038/35036318

Suchyna, T. M., Johnson, J. H., Hamer, K., Leykam, J. F., Gage, D. A., Clemo, H. F., Baumgarten, C. M., & Sachs, F. (2000). *Identification of a Peptide Toxin from Grammostola spatulata Spider Venom that Blocks Cation-selective Stretch-activated Channels*. *115*(May).

Suchyna, T. M., Tape, S. E., Koeppe, R. E., Andersen, O. S., Sachs, F., & Gottlieb, P. A. (2004). Bilayer-dependent inhibition of mechanosensitive channels by neuroactive peptide

enantiomers. *Nature*, *430*(6996), 235–240. https://doi.org/10.1038/nature02743

Sukharev, S. I., Blount, P., Martinac, B., Blattner, F. R., & Kung, C. (1994). A large-conductance mechanosensitive channel in E. coli encoded by mscL alone. *Nature*, *368*(6468), 265–268. https://doi.org/10.1038/368265a0

Sun, W., Gao, X., Lei, H., Wang, W., & Cao, Y. (2022). Biophysical Approaches for Applying and Measuring Biological Forces. *Advanced Science*, *9*(5), 1–26. https://doi.org/10.1002/advs.202105254

Sunnerberg, J. P., Descoteaux, M., Kaplan, D. L., & Staii, C. (2021). Axonal growth on surfaces with periodic geometrical patterns. *PLoS ONE*, *16*(9 September), 1–20. https://doi.org/10.1371/journal.pone.0257659

Syeda, R., Florendo, M. N., Cox, C. D., Kefauver, J. M., Santos, J. S., Martinac, B., & Patapoutian, A. (2016). Piezo1 Channels Are Inherently Mechanosensitive. *Cell Reports*, *17*(7), 1739–1746. https://doi.org/10.1016/j.celrep.2016.10.033

Szczot, M., Liljencrantz, J., Ghitani, N., Barik, A., Lam, R., Thompson, J. H., Bharucha-Goebel, D., Saade, D., Necaise, A., Donkervoort, S., Foley, A. R., Gordon, T., Case, L., Bushnell, M. C., Bönnemann, C. G., & Chesler, A. T. (2018). PIEZO2 mediates injury-induced tactile pain in mice and humans. *Science Translational Medicine*, *10*(462), 1–9. https://doi.org/10.1126/scitranslmed.aat9892

Szczot, M., Nickolls, A. R., Lam, R. M., & Chesler, A. T. (2021). The Form and Function of PIEZO2. *Annual Review of Biochemistry*, *90*, 507–534. https://doi.org/10.1146/annurev-biochem-081720-023244

Tadge, T., Pattewar, A., More, N., Babu, S. S., Velyutham, R., & Kapusetti, G. (2024). The role of Piezo1 and Piezo2 proteins in tissue engineering: A Comprehensive review. *Engineered Regeneration*, *5*(2), 170–185. https://doi.org/10.1016/j.engreg.2024.03.001

te Riet, J., Katan, A. J., Rankl, C., Stahl, S. W., van Buul, A. M., Phang, I. Y., Gomez-Casado, A., Schön, P., Gerritsen, J. W., Cambi, A., Rowan, A. E., Vancso, G. J., Jonkheijm, P., Huskens, J., Oosterkamp, T. H., Gaub, H., Hinterdorfer, P., Figdor, C. G., & Speller, S. (2011). Interlaboratory round robin on cantilever calibration for AFM force spectroscopy. *Ultramicroscopy*, *111*(12), 1659–1669. https://doi.org/10.1016/j.ultramic.2011.09.012

Teixeira, A. I., Abrams, G. A., Bertics, P. J., Murphy, C. J., & Nealey, P. F. (2003). *Epithelial contact guidance on well-defined micro- and nanostructured substrates*. https://doi.org/10.1242/jcs.00383

Tonazzini, I., Jacchetti, E., Meucci, S., Beltram, F., & Cecchini, M. (2015). Schwann Cell Contact

Guidance versus Boundary -Interaction in Functional Wound Healing along Nano and Microstructured Membranes. *Advanced Healthcare Materials*, *4*(12), 1849–1860. https://doi.org/10.1002/adhm.201500268

Tonazzini, I., Meucci, S., Faraci, P., Beltram, F., & Cecchini, M. (2013). Neuronal differentiation on anisotropic substrates and the influence ofnanotopographical noise on neurite contact guidance. *Biomaterials*, *34*(25), 6027–6036. https://doi.org/10.1016/j.biomaterials.2013.04.039

Tortorella, I., & , Chiara Argentati , Carla Emiliani, Francesco Morena, and S. M. (2022). Biochemical Pathways of Cellular Neurodegenerative Diseases Pathogenesis. *Cells*, *11*, 3093.

Tufoni, C., Battistella, A., Luppi, S., Boscolo, R., Ricci, G., Lazzarino, M., & Andolfi, L. (2024). Flagellar beating forces of human spermatozoa with different motility behaviors. *Reproductive Biology and Endocrinology*, *22*(1), 1–10. https://doi.org/10.1186/s12958-024-01197-8

Uhler, C., & Shivashankar, G. V. (2017). Regulation of genome organization and gene expression by nuclear mechanotransduction. *Nature Reviews Molecular Cell Biology*, *18*(12), 717–727. https://doi.org/10.1038/nrm.2017.101

Vaisey, G., Banerjee, P., North, A. J., Haselwandter, C. A., & Mackinnon, R. (2022). Piezo1 as a force-through-membrane sensor in red blood cells. *ELife*, *11*, 1–21. https://doi.org/10.7554/ELIFE.82621

Van Helvert, S., Storm, C., & Friedl, P. (2018). Mechanoreciprocity in cell migration. *Nature Cell Biology*, *20*(1), 8–20. https://doi.org/10.1038/s41556-017-0012-0

Velasco-Estevez, M., Gadalla, K. K. E., Liñan-Barba, N., Cobb, S., Dev, K. K., & Sheridan, G. K. (2020). Inhibition of Piezo1 attenuates demyelination in the central nervous system. *Glia*, *68*(2), 356–375. https://doi.org/10.1002/glia.23722

Ventura, G., & Sedzinski, J. (2022). Emerging concepts on the mechanical interplay between migrating cells and microenvironment in vivo. *Frontiers in Cell and Developmental Biology*, *10*(September), 1–9. https://doi.org/10.3389/fcell.2022.961460

Verkest, C., Schaefer, I., Nees, T. A., Wang, N., Jegelka, J. M., Taberner, F. J., & Lechner, S. G. (2022). Intrinsically disordered intracellular domains control key features of the mechanically-gated ion channel PIEZO2. *Nature Communications*, *13*(1). https://doi.org/10.1038/s41467-022-28974-6

Viatchenko-Karpinski, V., & Gu, J. G. (2016). Mechanical sensitivity and electrophysiological properties of acutely dissociated dorsal root ganglion neurons of rats. *Neuroscience Letters*, *634*, 70–75. https://doi.org/10.1016/j.neulet.2016.10.011

Villarino, N. W., Hamed, Y. M. F., Ghosh, B., Dubin, A. E., Lewis, A. H., Odem, M. A., Loud, M.

C., Wang, Y., Servin-Vences, M. R., Patapoutian, A., & Marshall, K. L. (2023). Labeling PIEZO2 activity in the peripheral nervous system. *Neuron*, *111*(16), 2488-2501.e8. https://doi.org/10.1016/j.neuron.2023.05.015

Wadia, J. S., Chalmers-Redman, R. M. E., Ju, W. J. H., Carlile, G. W., Phillips, J. L., Fraser, A. D., & Tatton, W. G. (1998). Mitochondrial membrane potential and nuclear changes in apoptosis caused by serum and nerve growth factor withdrawal: Time course and modification by (-)-deprenyl. *Journal of Neuroscience*, *18*(3), 932–947. https://doi.org/10.1523/jneurosci.18-03-00932.1998

Wang, J., Jiang, J., Yang, X., Zhou, G., Wang, L., & Xiao, B. (2022). Tethering Piezo channels to the actin cytoskeleton for mechanogating via the cadherin-β-catenin mechanotransduction complex. *Cell Reports*, *38*(6), 110342. https://doi.org/10.1016/j.celrep.2022.110342

Wang, Li, Zhou, H., Zhang, M., Liu, W., Deng, T., Zhao, Q., Li, Y., Lei, J., Li, X., & Xiao, B. (2019). Structure and mechanogating of the mammalian tactile channel PIEZO2. *Nature*, *573*(7773), 225–229. https://doi.org/10.1038/s41586-019-1505-8

Wang, Lijun, You, X., Lotinun, S., Zhang, L., Wu, N., & Zou, W. (2020). Mechanical sensing protein PIEZO1 regulates bone homeostasis via osteoblast-osteoclast crosstalk. *Nature Communications*, *11*(1), 1–12. https://doi.org/10.1038/s41467-019-14146-6

Wang, Y., Chi, S., Guo, H., Li, G., Wang, L., Zhao, Q., Rao, Y., Zu, L., He, W., & Xiao, B. (2018). A lever-like transduction pathway for long-distance chemical- and mechano-gating of the mechanosensitive Piezo1 channel. *Nature Communications*, *9*(1). https://doi.org/10.1038/s41467-018-03570-9

White, J. P. M., Cibelli, M., Urban, L., Nilius, B., McGeown, J. G., & Nagy, I. (2016). TRPV4: Molecular conductor of a diverse orchestra. *Physiological Reviews*, *96*(3), 911–973. https://doi.org/10.1152/physrev.00016.2015

Woo, S.-H., Lukacs, V., De Nooij, J. C., Zaytseva, D., Criddle, C. R., Francisco, A., Jessell, T. M., Wilkinson, K. A., & Patapoutian, A. (2015). Piezo2 is the principal mechanotransduction channel for proprioception HHS Public Access Author manuscript. *Nat Neurosci*, *18*(12), 1756–1762. https://doi.org/10.1038/nn.4162.Piezo2

Woo, S. H., Ranade, S., Weyer, A. D., Dubin, A. E., Baba, Y., Qiu, Z., Petrus, M., Miyamoto, T., Reddy, K., Lumpkin, E. A., Stucky, C. L., & Patapoutian, A. (2014). Piezo2 is required for Merkel-cell mechanotransduction. *Nature*, *509*(7502), 622–626. https://doi.org/10.1038/nature13251

Wu, J., Lewis, A. H., & Grandl, J. (2017). Touch, Tension, and Transduction – The Function and

Regulation of Piezo Ion Channels. *Trends in Biochemical Sciences*, *42*(1), 57–71. https://doi.org/10.1016/j.tibs.2016.09.004

Xi, W., Delacour, D., Ladoux, B., Xi, W., Delacour, D., & Ladoux, B. (2021). *Designer substrates and devices for mechanobiology study To cite this version : HAL Id : hal-03453583*.

Yang, H., Liu, C., Zhou, R. M., Yao, J., Li, X. M., Shen, Y., Cheng, H., Yuan, J., Yan, B., & Jiang, Q. (2016). Piezo2 protein: A novel regulator of tumor angiogenesis and hyperpermeability. *Oncotarget*, *7*(28), 44630–44643. https://doi.org/10.18632/oncotarget.10134

Young, M., Lewis, A. H., & Grandl, J. (2022). Physics of mechanotransduction by Piezo ion channels. *Journal of General Physiology*, *154*(7), 1–13. https://doi.org/10.1085/jgp.202113044

Zarychanski, R., Schulz, V. P., Houston, B. L., Maksimova, Y., Houston, D. S., Smith, B., Rinehart, J., & Gallagher, P. G. (2012). Mutations in the mechanotransduction protein PIEZO1 are associated with hereditary xerocytosis. *Blood*, *120*(9), 1908–1915. https://doi.org/10.1182/blood-2012-04-422253

Zhang, Y., Zou, W., Dou, W., Luo, H., & Ouyang, X. (2024). Pleiotropic physiological functions of Piezo1 in human body and its effect on malignant behavior of tumors. *Frontiers in Physiology*, *15*(April), 1–20. https://doi.org/10.3389/fphys.2024.1377329

Zhao, Q., Zhou, H., Chi, S., Wang, Y., Wang, J., Geng, J., Wu, K., Liu, W., Zhang, T., Dong, M. Q., Wang, J., Li, X., & Xiao, B. (2018). Structure and mechanogating mechanism of the Piezo1 channel. *Nature*, *554*(7693), 487–492. https://doi.org/10.1038/nature25743

Zhu, Y., Garcia-Sanchez, J., Dalal, R., Sun, Y., Kapiloff, M. S., Goldberg, J. L., & Liu, W. W. (2023). Differential expression of PIEZO1 and PIEZO2 mechanosensitive channels in ocular tissues implicates diverse functional roles. *Experimental Eye Research*, *236*(October), 109675. https://doi.org/10.1016/j.exer.2023.109675